SELF-ASSEMBLED DNA NANOSTRUCTURES AND DNA-TEMPLATED SILVER NANOWIRES

by

Sung Ha Park

Department of Physics
Duke University

Date:_____

Approved:

_____
Gleb Finkelstein, Supervisor

_____
Thomas H. LaBean, Co-supervisor

_____
John H. Reif

_____
Henry S. Greenside

_____
Glenn S. Edwards

Dissertation submitted in partial fulfillment of
the requirements for the degree of Doctor
of Philosophy in the Department of
Physics in the Graduate School
of Duke University

2005

ABSTRACT

SELF-ASSEMBLED DNA NANOSTRUCTURES AND DNA-TEMPLATED SILVER NANOWIRES

by

Sung Ha Park

Department of Physics
Duke University

Date:_____

Approved:

_____
Gleb Finkelstein, Supervisor

_____
Thomas H. LaBean, Co-supervisor

_____
John H. Reif

_____
Henry S. Greenside

_____
Glenn S. Edwards

An abstract of a dissertation submitted in partial fulfillment of the requirements for the degree of Doctor of Philosophy in the Department of Physics in the Graduate School of Duke University

2005

Abstract

DNA-based nanotechnology has been attractive as a novel assembly method for fabricating nanostructures for the last two decades. Artificially designed, self-assembled DNA nanostructures have been reported with various geometrical structures and functionalities: one- and two-dimensional periodically patterned structures, three-dimensional polyhedra, nanomechanical devices, molecular computers, and organization of other functionalized molecules. This thesis describes self-assembled DNA nanostructures and DNA-templated metallic nanowires. One- and two- dimensional periodically patterned superstructures, such as filaments, lattices, nanoribbons, nanotracks, and nanogrids, utilizing newly conceived two distinct DNA motifs - three helix bundles, and the cross-tiles as well as synthetic double-stranded DNA molecules - will be discussed with unique design schemes and characteristics. DNA complexes have been visualized by high-resolution tapping mode atomic force microscopy under buffer. Their dimensions are shown to be in excellent agreement with designed structures. We have also presented fabrication of size-controllable, fully addressable, and precisely programmable DNA-based nanomatrices, consisting of two different cross-tiles using a novel stepwise assembly technique.

Especially in design and construction of functionalized electronic nanodevices, properly fabricated DNA lattices can serve as a precisely controllable and programmable scaffold for organizing functionalized nanomaterials. DNA-templated metallic nanowires are an example demonstration of DNA molecules' scaffold capability and have been

considered an interesting research subject for the last decade. Until recently, mostly native λ-DNA molecules have been used as template for fabricating various metallic nanowires, such as silver, gold, palladium, platinum, and copper. In this thesis, we also present fabrication of metallic silver nanowires templated on artificially designed one-dimensional DNA nanostructures as well as native λ-DNA molecules by a novel electroless deposition technique and demonstration of electrical measurements through silver nanowires at room temperature. DNA templated silver nanowires have a uniform width with a diameter down to ~15 nm, which are among the thinnest conductive metal wires available to date by any method. The wires have been contacted by leads formed by electron beam lithography and show mostly ohmic behavior with resistances of ~1 kΩ.

Acknowledgments

A thesis such as this could not have been written without substantial assistance from many people. Here I am pleased to be able to thank those who have given me that assistance. I should begin with my supervisors, Thomas H. LaBean and Gleb Finkelstein. I am deeply grateful and indebted to them for their excellent guidance and sincere encouragement during my graduate work. I'll never forget them in my life. I am also grateful to John H. Reif for his consistent encouragement, Hao Yan and Chengde Mao for their helpful discussion, Nadrian C. Seeman and Erik Winfree for their pioneering works in DNA self-assembly and algorithmic DNA assembly, Duke SMiF and Jie Liu for providing access to SEM, TEM and AFM, Chris Dwyer and Alvin R. Lebeck for helpful discussion, Moo-Young Han, Horst Meyer, Seog H. Oh, Mary A. Creason, and Donna Ruger for their kind support, and my thesis committee members, Henry S. Greenside and Glenn S. Edwards for their helpful advice.

I would also like to thank the DNA nanotechnology group members in Department of Computer Science including Liping Feng, Sang Jung Ahn, Masahito Yamamoto (a visiting professor), Peng Yin, Hanying Li, Dage Liu, and Natalie Johnson and the Electronic Nanostructures group members in Department of Physics including Alexander Makarovski and Mathew Prior for their invaluable support and discussions. I also appreciate Myung-Sook Park, Mariko Okosi, Tae Song Lee, Serguei Vorojtsov, and Meng-Ru Li for their wonderful encouragement and friendship. Finally, I would like to

thank my parents, Dae Il Park and Sook Ja Jeon for their endless love and support. I dedicate this thesis to them with all my heart.

Contents

List of Figures

List of Tables

Chapter 1
Introduction

1.1 DNA as a Nanomaterial

In 1953, Watson and Crick reported the structure of DNA [1]. DNA is a polymer of nucleotide units where a nucleotide unit consists of a phosphate, a sugar, and a base. In DNA there are four types of bases: adenine (A), cytosine (C), guanine (G), and thymine (T). It is here that the information which is stored in the DNA molecule is found because it is the order of the bases in the polymer which ultimately determines the protein to be encoded by a particular stretch of DNA molecules [2].

What Watson and Crick noticed was that DNA consists of two polynucleotide strands, which run in opposite directions. In Figure 1.1 shows a simplified diagram of the structure of a polynucleotide. Two polynucleotide strands are wound around each other to form a double helix and make two continuous strands from one end to the other. Sticking out from this staging and pointing inwards are the bases. These bases are like the steps on a spiral staircase. Here the bases come into contact with each other and therefore each step of the staircase is actually two bases, holding ‘hands’ by way of hydrogen bonding. An A-base on one strand always hydrogen bonds to a T-base on the other strand, while a C-base always hydrogen bonds to a G-base. Therefore, once we know the sequence of the bases on one strand, we automatically know the sequence of the other strands. The two

strands are said to be complementary to each other. If a model is made of the DNA molecules, it becomes apparent that the helix has a regular pattern. The helix is ~2.0 nm across, and has two grooves running around and along it. One groove is referred to as the major groove, while the other is the minor groove. One total rotation of the molecule takes place every 3.4 nm, while the distance between the bases is about 0.34 nm. A sketch of the double-helix is shown in Figure 1.2.

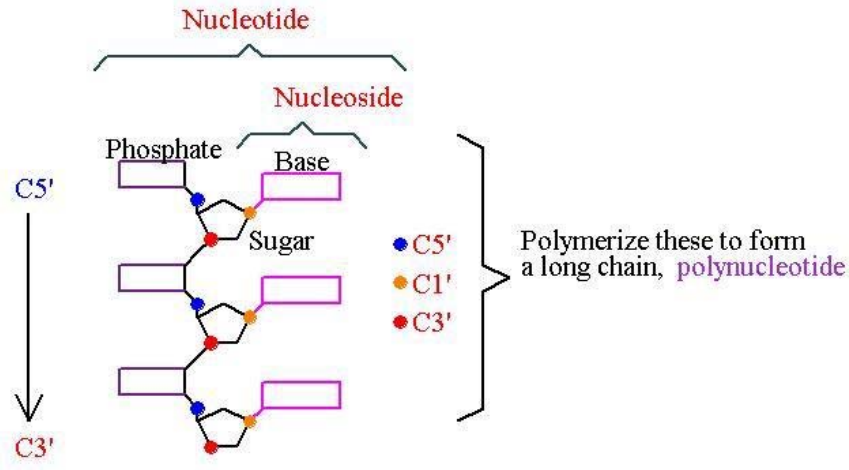

Figure 1.1: A simplified diagram of the structure of a polynucleotide. Together, a sugar and a base are collectively called a nucleoside. A nucleotide unit consists of a phosphate, a sugar, and a base.

Although it is well known as excellent molecules for storage of genetic information in biology and biochemistry, DNA has also been recognized as a useful and efficient building material in the field of nanotechnology [3-5]. DNA provides basic building blocks for constructing functionalized nanostructures with four major features:

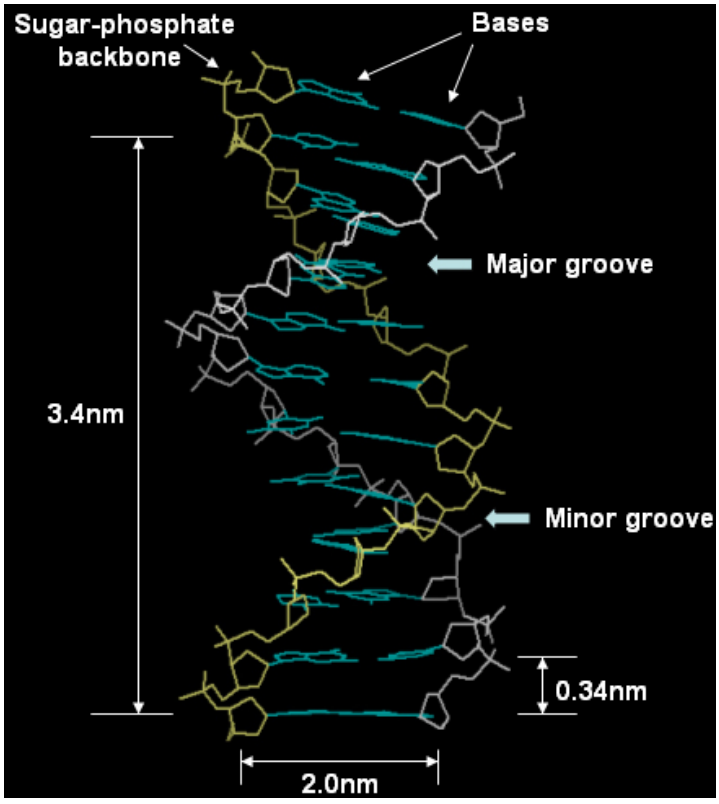

Figure 1.2: A schematic diagram of the double-helix.

molecular recognition, self-assembly, programmability, and predictable nanoscale structure. The limitations of conventional methods of top-down fabrication make bottom-up self-assembled nanostructures using DNA molecules a fascinating and attractive technique for near-term nano/bio technologies. Recently, self-assembled DNA nanostructures utilizing branched DNA tiles have been reported on (i) various artificial geometrical structures like one- and two-dimensional periodically patterned structures [6-15], and three-dimensional polyhedra [16, 17], and (ii) functionalized lattices such as mechanical devices [18-24], molecular computers [25-31], and organizing other functionalized molecules [32-34].

1.2 Overview of Thesis

This thesis documents our investigation of self-assembled DNA nanostructures and DNA templated silver nanowires. It consists of six chapters. In chapter 1, sections 1.3 and 1.4, we briefly review the properties of DNA sequence design and five distinct examples of self-assembled DNA nanostructures utilizing branched DNA tiles: (i) 1D-nanotubes, (ii) 2D periodically patterned structures, (iii) three-dimensional polyhedra, (iv) nanomechanical devices, and (v) DNA computers.

In chapter 2, we present a new type of DNA nanostructure, the three-helix bundle (3HB), which consists of three double-helical DNA domains connected by six immobile crossover junctions such that the helix axes are not coplanar. The 3HB motif presents a triangular cross-section with one helix lying in the groove formed by the other two. By differential programming of sticky-ends, 3HB tiles can be arrayed in two distinct lattice conformations: one-dimensional (1D) filaments and two-dimensional (2D) lattices. Filaments and lattices have been visualized by high-resolution tapping mode atomic force microscopy (AFM) under buffer. Their dimensions are shown to be in excellent agreement with designed structures.

Self-assembling nanostructures composed of DNA molecules offer great potential for bottom-up nanofabrication of objects and materials with smaller features than ever previously possible. Future advances in DNA-based nanotechnology depend not only on expanding the toolbox of available structures, but also on developing new structures with features useful for organizing functional molecules for diverse applications. Another new DNA motif described in chapter 3 provides such features. A cross-tile consisting of four

four-arm junctions oriented with a square aspect ratio is designed and fabricated. Programmable self-assembly of cross-tiles resulted in four distinct lattice morphologies: uniform-with nanoribbons and nanogrids made from a single unit cross-tile, and nanotracks and nanogrids using two unit cross-tiles.

Even though it has excellent intrinsic characteristics such as molecular scale recognition, self-organization, programmability and structuring properties, DNA-based nanostructure is still made of limited applications in the nanotechnology because of the lack of fixed-size controllability and full addressability. In chapter 4, we present fabrication of size-controllable and fully-addressable DNA-based nanomatrices (NM) which consist of two different cross-tiles using a novel stepwise assembly technique. The reliable and easily reproducible fixed-size DNA nanostructures as templates can lead a major step toward developing nano/bio technologies. In this chapter, we also demonstrate construction of DNA superstructures assembled step-by-step. They consist of heterogeneous DNA motifs, cross-tiles and duplex DNA molecules for controlling length and directionality of the superstructures.

Direct electrical transport measurements in DNA molecules have been considered an interesting research subject for last few decades. Even though some conductivity experiments with DNA have shown semiconducting or superconducting behavior, other studies have concluded that DNA molecules are insulators. Rather than relying on electrical transport through DNA itself, we have made use of DNA nanostructures as templates for the specific deposition of highly conductive metallic nanowires. DNA-templated functionalized nanowires represent a potential breakthrough in the self-

assembly of nanometer-scale electronic circuits because they can be targeted to connect specific locations on larger-scale structures. Until recently, mostly native λ-DNA molecules have been used as template for fabricating various metallic nanowires. In chapter 5, we present fabrication of metallic silver nanowires templated by a novel electroless deposition technique on artificially designed 1D DNA nanostructures, such as the cross-tile nanoribbons, triple-crossover nanotubes, 3HB filaments and synthetic double stranded DNA (dsDNA) nanowires, as well as native λ-DNA molecules. We characterize the electrical properties of silver nanowires at room temperature.

In Chapter 6, the final chapter of this thesis, we review the main results of our experiments and discuss the direction of future work in DNA self-assembly and DNA-based nanoelectronics: the possibility of the construction of functionalized electronic devices such as single electron transistors, spin-related devices, and quantum-dot cellular automata based on DNA as templates. Finally, detailed DNA sample preparation, two-step silver metallization procedure, and AFM imaging method under buffer are discussed in the appendix.

1.3 Properties of DNA Base Sequence Design

Oligonucleotide sequences were designed using a random hill-climbing algorithm to maximize the likelihood of formation of the desired base-pairing structures while minimizing the chances of spurious pairings [35]. The distinct feature of the sequence-symmetry minimization algorithm employed is the treatment of short sequences as ‘vocabulary elements whose repetition decreases control over the resulting secondary

structure. Even though it is laborious to predict the structure of a molecule of arbitrary sequence, Seeman at New York University found it simple to construct sequences for molecules so that they will form a desired secondary structure. The basic procedure rule is that DNA molecules will form continuous perfectly paired double-helical segments in preference to other arrangements. Given enough perfect pairs, he is able to force oligonucleotide strands to assume secondary structures that would not otherwise form

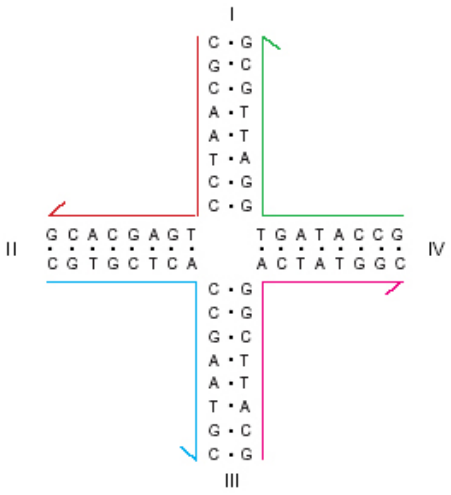

Figure 1.3: A branched DNA molecule with four arms. The four strands identified by color, combine to produce four arms, labeled with Roman numerals. The branch point of this molecule is fixed. (From Ref. [35].)

spontaneously. Here, only two hydrogen bonding schemes are defined by the classical base pairs, A-T and G-C. Therefore the author treats longer contiguous segment, i.e., trimeric, tetrameric, pentameric or hexameric sequences, as the unique 'vocabulary' elements to 64 (trimers), 256 (tetramers), 1024 (pentamers) or 4096 (hexamers), depending on the length selected. An example shown in Figure 1.3 contains four strands

designed by means of this procedure: Each strand consists of 13 overlapping tetramers. Each of the 52 tetramer elements in the four-stranded complex is unique. Therefore, sequence-symmetry has been minimized here so that no tetrameric 'vocabulary' element is ever repeated.

1.4 Examples of self-assembled DNA Nanostructures

Self-assembled DNA 1D- and 2D- nanostructures are made from various DNA motifs, for examples, double-crossover (DX) [36], triple-crossover (TX) [37], and cross-tile also known as four four-arm junctions (4 × 4) [38]. Cross-tile will be discussed in detail in

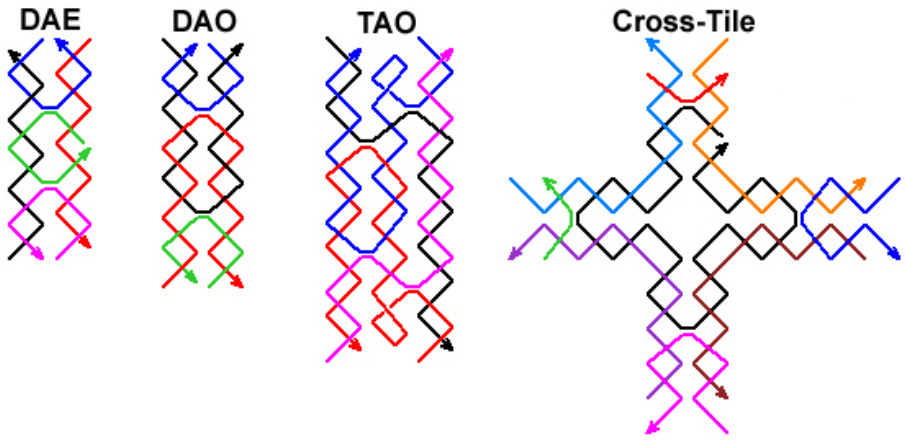

Figure 1.4: Four distinct DNA motifs for constructing complex 1D DNA nanotubes. The structures shown, DAE, DAO, and TAO are named by the acronym describing their basic characteristics. Names begin with 'D' for double-crossover, and 'T' for triple-crossover. The second character indicates the relative orientations of their two double-helical domains. Here 'A' stands for anti-parallel. The third character refers to the number of helical half-turns between crossovers, 'E' for an even number and 'O' for an odd number. A fourth tile, cross-tile, contains four four-arm DNA branched junctions pointing in four directions (north, south, east, and west in the tile plane) also know as 4 × 4 tile. Arrows indicate simplified strands running from 5' to 3'.

chapter 3. Schematic drawings of four distinct DNA motifs for constructing complex 1D- and 2D- DNA superstructures are shown in Figure 1.4. DNA superstructure morphology (tube-1D [39] versus sheet-2D) is controlled in these tiling systems by a variety of means, including lattice corrugating schemes, disulfide bridge formation, and counter ion concentration.

Recently Mitchell *et al.* demonstrated 1D DAE-O double-crossover tile nanotubes [13]. A system of DNA tiles that is designed to assemble to form 2D arrays is observed to form narotubes either with flat ring layers or with spiral layers producing a range of chiral tubes (Figure 1.5). As with the study described above, double crossover tiles (this time of the DAE-O variety) with the four single stranded sticky ends on each tile were arranged such that α and β tiles tessellate as shown in Figure 1.5b. The β tiles contained a 5' biotinylated strand to enable streptavidin binding to be used as an observable marker. Hybridization was accomplished by cooling the sample solution by a linear gradient from 96 ºC to room temperature over the course of 96 hours.

In a standard 1×TAE/Mg^{2+} buffer, containing 20 mM Tris-acetate (pH 8.3) supplemented with 12.5 mM $MgCl_2$, the tiles form ribbon structures many micrometers in length and 40 ~ 250 nm in width after hybridization (Figure 1.5e). Higher magnification reveals transverse streptavidin bands with periodicity 31 ± 2 nm (Figure 1.5f), consistent with the designed 2D array structure with the long axis of the tiles aligned along the ribbons. A natural explanation for the parallel edges of these structures is that arrays of tiles curl and close upon themselves to form tubes (Figure 1.5e). Unambiguous evidence for the formation of tubes is provided by micrographs such as Figure 1.5g in which lines

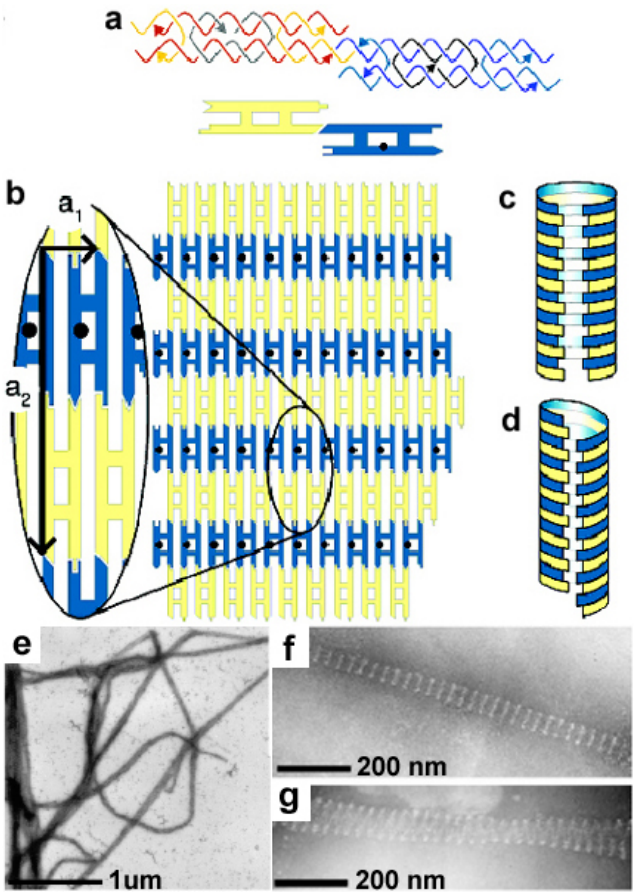

Figure 1.5: Self-assembly of DNA tiles into sheets and tubes. (a) Structure of the double crossover tiles: different colored arrows indicate simplified strands running from 5' to 3'. The 6 nucleotide (nt) single-stranded sticky ends on the α tile are complementary to those on the β tile; complementary shapes on the schematic representations of the tiles indicate complementary sticky ends. The 5' biotin label on the β tile is represented by a black dot. (b) α and β tiles tessellate to form extended two-dimensional arrays. Here 2D sheets can fold and close upon themselves to form tubes, producing either alternating rings (c) or nested helices (d) of α and β tiles. (e) through (g) Transmission electron micrographs of negatively stained DNA nanotubules and arrays. Electron transparent dots correspond to protein labels bound to the centers of β tiles. (From Ref. [13].)

of streptavidin labels zigzag across a ribbon. In all such cases the line is continuous where it changes direction at the edge of the ribbon, providing they represent helical (spiral) tubes with a structure such as that illustrated in Figure 1.5d. In buffer with higher salt concentration mixed complex morphologies (1D-tubes and 2D-sheets) were observed.

In 1998, Winfree *et al.* reported the assembly of 2-D lattices from DX tiles [9]. The DX tiles self-assemble in solution to form single-domain lattice as large as 2 μm × 8 μm, as visualized by AFM. Authors use two different DX tiles, A and B, which make a striped lattice (Figure 1.6a). By incorporating a DNA hairpin into a DX tile to serve as a marker, they have produced stripes above the surface at intervals of ~25 nm. The antiparallel DX tile consists of two juxtaposed immobile 4-arm junctions arranged so that at each junction the non-crossover strands are antiparallel to each other. The design depends on the twist of the DNA double-helix. DAO tiles have an odd number of half-turns between the crossover points, whereas DAE tiles have an even number of half-turns. Schematic diagrams of the DAO and DAE tiles used in this study are shown in Figure 1.6b. The DAO tiles consist of four strands of DNA, each of which participates in both helices. The DAE tiles consist of three strands that participate in both helices (yellow, light blue, green), and two strands that do not cross over (red, dark blue). Each corner of each DX unit has a single-stranded sticky end with a unique sequence; specific association of DX units is controlled by choosing sticky-ends with Watson–Crick complementarity.

DX units can be designed that will fit together into a 2D-lattice. Winfree *et al.* use two separate systems to implement the two-unit lattice, one consisting of two DAO units,

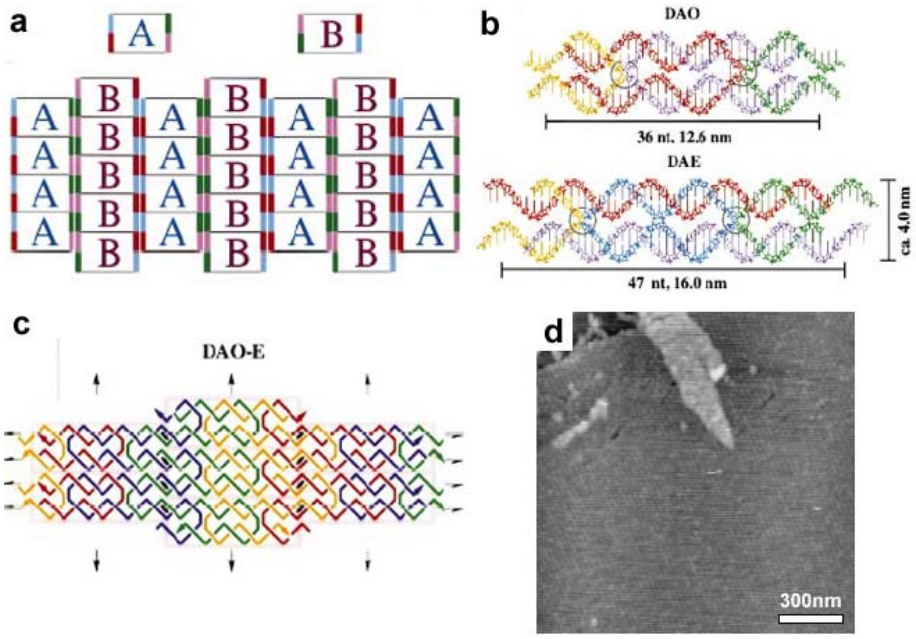

Figure 1.6: Design of DX molecular structure and arrangement into 2-D lattices. (a) A schematic drawing of 2-D lattices consisting of two units of DX molecules. Type A units have four colored edge regions, each of which match exactly one colored region of the adjacent type B units. (b) Model structures for DAO and DAE type A-units. Each component oligonucleotide is shown in a unique color. The crossover points are circled. (c) The lattice topologies produced by the DAO-E units. A unique color is chosen for each strand type which would be formed after covalent ligation of units. Black ellipses indicate dyad symmetry axes perpendicular to the plane; black arrows indicate dyad axes in the plane (full arrowhead) or screw axes (half arrowhead). (d) DAO-E AB lattice. Stripes have 25 ± 2 nm periodicity; the expected value is 25.2 nm. (From Ref. [9].)

the other consisting of two DAE units. The lattices produced by these systems are called DAO-E (Figure 1.6c) and DAE-O, respectively, to indicate the number of half-turns between crossover points on adjacent units. Covalently joining adjacent nucleotides at nicks in the lattice, by chemical or enzymatic ligation, would result in a 'woven fabric' of DNA strands. Ligation of the DAO-E design produces distinct strand types, each of which continues infinitely in the vertical direction. A- and B- units are annealed separately, then combined and annealed together to form AB-lattices. The resulting

solution is deposited on a mica substrate, and then imaged under isopropanol by contact mode AFM. The self-assembling AB-lattice can serve as scaffolding for other molecular structures. Here B tile have been decorated with two DNA hairpin sequences inserted into its component strands. Then, the vertical columns of the lattice become dramatically apparent as stripes in AFM images, further confirming the proper self-assembly of the 2-D lattices. Figure 1.6d shows an AFM image: the spacing of the decorated columns is 25 ± 2 nm for the DAO-E lattice, indicating that every other column is decorated, in accord with the design.

Shih *et al.* reports the design and construction of 3D-octahedron which consists of seven paranemic-crossover (PX) [8] tiles and five DX tiles, joined at six four-way junctions (Figure 1.7a) [17]. PX and DX tiles have been designed as pairs of double-helices that are arranged in a side-by-side scheme. Each of the twelve tiles of the octahedron contributes one double-helix to a 'core' layer and the other to a concentric 'peripheral' layer. The four-way junctions connect only the 'core' layer double-helices. Each four-way junction displays on its concave face the minor grooves of its four proximally surrounding base pairs. All four strands at all six junctions contain two unpaired thymidine residues at the crossover point to allow some flexibility for assembly.

The 'core' layer double-helix of each of the twelve tiles contains 40 base pairs, corresponding to approximately four full turns of DNA molecules and a length of about 14 nm. For eleven of the tiles, the 'peripheral' layer double-helix contains 30 or 32 base pairs and is capped at both helical ends by a hairpin loop of four thymidine residues. The twelfth tile is slightly longer, containing 35 base pairs, and is capped at only one end. DX

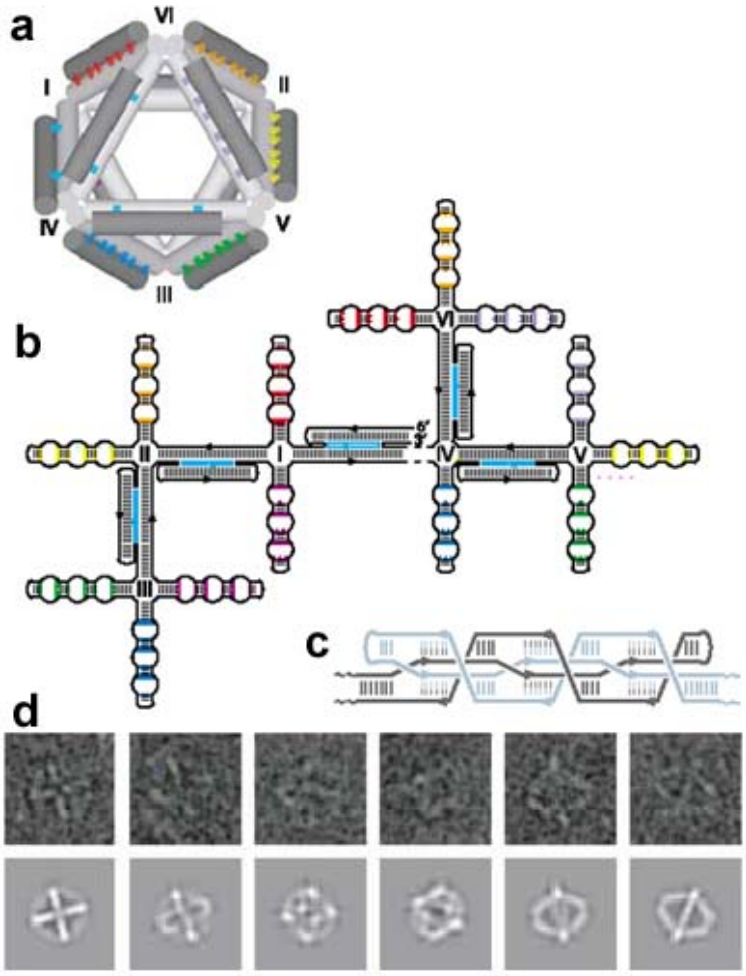

Figure 1.7: Design and data of the DNA-octahedron. (a) Three-dimensional structure involving twelve tiles (octahedron edges) connected by six flexible joints (octahedron vertices). Five of the tiles are DX (cyan) and seven are PX tiles (rainbow colors). The joints are four-way junctions that connect the 'core' layer double-helices of each tile. (b) Secondary structure of the branched-tree folding intermediate. The structure consists of a single heavy chain (black) and five unique light chains (cyan). Like colors indicate half-PX loops whose sequence-specific cross-association generates a tile that serves as an edge of the DNA-octahedron. Colored stripes coincide with strand crossover positions. Folding to the structure in the upper left is complete when all seven PX tiles have formed. (c) Schematic of a PX tile. (d) Raw images of individual octahedrons and corresponding projections of the three-dimensional map. (From Ref. [17].)

tiles have been shown to be about twice as rigid as standard duplex DNA molecules. Assuming that PX tiles have similar rigidity, each of the tiles would be expected to have a stiffness corresponding to a rod that is roughly one-eighth of a persistence length. Thus the self-assembled DNA-octahedron is expected to be a highly rigid object. The DNA-octahedron was tested using cryo-electron microscopy. Figure 1.7d shows representative cryo-electron micrographs of individual octahedrons and corresponding projections of the computer generated three-dimensional map.

Controlled mechanical movement in molecular scale devices is one of the key goals of nanotechnology. DNA is an excellent candidate for the construction of such devices due to the specificity of base pairing and its robust physicochemical properties. Herein we have reported the construction of a robust sequence dependent DNA device, which we call a nanoactuator, and the incorporation of such a device into a 2D parallelogram DNA lattice. Figure 1.8 illustrates the design and the operation of the nanoactuator device. The two states of the device are shown as S1 and S2. S1 consists of four strands assembled through Watson–Crick base pairing to form a bulged three arm DNA branch-junction. A DNA device based on a bulged three-arm junction is an excellent candidate to serve as actuator for DNA lattices. The stem-loop joining the two strands of the duplex contains 21 nucleotides and is composed of a loop of two deoxythymidine nucleotides, a seven-base-pair duplex region (contains two mismatched pairs), and a loop of five deoxythymidine nucleotides. In Figure 1.8, the strand in red is a set strand (SS1) that sets the nanoactuator device in the S1 state. S2 consists of the same three black strands as in S1, but a blue strand (SS2), which has a region fully

complementary to the stem-loop sequence, replaces the red strand. SS2 serves to open up the stem-loop in S1 and set the conformation of the nanoactuator device to the S2 state. The mismatched base pairs (in pink) are included in the stem-loop of S1 to avoid the formation of an unwanted kinetically trapped cruciform junction, a possible secondary structure to the S2 state of the nanoactuator device.

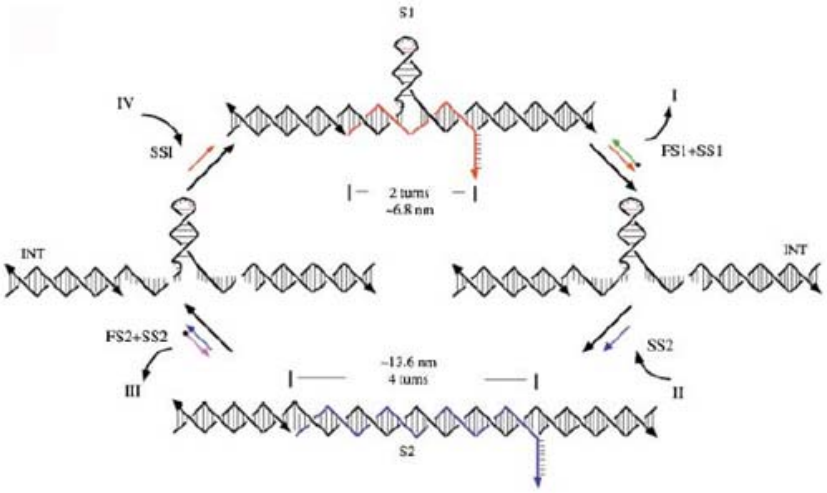

Figure 1.8: Schematic drawing of the design and operation of the nanoactuator device. I-IV represents the four steps to complete one cycle of the device operation.

To realize potential applications of the DNA nanoactuator device constructed here, the device must be integrated into nanorobotics or patterned arrays so that a functional network of nanoactuator devices can be built. We demonstrated a major step toward this goal by implementing the device constructed here into a 2D DNA lattice, and the state of the lattice can be actuated through the operation of this device. Figure 1.9 illustrates the design of such a structure. The nanoactuator device is incorporated into a 2D DNA lattice constructed previously by Mao *et al.* [10], which was demonstrated to display a rhombus-

like cavity with the size of ~14 nm in each of the two dimensions. The unit of the previously demonstrated parallelogram contains four four-arm branched junctions (Figure 1.9a), which were fused into a rhombus-like molecule. The branch points, which define vertices, are each separated by four double-helical turns. The rhombuses were directed to self-assemble by hydrogen bonding into a 2D periodic array, whose spacing is six turns in each direction. In our design, we modified the molecule and incorporated two nanoactuator devices into two opposite edges of the unit (Figure 1.9b). The operation of the nanoactuator devices will result in a contraction/extension motion of the 2D lattice assembled from the designed unit, as illustrated in lower panel of Figure 1.9b.

We performed the interconversion of the nanoactuator device in solution and demonstrated the motion of the lattice by imaging samples deposited on mica using AFM. The AFM images in Figure 1.9c illustrate the change of the DNA lattices upon the operation of the nanoactuator device. In the upper panel of Figure 1.9c, the three AFM images demonstrate the switching of the nanoactuator device from S1 to the intermediate state and then to S2. A change in the size of the cavity in the lattice was observed after the operation was complete. The dimensions of each rhombus cavity in the lattice change from ~14 nm × 14 nm to ~14 nm × 20 nm after the operation, which is consistent with the parameters in the design. The three images in lower panel of Figure 1.9c show the switching of the nanoactuator device from S2 to the intermediate state and then to S1. The dimensions of each rhombus cavity change from ~14 nm × 20 nm to ~14 nm × 14 nm. These clearly confirm that the operation of the nanoactuator devices results in a contraction and extension of the lattice. Thus, the DNA nanoactuator device is

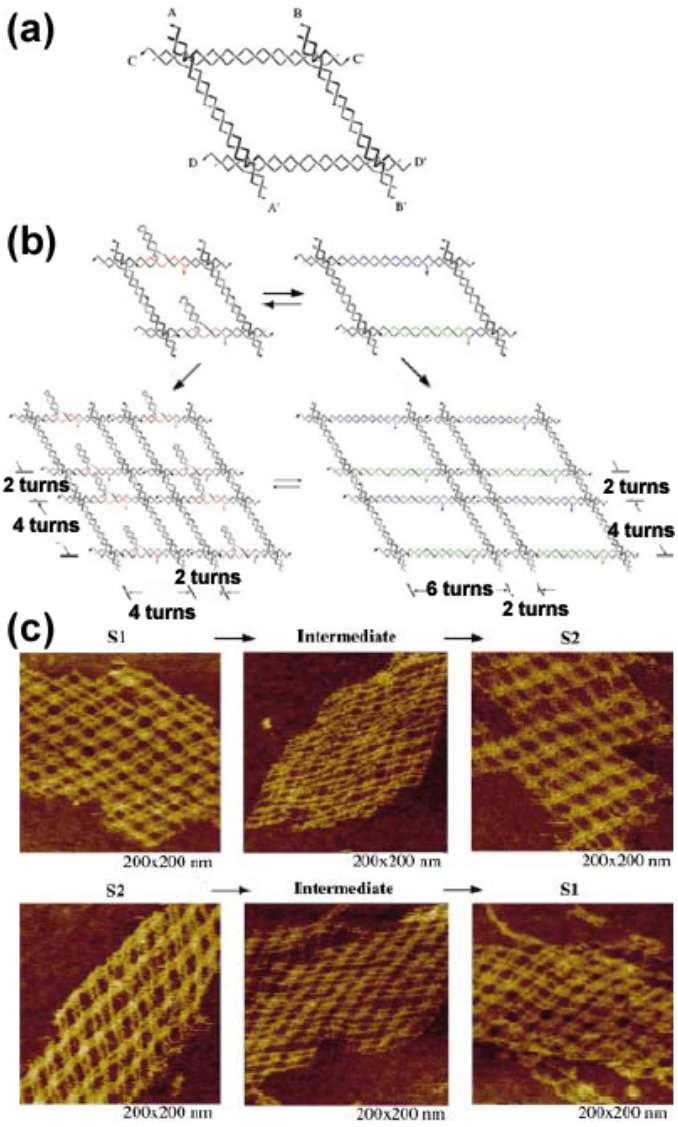

Figure 1.9: (a) Schematic drawing of the two-state 2D lattices actuated by DNA nanoactuator devices. A unit for self-assembly of parallelogram lattice containing complementary sticky ends, for example, A and A', which self-assemble into a 2D lattice. (b) Incorporation of DNA nanoactuator devices into 2D lattice. Two nanoactuator devices with different base sequences are incorporated into the opposite arms of the rhombus-like motif. The two states of these nanoactuator devices result in two different lattice components. Sticky-ended association leads to 2D lattices. Periodicity of the lattice is illustrated by their helical turns. (c) AFM evidence for the two state DNA lattice actuated by DNA nanoactuator devices.

functioning in a 2D lattice powered by DNA fuel strands. The AFM images of the intermediate state shown in Figure 1.9c demonstrate that the lattices in the intermediate state are not as regular as those in the S1 and S2 states. However, the lattice in the intermediate state does not fall apart during the transition of the device, which strongly suggests the robustness of the lattice during the operation of the nanoactuator devices.

The last example in this section of functionalized self-assembled DNA-based nanotechnology is the field of DNA-based computers proposed by Adleman in 1994 [25]. He used DNA to solve a variant path of the 'traveling salesman' problem. The idea is to establish whether there is a path between two cities, given an incomplete set of available roads. The author used DNA strands to represent cities and roads, and encoded the sequences so that a strand representing a road would connect (based on DNA base pairing) to any two strands representing a city. By mixing together the strands, joining the cities connected by roads, and weeding out any 'wrong answers', he showed that the strands could self-assemble to solve the problem [3].

The first connection between DNA-based computation and DNA-based nanotechnology was demonstrated by Winfree [26]. He proposed that short branched DNA molecules could be programmed to undergo algorithmic self-assembly and thus serve as the basis of computation. Figure 1.10 shows a schematic diagram of a binary counter. The goal is to count 1, 2, 3, 4, …, but in base 2, where it would be 1, 10, 11, 100, …, with subsequent numbers written above the previous ones. Shapes on the tiles represent information used in the computation: the top and bottom sides encode the value of bits in the counter, while the left and right sides are use to carry the rollover bit. The

seed tile, S, triggers the computation, and the two boundary tiles (bottom and right) provide initial conditions. The bottom boundary tile produces a series of rounded tops, encoding the initial counter bits. The boundary tiles on the right produce a series of 'commands' to increment the rightmost bit in every row. The four rule-tiles can then be seen to effect the following rule: if there is no rollover from the bit on the right, this bit stays the same; but if there is a rollover from the bit on the right, 0 becomes 1, and 1 rolls

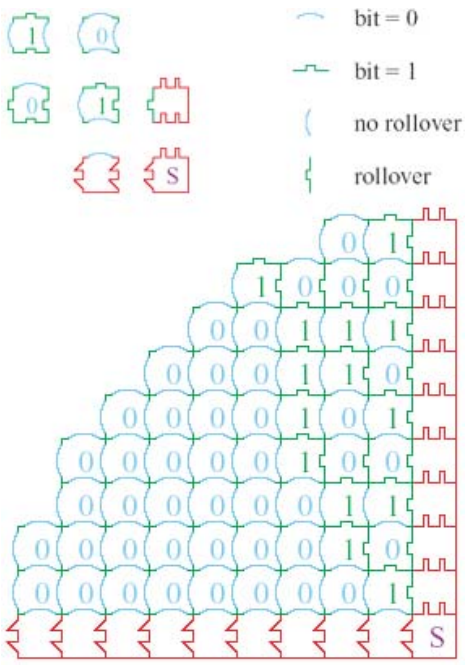

Figure 1.10: A system of 3 input tiles and 4 rule tiles that form an aperiodic tiling. The rows in the tiling are the consecutive integers, represented in binary. (From Ref. [26].)

over to 0. It is important to know that there are two new ingredients in this example. First, to ensure that the correct pattern results; the three input-tiles are assembled before the rule-tiles are used. Second, to avoid getting stuck with an incorrect partial tiling; one

must add rule tiles only when both the tiles below and to their right are already present. This condition also prevents the formation of tilings in the absence of the input assembly, such as an infinite periodic lattice containing only the 'all-0' tile.

1.5 Summary

DNA, known as the predominant chemical for duplication and storage of genetic information in biology, has also been shown to be highly useful as a nanomaterial for construction of micron-scale objects with nanometer-scale feature resolution. A variety of unusual DNA motifs whose designs are based on the immobile DNA branched-junction, a stable analogue of the Holliday intermediate from genetic recombination, have been used for self-assembly of periodic arrays. 1D- and 2D- DNA complexes formed by tiling self-assembly have shown the promise of this approach in directing the formation of highly structured materials with specific nanoscale features. Functionalized 'working' lattices such as mechanical devices and biomolecular computers can be made by programmable DNA nanostructures as well.

Chapter 2
Three-Helix Bundle

Widely known for storage of genetic information in biology, DNA has also been recognized as a useful building material in the field of nanotechnology. The limitations of conventional methods of top-down fabrication make bottom-up self-assembled nanostructures using DNA molecules an attractive technique for near-term nano/bio technologies. Here, we present a DNA nanostructure, the three-helix bundle (3HB), which consists of three double helical DNA domains connected by six immobile crossover junctions such that the helix axes are not coplanar. The 3HB motif presents a triangular cross-section with one helix lying in the groove formed by the other two. By differential programming of sticky-ends, 3HB tiles can be arrayed in two distinct lattice conformations: one-dimensional filaments and two-dimensional lattices. Filaments and lattices have been visualized by high-resolution, tapping mode atomic force microscopy (AFM) under buffer. Their dimensions are shown to be in excellent agreement with designed structures.

2.1 Design and Characteristics of 1D- and 2D- 3HB

A newly conceived motif, the 3HB consists of three double helical DNA domains joined in cyclic fashion at six strand-exchange points, with two crossover junctions between

each pair of helices. Using DNA's inherent programmability, molecular recognition, and self-assembly characteristics, we have designed and constructed simple but unique DNA nanostructures: 1D-3HB tiles for formation of one-dimensional chains or filaments of tiles and 2D-3HB for assembly of two dimensional tile lattices. A 1D-3HB tile consists of nine different oligos which, when hybridized by slow annealing, form a bundle with three duplex domains connected by six immobile crossover junctions. Neighboring crossover points involve opposite strands of DNA, therefore dihedral angles between crossovers are calculated to be 60°, since the minor groove gives us -146°, and then six base-spacings of 34.3°, each gives +206°, for a rotation around the helix axis of -146° + 6(34.3°) = 60°. A schematic diagram of the strand trace and a cartoon of the self-assembled 1D filament are shown in Figure 2.1a and 2.1b. The unit length of a 1D-3HB tile is ~17.0 nm, which corresponds to five full turns of the helices (52 base pairs). The complementary sticky-ends of a, b, and c are a', b', and c', thus 1D-3HB tiles hybridize into a single layer linear array, forming 1D filaments as shown.

2D-3HB tiles also consist of nine strands, but have only 4.5 full turns of double-helix (47 base pairs), for a unit length of ~15.3 nm. A schematic diagram of a tile and a cartoon of self-assembled 2D lattice are shown in Figure 2.1c and 2.1d. Figure 2.1e is a front view of an atomic-scale model of the 3HB tile looking down the helix axis. The odd number of helical half-turns in 2D-3HB tiles provides alternate facings of adjacent tiles (as shown in Figure 2.1d) in the east-west direction in the lattice plane, giving the 2D array a so-called corrugated design. We intentionally removed the sticky ends of the out-of-plane helix domains (yellow cylinders in Figure 2.1c) and matched the complementary

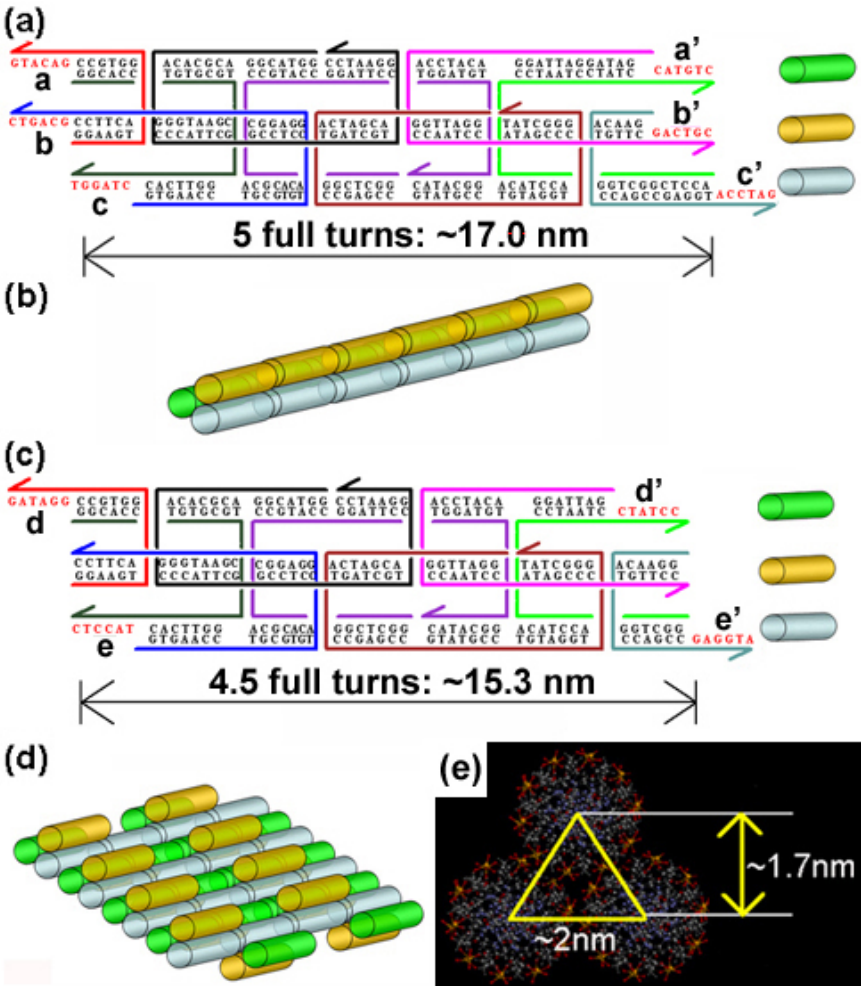

Figure 2.1: Schematic drawings of self-assembled 1D- and 2D- 3HBs. (a) 1D-3HB has nine different oligonucleotides which form 3-helix bundles with six crossovers. Different color-coded arrows indicate simplified strands running from 5' to 3'. Unit length of 1D-3HB is ~17 nm. Here, the complementary sticky-ends of a, b, and c are a', b', and c' respectively. Identification of the three helices in the strand trace diagram with the helices of the simple tube cartoons are given by the color coded tubes to the right. (b) A cartoon of filaments formed from 1D-3HB tiles. (c) 2D-3HB also consists of nine different strands but is 4.5 full turns, ~15.3 nm. The odd number of helical half-turns causes neighboring tiles to face alternating directions in the lattice plane. The complementary sticky-ends of d and e are d' and e', respectively. (d) A cartoon of 2D-3HB lattice. (e) Front view of an atomic scale model of a 3HB tile. Because the diameter of double-stranded DNA is ~2 nm, the height distance between centers of the lower duplexes and the upper is ~1.7 nm.

sequences of the other two as shown in Figure 2.1c. This slight reprogramming of the DNA molecules changes the resulting superstructure morphology dramatically from uniform 1D filaments to 2D lattices with upward- and downward- facing stripes.

Formation of single species with expected molecular weights and designed strand stoichiometry was demonstrated using gel electrophoresis of 3HB tiles without appended sticky-ends (Figure 2.2). Thermal stability was also demonstrated; melting curves show a cooperative unfolding with a T_m of ~57 °C (Figure 2.3).

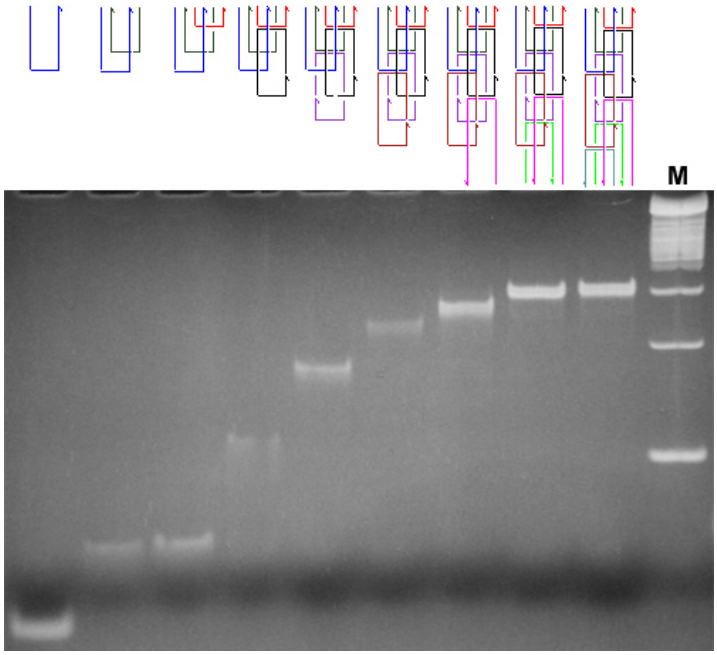

Figure 2.2: Characterization of the 3HB tile structure using non-denaturing electrophoresis. A 10% polyacrylamide gel (ethidium bromide stained) showing association complexes between various equimolar combinations of the 3HB DNA complex component strands. Equimolar mixtures at 1 μM concentration per included strand were annealed and run on the gel at room temperature. Strands included in the annealings are indicated in the drawing above each lane. The last lane contains 50 bp DNA ladder size markers (M).

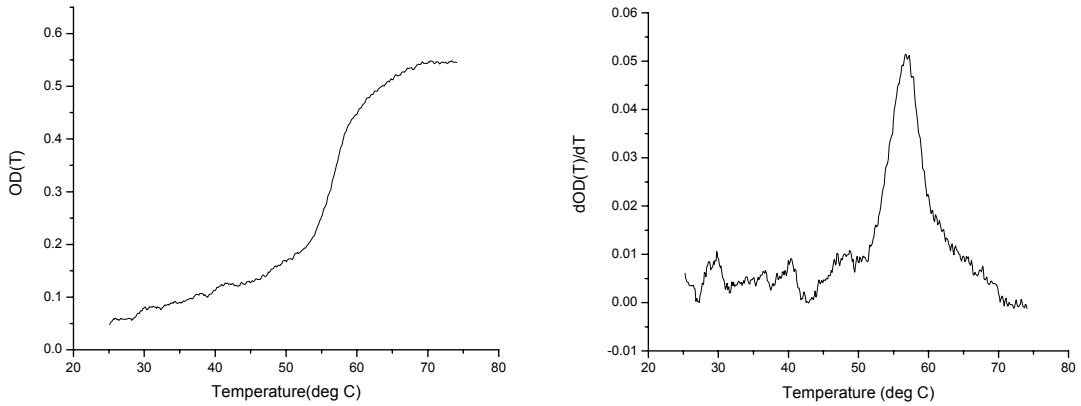

Figure 2.3: Melting behavior of 3HB tile without sticky-ends. The optical density at 260 nm as a function of temperature (left panel). The derivative of the melting data shows several different melting domains with the most significant overall transition at around 57 °C (right panel).

2.2 Results and Discussion of 1D- and 2D- 3HB

The DNA nanostructures have been visualized by atomic force microscopy, which provides high-resolution imaging (down to ~2 nm). Figure 2.4a and 2.4b show AFM images of 1D filaments with scan sizes 1 μm × 1μm and 300 nm × 300 nm, respectively. AFM images were taken using tapping mode under physiological buffer as described in the appendix A. The images show many individual filaments crowded together on the mica surface. Filaments have measured heights of 1.8 ± 0.2 nm, and their lengths vary from a few hundred nanometers to a few microns (tens to hundreds of tiles). In high-resolution AFM images of filaments (Figure 2.4b), we clearly see individual 1D-3HB tiles (circled in blue) with a length of ~16.5 nm, in good agreement with the original design of ~17.0 nm. Height measurements of the filaments can be shown in Figure 2.4d.

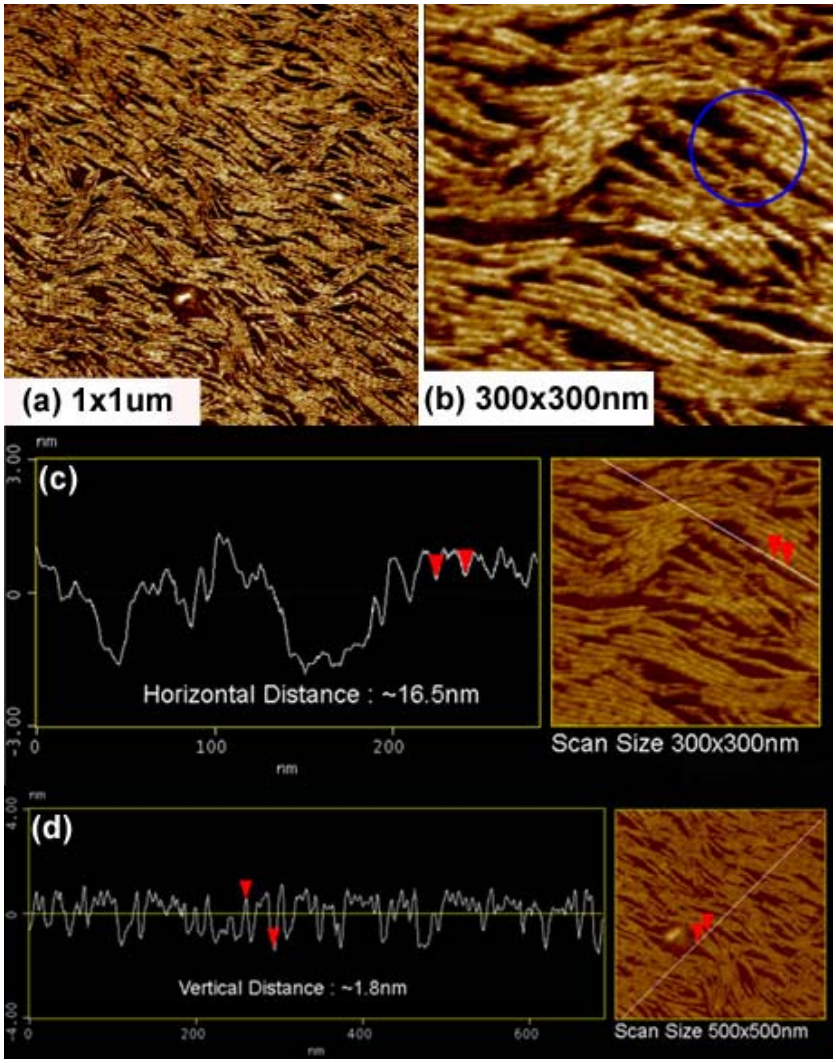

Figure 2.4: (a) AFM images of 1D-3HB filaments. Height of individual filaments is 2.0 ± 0.2 nm, and length varies from a few hundreds nanometers to a few microns. (b) High-resolution AFM image of the filaments with 300 nm × 300 nm scan size. Individual unit-tiles can be seen clearly (circled in blue). (c) Section profiles from AFM images of the 1D filaments. After formation, we observe horizontal lengths for the unit 1D-3HB tile at about 16.5 nm, in good agreement with the designed structure, ~17.0 nm. (b) Vertical distance (height) of the 1D-3HB filaments is 1.8 ± 0.2 nm.

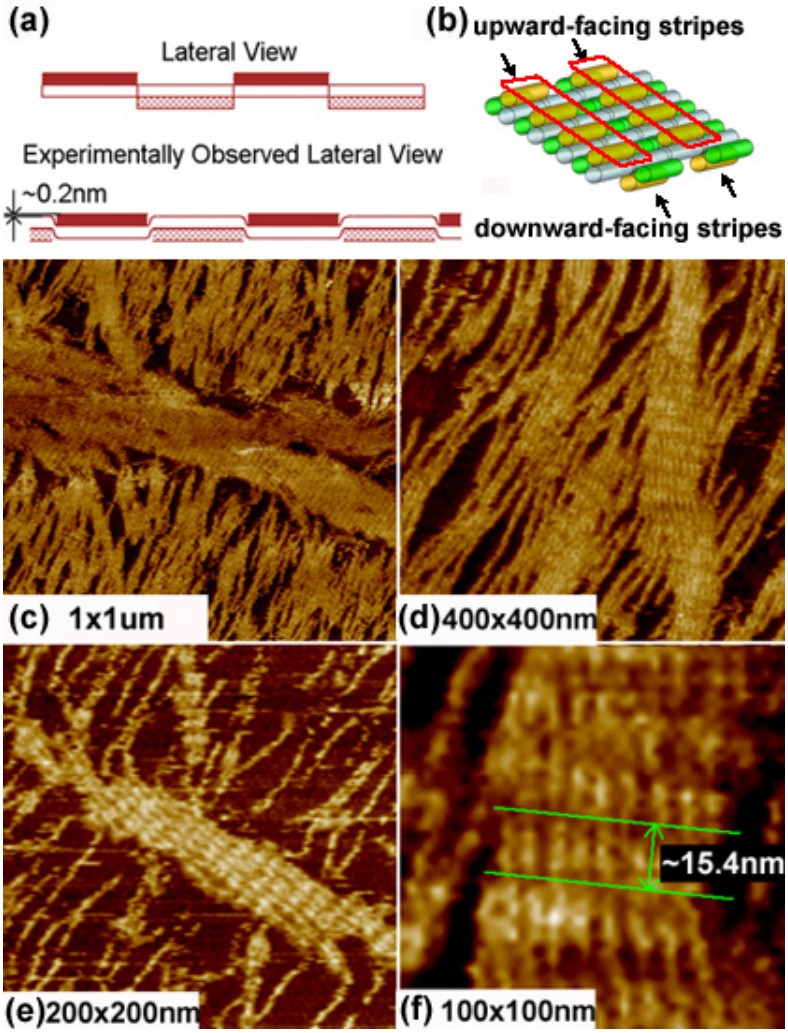

Figure 2.5: (a) Schematic diagrams of a 2D-3HB lattice rigid model lateral view (top) and a lateral view of a more flexible model closer to the experimental observations (bottom). (b) Cartoon of lattices with upward- and downward-facing stripes highlighted. (c-f) AFM images of the 2D-3HB lattices. Scan size of images are (c) 1 μm × 1 μm, (d) 400 nm × 400 nm, (e) 200 nm × 200 nm, and (f) 100 nm × 100 nm. 2D-3HB tiles are clearly visible and the average length of the tiles is ~15.4 nm.

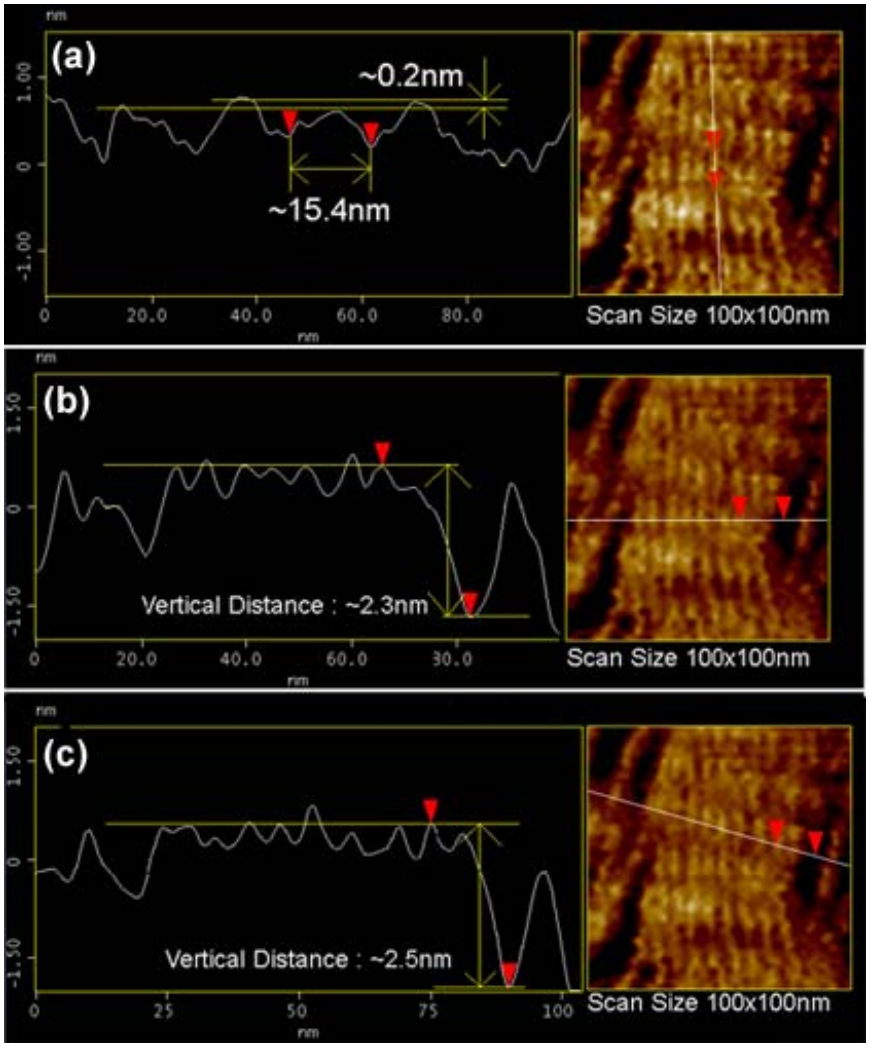

Figure 2.6: (a) ~ (c) Section profile of AFM images of 2D-3HB lattices. Tile heights are ~2.5 nm for upward-facing stripes and ~2.3 nm for downward-facing. Thus, the height difference between alternating stripes is ~0.2 nm, with upward-facing stripes slightly lower. The horizontal unit distance is ~15.4 nm matching the designed distance of ~15.3 nm.

A schematic diagram of 2D-3HB lattice shown as a rigid model in lateral view is given in Figure 2.5a (top). Experimentally we observed a more flexible lattice with upward-facing stripes sagging slightly lower to the substrate as shown in Figure 2.5a (bottom). The height of upward-facing stripes is ~2.5 nm and that of downward-facing

stripes is 2.3 nm, measured from the mica surface. Thus the experimentally determined height difference between alternating stripes is ~0.2 nm. Height analysis AFM images are given in Figure 2.6. The cartoon in Figure 2.5b highlights the different stripes observed on the lattices. Figures 2.5c through 2.5f show high-resolution AFM images of 2D lattices. From these AFM images, 2D-3HB tiles and stripes are clearly visible; the average length of the tiles is ~15.4 nm, in excellent agreement with the designed distance of ~15.3 nm.

2.3 Summary

We have designed and constructed novel DNA nanostructures, 1D- and 2D- three-helix bundle tiles that self-assemble into filaments and lattices. Uniform-width filaments can serve as templates for highly conductive metallic nanowires which we will discuss in chapter 5. Theoretically, they can also be used as templates for other materials such as semiconducting, superconducting, or magnetic nanowires, for a variety of applications in future electronic devices. We have also presented 2D lattices using slightly modified 3HB tiles. Unit tiles of 2D-3HB have an odd number of helical half turns (4.5 full helical turns), and therefore present alternating stripes with the extra helix either above or below the lattice plane. With tile sets containing greater numbers of sticky-ends, 2D-3HB lattices could serve as addressable templates for protein or metallic nanoparticle period arrays for use in molecular machines or quantum-dot cellular automata.

Chapter 3
Cross-Tile

Self-assembling nanostructures composed of DNA molecules offer great potential for bottom-up nanofabrication of objects and materials with smaller features than ever previously possible. Future advances in DNA-based nanotechnology depends not only on expanding the toolbox of available structures, but also on developing new structures with features useful for organizing functional molecules for diverse applications. A new DNA motif described here provides such features. Cross-tile consisting of four four-arm junctions oriented with a square aspect ratio was designed and constructed. Programmable self-assembly of cross tiles resulted in four distinct lattice morphologies: uniform-with nanoribbons and nanogrids made from a single unit cross-tile, and nanotracks and nanogrids using two unit cross-tiles.

3.1 Design and Characteristics of Cross-Tile

The cross-DNA motif shown in Figure 3.1a contains four four-arm DNA branched-junctions pointing in four directions (North, South, East, and West in the tile plane). This structure contains nine strands, with one strand (shown in cyan) going through every junction. There is a bulged T_4 loop at each of the four corners inside the tile cavity. These

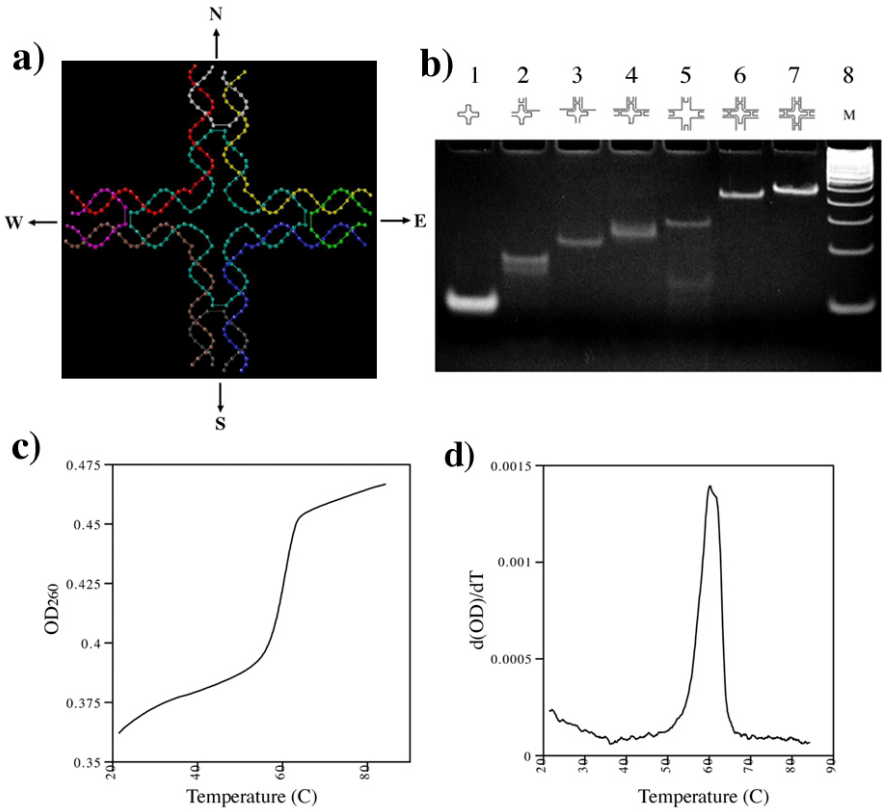

Figure 3.1: (a) Cross-DNA tile strand structure. Unit cross-tile is oriented in each direction (north, south, east, and west). The cyan strand participates in all four junctions and contains T_4 loops connecting adjacent junctions. (b) Non-denaturing electrophoresis of the cross-tile. An 8% polyacrylamide gel (ethidium bromide stained) showing association complexes between various equimolar combinations of the cross-tile component strands. Equimolar mixtures at 1 μM concentration per included strand were annealed and electrophoreses at room temperature. Strands included in the annealing are indicated in the drawings above each lane. The right-most lane contains 50 bp linear marker. (c) Thermal transition profiles. The relative change in optical density at 260 nm as a function of temperature. (d) The differential melting behavior of the cross-tile.

bulged loops were designed to avoid stacking between adjacent four-arm junctions and should cause the arms to point to four different directions.

We have characterized the formation of the structure using non-denaturing gel electrophoresis and thermal transition analysis. Formation of specific molecular weight complexes by annealing stoichiometric mixtures of all nine and various subsets of the nine oligonucleotides is shown in Figure 3.1b; lane 7 corresponds to the 1:1 ratio combination of all nine oligos. This complex moves slower and has the highest molecular weight compared to the other oligo combinations. The cross-tile complex runs as a single band on non-denaturing gels, without any higher molecular weight (unexpected base pairs between two or more complexes) and lower molecular weight byproducts (dissociated complex), indicating the cross-tile is a stable structure in the chosen buffer. Melting curves of DNA complexes provide a measure of stability and cooperativity of internal interactions indicated, respectively, by the temperature at the transition midpoint and the width or range of the transition. Figure 3.1c illustrates the thermal transition profile of the cross-tile. Figure 3.1d shows these same data in differential form. The results show that the cross-tile complex melts cooperatively, as a single transition, with T_m = 60 °C.

3.2 1D Nanoribbon Using a Single Unit Cross-Tile

Based on the structure shown in Fig. 3.1a, two other versions of the cross-tile were prepared using a single unit cross-tile by designing sticky-ends which led us to self-assemble and visualize two different types of lattice morphologies using the same tile

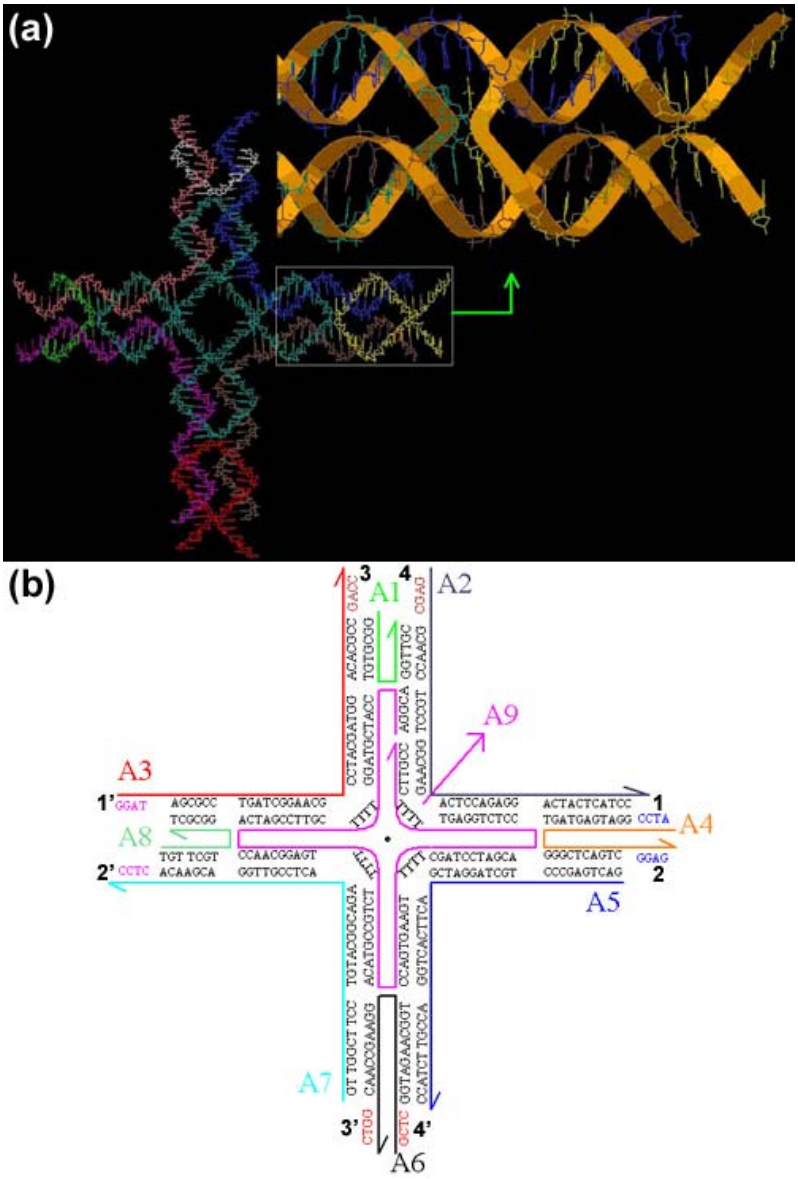

Figure 3.2: (a) An atomic-scale unit cross-tile with the zoom-in view of four-arm junction. (b) The 1D nanoribbon unit cross-tile's strand structure and sequences. The complementary sticky-ends of *1*, *2*, *3*, and *4* are *1'*, *2'*, *3'*, and *4'*, respectively.

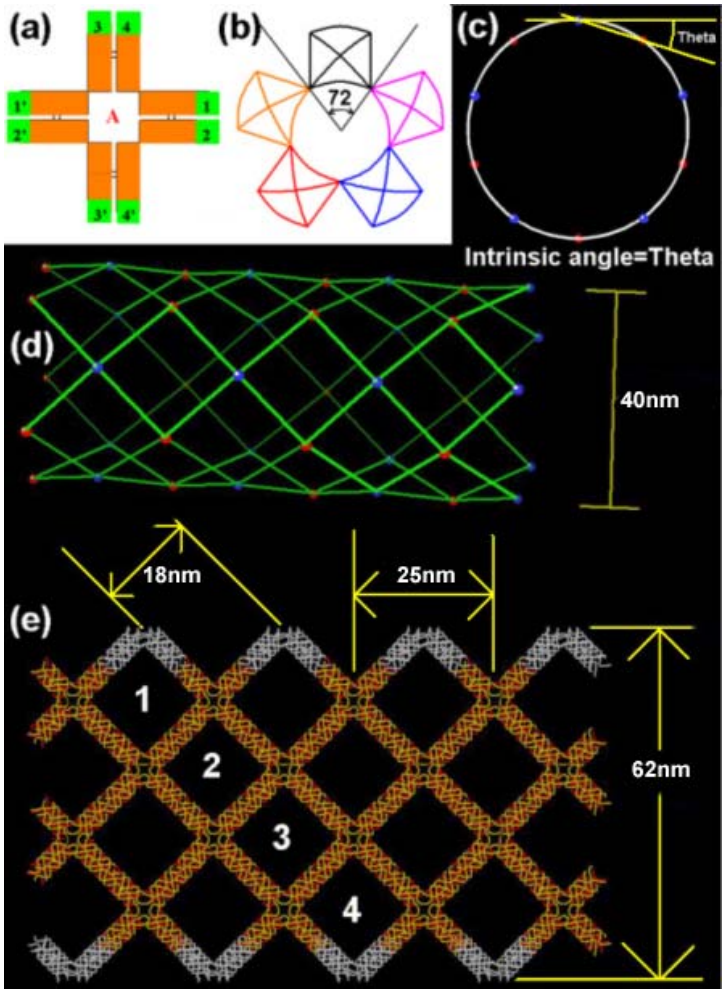

Figure 3.3: (a) Schematic diagram of the unit cross-tile of the nanoribbon. Here, the sticky-end *1* complements with *1'*, *2* to *2'* etc. (b) An example of front-view of the 1D nanoribbon. (c) End-on view of a tube showing 5 cross tiles in the terminal ring. From this model we can calculate an intrinsic angle of ~36 degrees. (d) A model of the nanoribbon structure. Side-view of a proposed tube structure where each dot represents the center of a cross-tile (blue and red dots are on separate ring layers). (c) Overhead-view of a tube squashed onto the surface of the substrate and forming a ribbon with four diagonal square cavities and ~63 nm width. Note the saw-tooth edge formed by folding one row of cross tiles along a diagonal running through their most flexible region, the TTTT loops between adjacent arms. The jagged edges along with the 45 degree diagonal containing four cavities are typically observed in high resolution AFM images of the ribbons.

structure by only slightly reprogramming the sticky-end association. In this system, we can control the preferred lattice formation by varying the assembly strategy and strand design of the cross-tile nanostructure. Both designs resulted in lattices containing periodic square cavities. Interestingly, one strategy (the original design) produced a high preponderance of uniform-width ribbon structures (see Figure 3.3). In this design the distance between adjacent tiles is an even number of helical half-turns (four full turns) so that the identical face of each tile points toward the same lattice face. Figure 3.4 shows four AFM images of the nanostructures formed from the original design. Self-assembly of the original design resulted in long (~5um in average) ribbon-like lattice with uniform-width depending on the number of diagonal square holes in the nanoribbons (see Figure 3.3e and Table 3.1).

Number of diagonal square	Diameter (D) : nm	Width (W) : nm	Intrinsic Angle (θ) : Degree
4	40	62	36
5	48	76	30
6	57	89	26

Table 3.1: Based on the number of diagonal square holes, we can estimate each ribbon's diameter, width, and intrinsic tile curvature.

The regularity of the periodic cavities is striking, as well as the observation that some of the nanoribbons revealed a single layer flat grid lattice unrolled at the open end of the ribbon (Figure 3.4d). This observation strongly suggests that the ribbon structure results from tube-like structures which flatten when the sample is deposited onto mica. An AFM image height profile in Figure 3.5 clearly shows that the nanoribbon structure

has two layers compared to the flat lattice. Also the edges of the ribbon appear slightly higher (~0.12 nm) than the middle, indicating a finite radius of curvature for the squashed tube structure. The formation of tube-like lattices could be due to the fact that each component tile is oriented in the same direction in the designed lattice planes, therefore any incidental curvature resident in each tile could accumulate and cause circularization of the lattice. This hypothesis is tested and supported by the corrugated design described in Section 3.3.

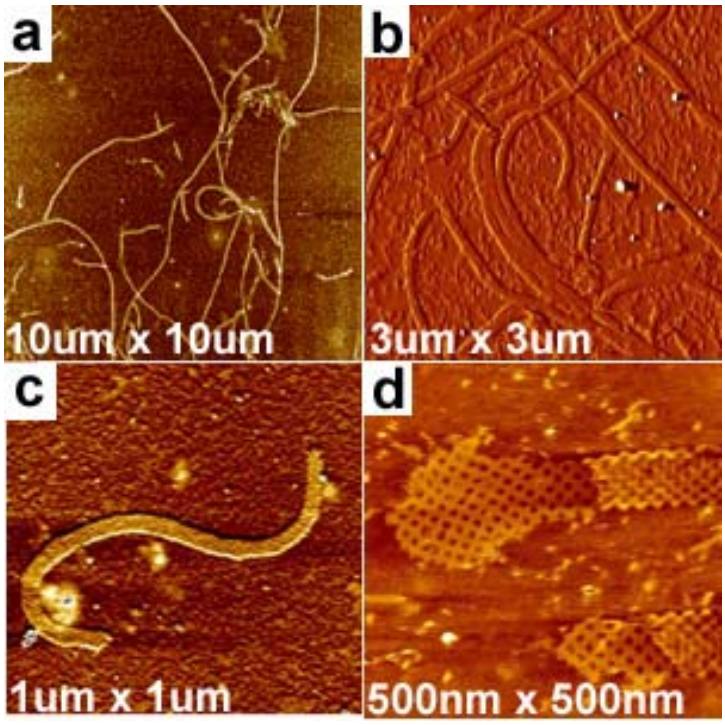

Figure 3.4: (a) through (d) are AFM images of uniform-width nanoribbons with various scan sizes.

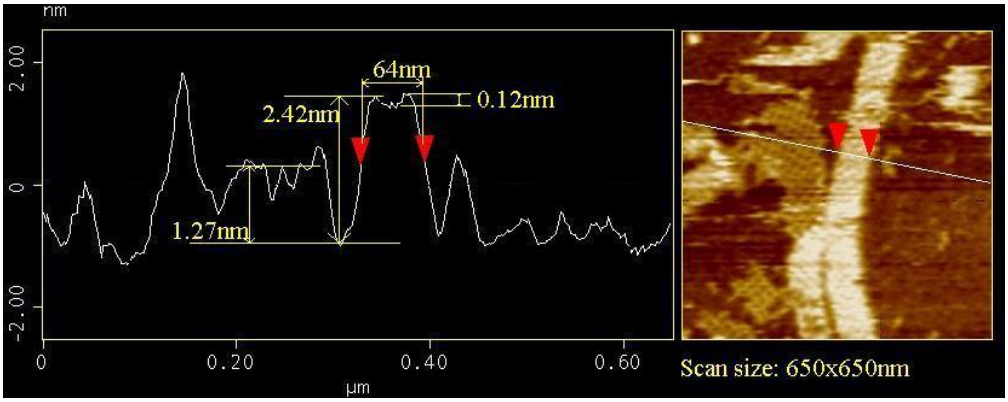

Figure 3.5: A cross-section height profile analysis of an AFM image which contains nanoribbon and single-layered flat lattice. The AFM image clearly shows that the nanoribbon structure has two layers compared to the flat lattice. Also the edges of the ribbon appear slightly higher (~0.12 nm) than the middle, indicating a finite radius of curvature for the squashed tube structure.

3.3 2D Nanogrid Using a Single Unit Cross-Tile

This is a second design strategy aimed at eliminating the lattice curvature and producing larger pieces of flat nanogrid with square aspect ratio. This strategy, referred to as the corrugated design, causes adjacent tiles to associate with one another such that the same face of each tile is oriented up and down alternately in neighboring tiles, therefore the surface curvature inherent in each tile should be canceled-out within the assembly. A schematic drawing of the unit corrugated cross-tile is shown in Figure 3.6a with sticky-ends association. Figure 3.6b gives an AFM image showing the self-assembled lattice with the corrugated design. The designed distance between adjacent tile centers is 4.5 helical-turns plus two DNA-helix diameters, totaling ~19.3 nm. The AFM measured distance from center to center of adjacent tiles is ~19 nm, in good agreement with our design (Figure 3.6c). Large lattice pieces, up to several hundred nanometers on each edge,

were observed in which the cavities appeared square. 2D Lattice displaying a square aspect ratio would be useful for forming regular pixel grids for information readout from nanoarrays, for example, by encoding information in a pattern of topographic markers. The large cavities in the nanogrid are bordered by segments of four separate tiles. The multi-tile cavities allow for combinatorially defined binding cavities, which may find applications in constructing patterns with addressable features.

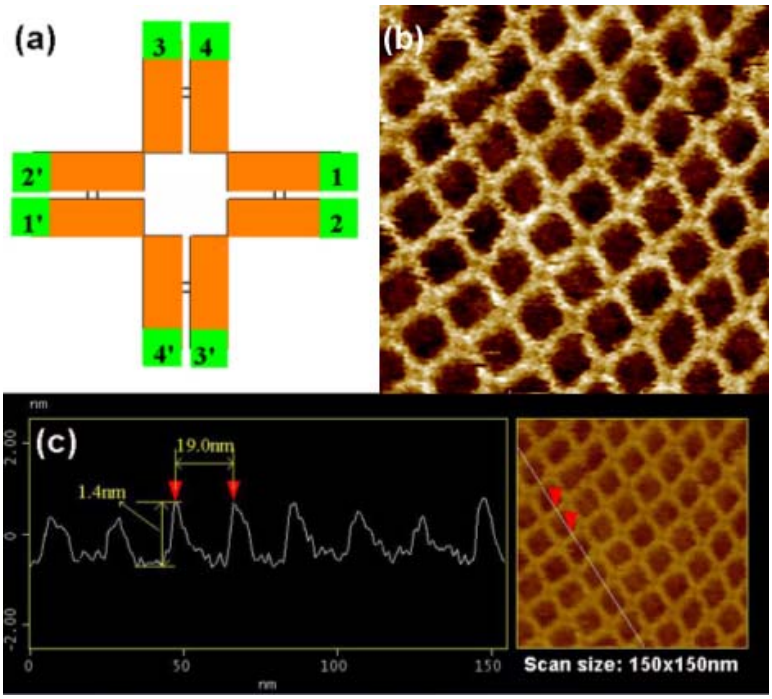

Figure 3.6: (a) Schematic diagram of the unit cross-tile of the nanogrid. (b) AFM image of the nanogrid with scan size of 150 nm × 150 nm. (c) Section profile of the nanogrid. Average spacing is about 19.0 nm, in good agreement with the designed structure, 19.3 nm.

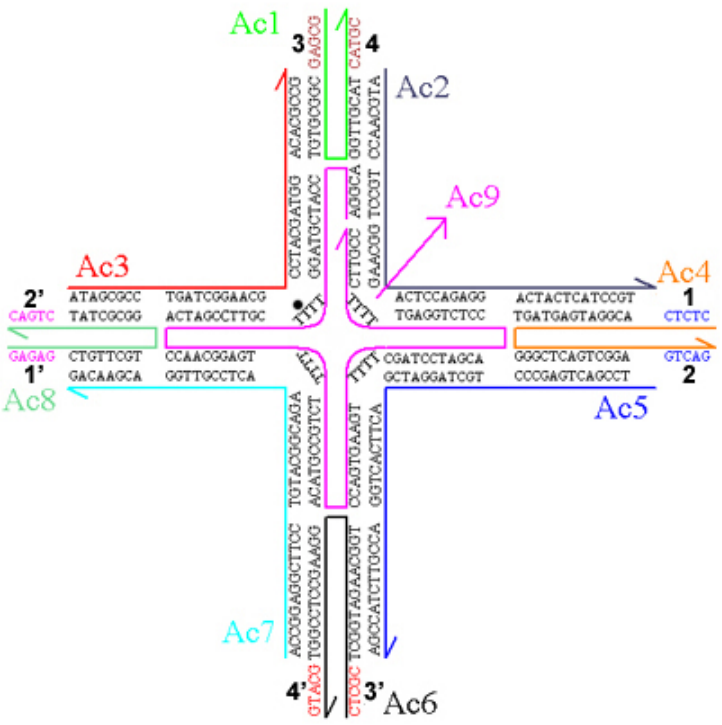

Figure 3.7: The 2D nanogrid unit cross-tile's strand structure and sequences. The complementary sticky-ends of *1*, *2*, *3*, and *4* are *1'*, *2'*, *3'*, and *4'*, respectively.

One major application of DNA nanotechnology is to use self-assembled DNA lattices to scaffold assembly of other molecular components. 2D nanogrids provide us with an excellent candidate to do so, due to the property of large cavity size which serves as binding or tethering sites for other molecular component. For instance, the loops at the center of each cross-tile can be modified with appropriate functional groups and used as scaffold for directing periodic assembly of desired molecules. Here we have used the nanogrids as templates to self-assemble streptavidin (SA) into periodic protein arrays. The cross-tile used in Figure 3.6 was modified by incorporating a biotin group into one of the loops at the center of the tile structure (see Figure 3.7). By adding SA to the solution

of the self-assembled 2D nanogrids, the interaction of SA-biotin will lead to periodic SA arrays (see schematic drawings of Figure 3.8a). We have been able to visualize the formation of the protein arrays on the DNA nanogrids by AFM imaging. Figure 3.8b shows an AFM image of the DNA-protein array. SA has a diameter of ~5 nm. Binding of SA to the 2D nanogrids generates bumps at the center of the cross-tile. This is clearly observed in the AFM image shown in Figure 3.8b. Some regions where there are no SA binding strongly supports the successful assembly of SA protein arrays on the 2D nanogrids. Comparison of SA-bound nanogrids and SA-unbound nanogrids reveals the difference caused by binding of SA to the nanogrids.

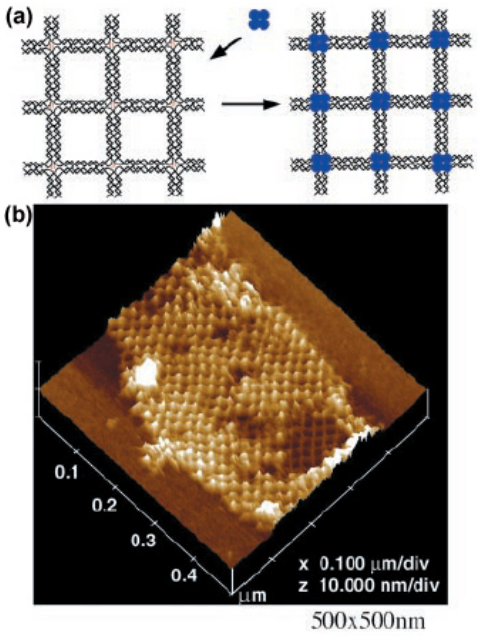

Figure 3.8: Self-assembly of protein arrays templated by the DNA nanogrids. (a) Schematic drawings of the DNA nanogrids scaffolded assembly of streptavidin. *Left*: The DNA nanogrids with a biotin group incorporated into one of the loops at the center of each tile. *Right*: Binding of streptavidin (represented by a blue tetramer) to biotin group will lead to protein nanoarrays on DNA lattices. (b) AFM image of the self-assembled protein arrays; scales are shown below the image.

3.4 1D Nanotrack Using Two Unit Cross-Tiles

Here, we demonstrate the precise control of periodic spacing between individual protein molecules by programming the self-assembled DNA templates made from two unit cross-tiles. In particular, we report the application of two self-assembled periodic DNA structures, 1D nanotrack, as a template for programmable self-assembly of SA protein arrays. These programmable protein assemblies utilize a two-tile system (A-tile and B-tile) as selectable templates for protein binding where A-tile and B-tile associate with each other, alternatively, through rationally designed sticky-ends and self-assemble into 1D nanotracks. A-tile and B-tile can be selectively modified such that either one or both

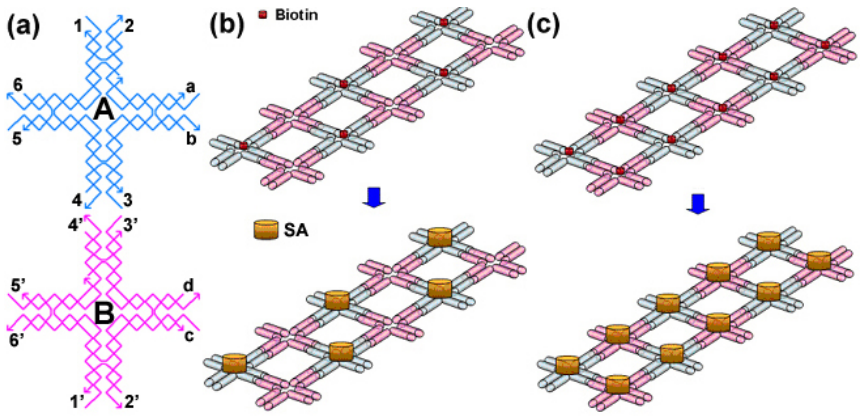

Figure 3.9: Schematic drawings of the precisely controlled protein self-assembly on programmable DNA scaffolds. (a) Strand structure of cross-tiles, A (blue) and B (pink) for the construction of the 1D AB nanotrack. Complementary sticky-end pairs are labeled as numbers, *n* and *n'*. In contrast, *a*, *b*, *c*, and *d* are non-complementary sticky-ends. (b) and (c) illustrate schematic cartoons for the self-assembly of streptavidin templated by 1D A*B nanotrack and A*B* nanotrack, respectively. Biotin groups and streptavidin molecules are represented as smaller red dots and larger yellow cylinders, respectively.

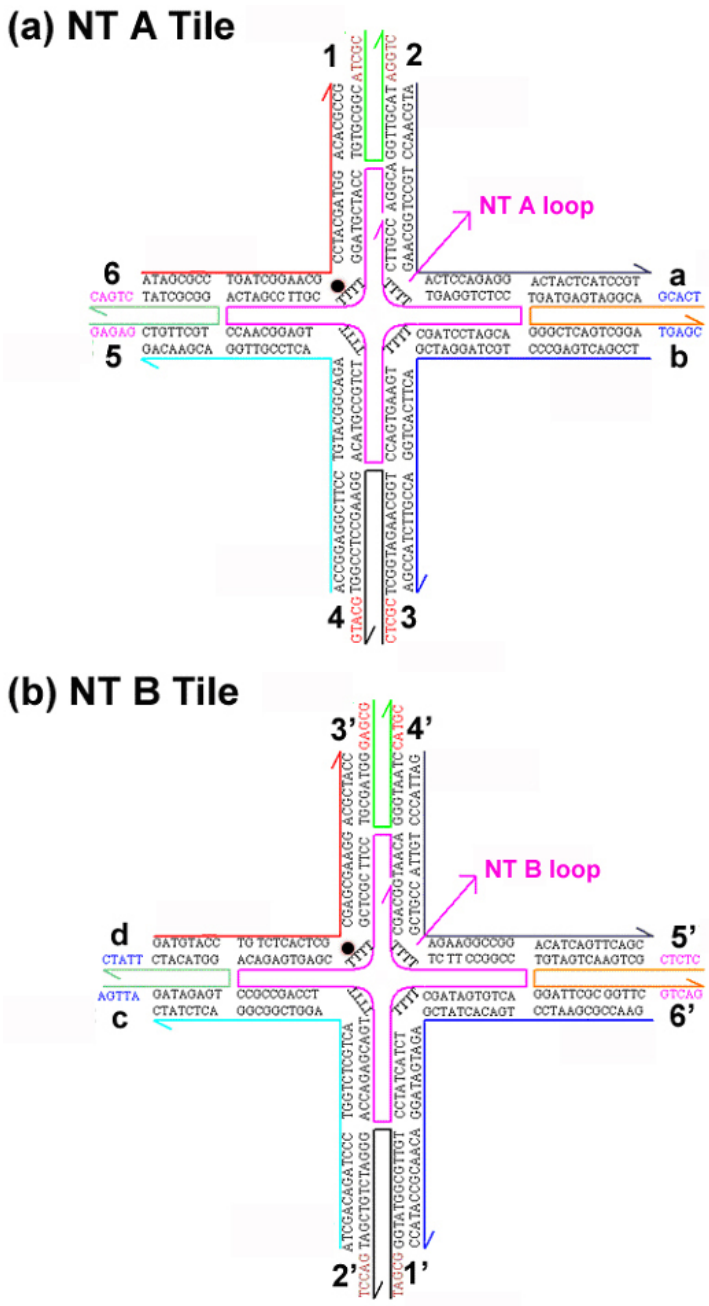

Figure 3.10: Strand structures and DNA sequences used for the 1D nanotrack construction. Here, (a) and (b) are the structures of nanotrack A and B cross-tiles containing base sequences, respectively. Each tile consists of nine different strands indicated by different colors. Black dots in the NT A-loop and NT B-loop strands indicate possible biotin sites. Biotin functionalization was incorporated during oligonucleotide synthesis as an internal biotin-dT monomer. For the A- and B- tiles, there is no biotin. For the A* and B*, the strand contains biotin.

tile types carry biotin groups. In consequence, the combination of selectively modified A- and B- tiles in the self-assembly and subsequent binding of SA to biotin leads to varied periodic spacing of the protein molecules on the DNA lattices.

Figure 3.9a, 3.9b, and 3.9c illustrate schematic drawings of the AB-tile system for the 1D nanotrack assembly and the subsequent SA attachment to form two distinct protein arrays. The basic DNA building blocks, A-tile and B-tile (Figure 3.9a), were derived from the cross-tiles. The sticky-ends of A- and B- tiles are designed such that complementary sticky-end pairs are indicated as numbers *n* and *n'*. By keeping the core structure of the cross AB-tiles and intentionally introducing non-complementarity into the sticky-ends on one side of the A- and B- tiles (indicated as sticky-ends *a*, *b*, *c*, and *d* in Figures 3.9a and 3.10), self-assembly of 1D DNA nanotrack (Figures 3.9b and 3.9c) can be obtained. Selective biotin incorporation indicated as a red dot in just A-tile as shown in Figure 3.9b or in both A- and B- tiles as shown in Figure 3.9c into the central loop of the AB-tile system results in two forms of the nanotrack: the A*B nanotrack (Figure 3.9b), where only tile A is biontinylated, and the A*B* nanotrack (Figure 3.9c), where both tile types are biotinylated. SA binding (indicated as yellow cylinders) to these two forms of nanotracks in turn results in two distinct self-assembled SA arrays, as shown in Figure 3.9b and 3.9c. SA on A*B* nanoarray is designed to be twice as dense as A*B arrays.

Following formation of lattice and subsequent binding of streptavidin, the lattices were examined by AFM imaging. Figures 3.11a and 3.11b are AFM images of the bare 1D A*B DNA nanotracks and A*B* DNA nanotracks, respectively. Figure 3.11c and

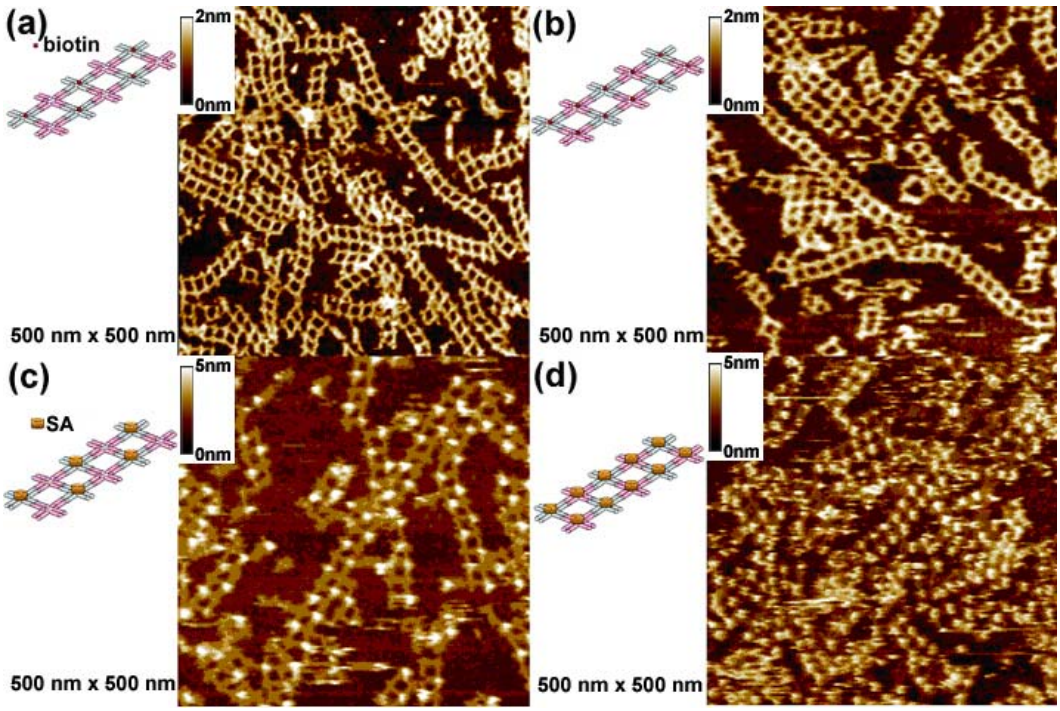

Figure 3.11: AFM images of the programmed self-assembly of streptavidin on 1D DNA nanotracks. (a) and (b) are AFM images of bare A*B and A*B* nanotrack before streptavidin binding, respectively. (c) and (d) are AFM images of A*B and A*B* nanotrack after binding of streptavidin. All AFM images are 500 nm × 500 nm.

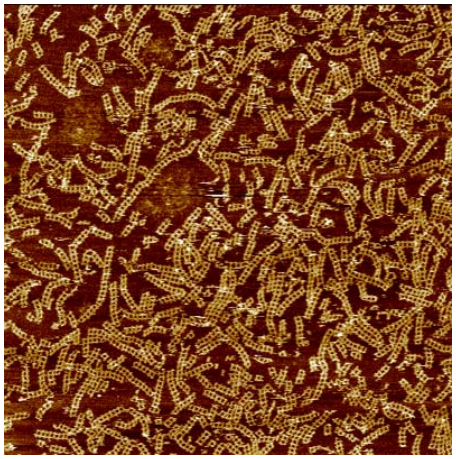

Figure 3.12: Wider area AFM scan, 2 μm × 2 μm of AB nanotrack. Following sample binding onto mica, it was observed that the DNA nanostructure was bound almost everywhere on the surface. This large area scan shows that the vast majority of DNA in the sample could be found in the desired structure.

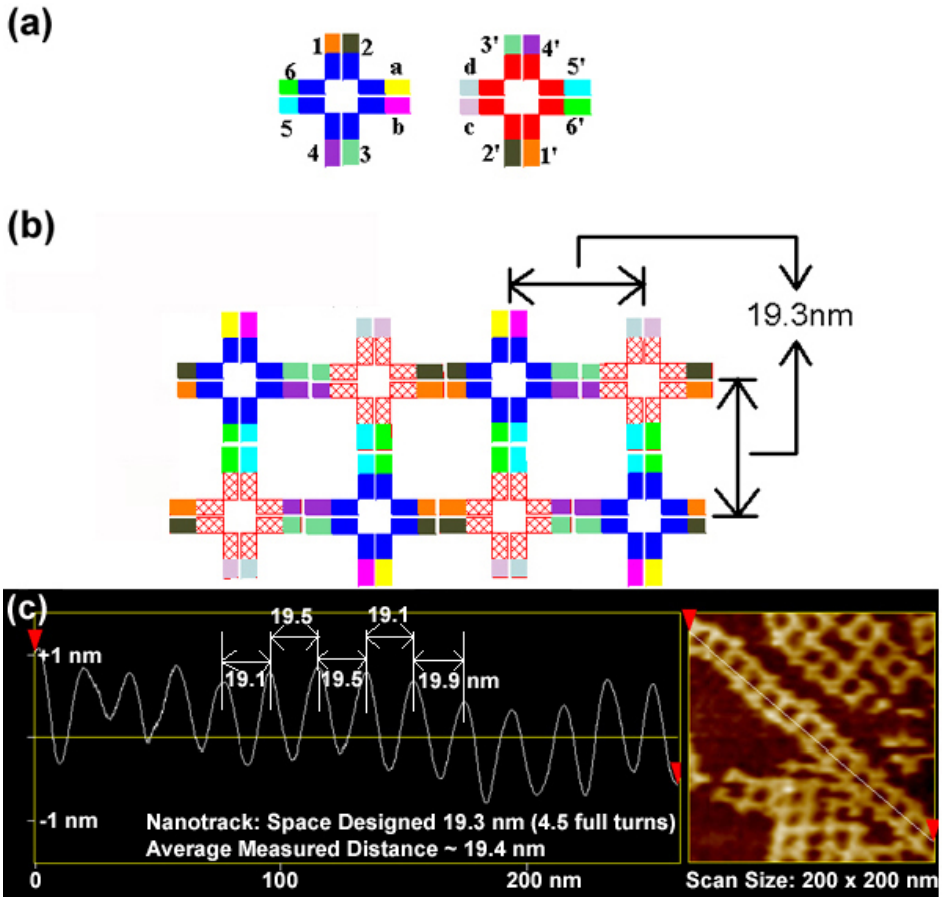

Figure 3.13: (a) Schematic diagram of the unit tiles of the nanotrack. (b) Schematic drawing of the nanotrack. A-tiles are in blue, B-tiles in red, solid colors represent tiles facing in the orientation as in (a), while cross-hatched colors represent tiles which have been flipped over so the side which was facing into the page is now facing out of the page. After formation of the nanotrack, we observe only one size of grid spacing 19.3 nm which corresponds to 4.5 full-turns of double helix. (c) Section profile of the nanotrack. Average spacing is about 19.5 nm, in very close agreement with the design.

3.11d show the two distinct forms of proteins nanoarrays resulting from SA binding to lattices A*B and A*B*, respectively. SA has a diameter of ~4 nm. Its binding to the self-assembled A*B and A*B* arrays generates topographical features on the mica surface which are higher than bare DNA lattices and are visualized as brighter bumps at the appropriate tile centers. AFM images in both Figure 3.11c and 3.11d clearly demonstrate the regular periodicity of the SA molecules templated on the 1D DNA nanotrack. The measured average distance between each pair of adjacent streptavidin molecules is about ~36 nm in Figure 3.11c and ~18 nm in Figure 3.11d, which is in good agreement with the designs. AFM height measurements show that SA molecules in Figure 3.11c and 3.11d have an average height of ~3.8 nm, compared to the height of ~1.2 nm measured on bare DNA lattices in Figures 3.11a and 3.11b. This further confirms that the periodic bumps in the nanotracks result from the binding of SA to the DNA tiles.

3.5 2D Nanogrid Using Two Unit Cross-Tiles

A system of programmable protein arrays with increasing complexity would benefit from an ability to design various DNA templates from an identical core structure. Figure 3.14 illustrates schematic drawings of the AB-tile system for the 2D nanogrid assembly and the subsequent SA attachment to form two distinct protein arrays. The sticky-ends of tiles A and B are designed such that complementary sticky-end pairs are indicated as numbers *n* and *n'*. The association of the programmed sticky-ends between A- and B- tiles will result in a 2D lattice composed of alternating A- and B- tiles, as shown in Figures 3.14b and 3.14c. To template the assembly of SA molecules, the loops at the center of the

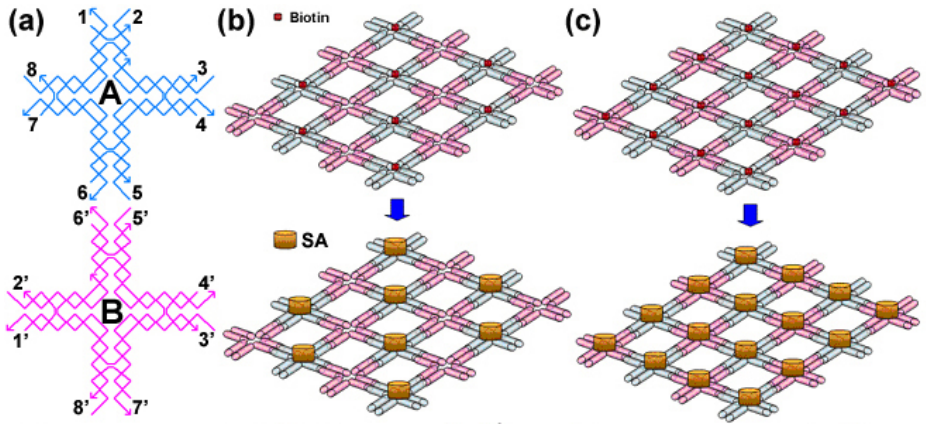

Figure 3.14: Schematic drawings of the precisely controlled protein self-assembly on programmable DNA scaffolds. (a) Strand structure of cross-tiles, A (blue) and B (pink) for the construction of the 2D nanogrids. Complementary sticky-end pairs are labeled as *n* and *n'*. (b) and (c) show schematic cartoons of the AB-tile self-assembly and subsequent binding of streptavidin onto A*B lattice and A*B* lattice, respectively.

A- and B- tiles were selectively modified to incorporate a biotin group indicated as a red dot in just A-tile as shown in Figure 3.14b or in both A- and B- tiles as shown in Figure 3.14c. Biotinylated A- and B- tiles are denoted as A* and B*, respectively. The lattice in Figure 3.14b is composed of A*-tile and B-tile and hence is denoted as A*B lattice, while the one in Figure 3.14c consisting of A*- and B*- tiles is denoted as A*B* lattice. The binding of SA to the biotin sites in A*B lattice or A*B* lattice results in two distinct forms of SA nanoscale arrays with different periodic spacing between adjacent protein molecules.

The formation of 1D AB nanogrid and the subsequent binding of SA were also confirmed with AFM imaging. Figures 3.16a and 3.16b are AFM images of the bare 1D A*B DNA nanogrid and A*B* DNA nanogrid, respectively. Figures 3.16c and 3.16d show the two distinct forms of protein arrays resulting from streptavidin binding to

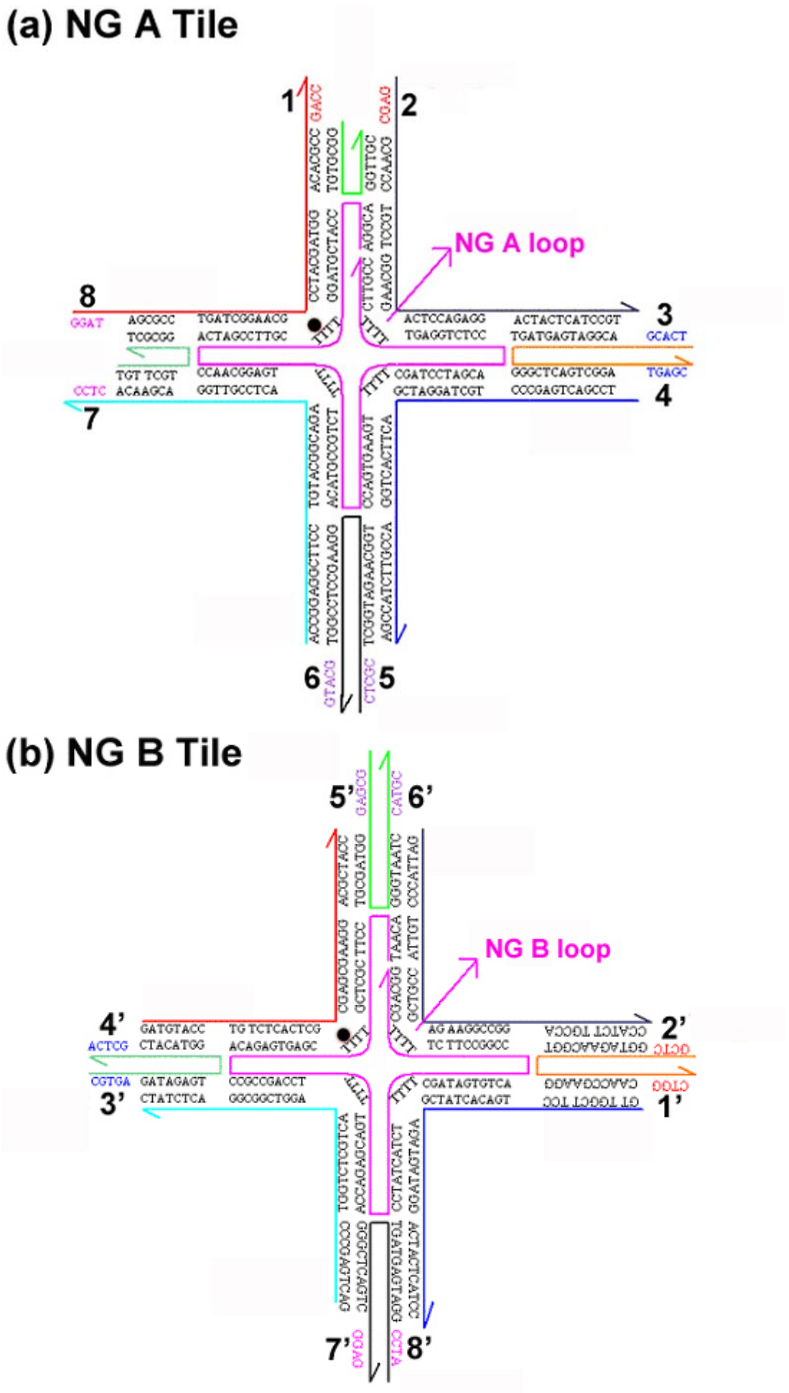

Figure 3.15: Strand structure and DNA sequences used in 2D nanogrid construction. Here, (a) and (b) are for the A-tile and B-tile, respectively. Each tile consists of nine different strands indicated by different colors. The black dots on the NG A-loop and NG B-loop strands indicate the site of biotin modification.

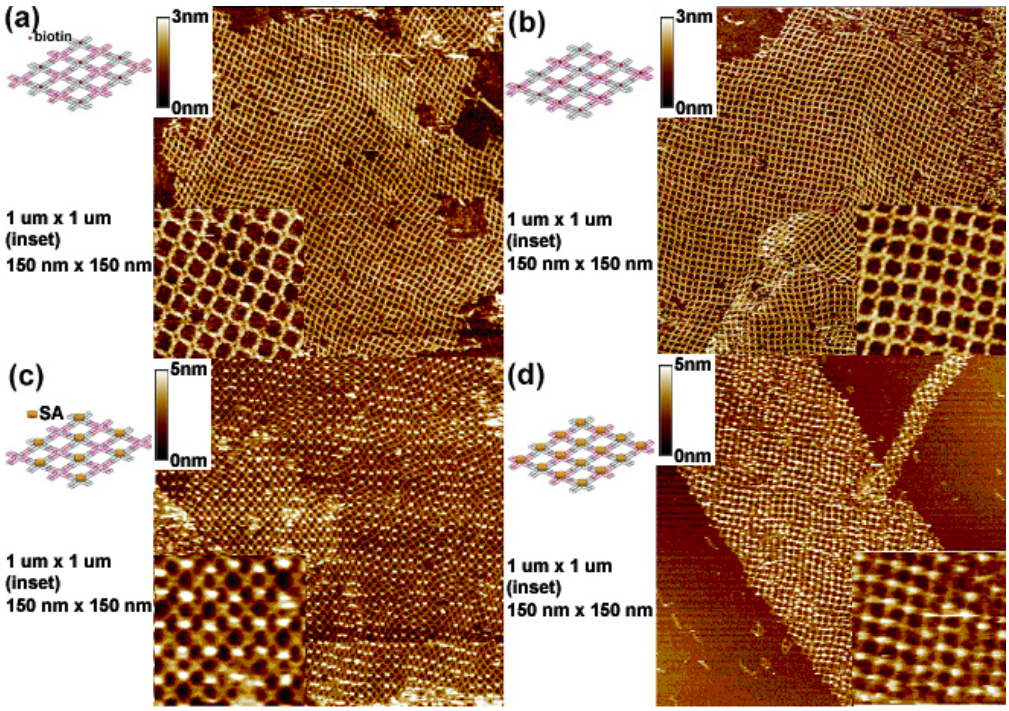

Figure 3.16: AFM images of the programmed self-assembly of streptavidin on 2D DNA nanogrids. (a) and (b) are AFM images of bare A*B and A*B* nanogrids before streptavidin attachment. (c) and (d) are AFM images obtained after binding of streptavidin to the bare DNA nanogrids A*B and A*B*, respectively. Scan sizes of all AFM images are 1 μm × 1 μm with 150 nm × 150 nm zoom-in insets.

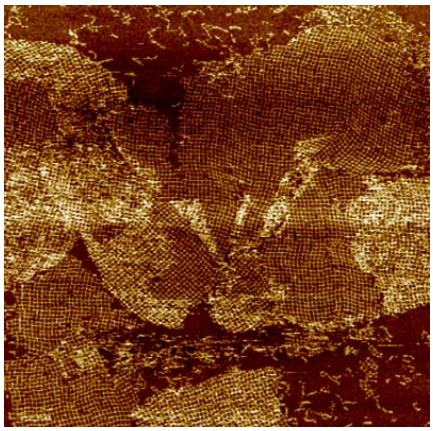

Figure 3.17: Wider area AFM scan, 2 μm × 2 μm of AB nanogrid. Following sample binding onto mica, it was observed that the DNA nanostructure was bound almost everywhere on the surface. This large area scan shows that the vast majority of DNA in the sample could be found in the desired structure.

nanogrid A*B and A*B*, respectively. The measured average distance between pairs of adjacent SA molecules is about ~36.9 nm in Figure 3.16c and ~18.5 nm in Figure 3.16d, which is in excellent agreement with the designed structures. AFM height measurements reveal the binding of SA compared to bare DNA nanogrid in Figures 3.16a and 3.11b and provide clear evidence that the assemblies formed as designed.

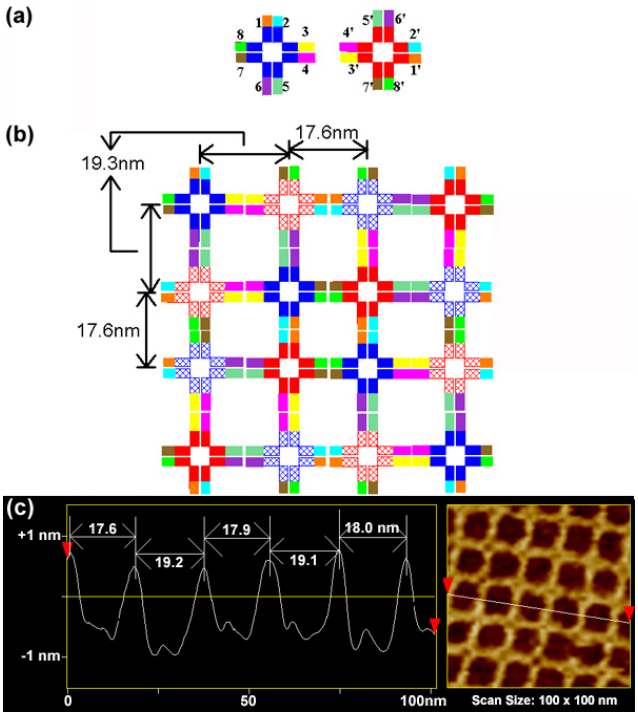

Figure 3.18: (a) Schematic diagram of the unit tiles of the nanogrid. (b) Schematic drawing of the nanogrid showing the corrugation pattern and alternation of wide and narrow grid spacing. A-tiles are in blue, B-tiles in red, solid colors represent tiles facing in the orientation as in (a), while cross-hatched colors represent tiles which have been flipped over so the side which was facing into the page is now facing out of the page. It can be seen that the neighboring tiles each need to be both flipped relative to the plane and rotated within the plane in order to properly match their sticky-end pairs. This arrangement results in a corrugation scheme in which A-tiles and B-tiles both occur in flipped orientations within the plane of the lattice. (c) Section profile of an AFM image of the nanogrid. After formation of the nanogrid, we observe alternating rows of different sized grid spacing, 19.3 and 17.6 nm which correspond to 4.5 full-turns and 4 full-turns, respectively, in excellent agreement with the designed structure.

3.6 Summary

In summary, we have rationally designed, assembled, and examined a set of programmed self-assembling nanostructures: nanoribbon and nanogrid made from a single cross-tile, and nanotrack, and nanogrid using two different cross-tiles. The DNA nanostructures described here provide regular lattice with a high preponderance of empty space in cavities which is useful for docking and organizing other materials. We have demonstrated 1D- and 2D- protein arrays with precisely controlled spacing and periodicity, templated on two types of DNA nano assemblies: the 1D nanotracks and the 2D nanogrids. This is one step forward toward more programmable and complex assembly of protein arrays at the nanoscale. The cross-tile can be easily programmed by varying sticky-ends to form more sophisticated arrays for applications in construction of logical molecular devices. For instance, quantum-dot cellular automata arrays may be constructed by specifically incorporating metal nanoparticles into the nanogrids. The nanogrids may also be useful as nanoscale contact-masks for transferring patterns onto surfaces via vapor deposition. The cavities can also be used as pixels in a uniform-pixel array which could be applied to AFM visual readout of self-assembly DNA computations such as binary-counting lattice.

Chapter 4

Stepwise Assembly Using Two Cross-Tiles

Even though it has excellent intrinsic characteristics such as molecular-scale recognition, self-organization, programmability and structuring properties, DNA-based nanostructure is still made of limited applications in the nanotechnology because of the lack of fixed-size controllability and full addressability. In this chapter, we present fabrication of size-controllable and fully-addressable DNA-based nanomatrices (NM) which consist of two different cross-tiles using a novel stepwise-assembly technique. The reliable and easily reproducible fixed-size DNA nanostructures as templates can lead to a major step toward developing nano/bio technologies. We also demonstrate construction of DNA superstructures assembled step-by-step. They consist of heterogeneous DNA motifs, cross-tiles and duplex- DNA molecules for controlling length and directionality of the superstructures.

4.1 Fully Addressable Fixed-size Nanomatrices

4.1.1 Design and characteristics of nanomatrices

Although fixed-size complex superstructures made of RNA have been presented recently [40], a stable and rigid nanostructure composed of DNA molecules with the novel

properties -size controllable, fully addressable, and precise programmable capabilities- has not been fully demonstrated. The two major schemes that we implement are: (i) construction and generalization of the fully addressable, finite-size 'N(row) x N(column)' NM from the aforementioned cross-tiles, and (ii) fabrication of superstructures composed of 2 × 2 NMs and double-stranded DNA (dsDNA) molecules utilizing a novel stepwise-assembly technique.

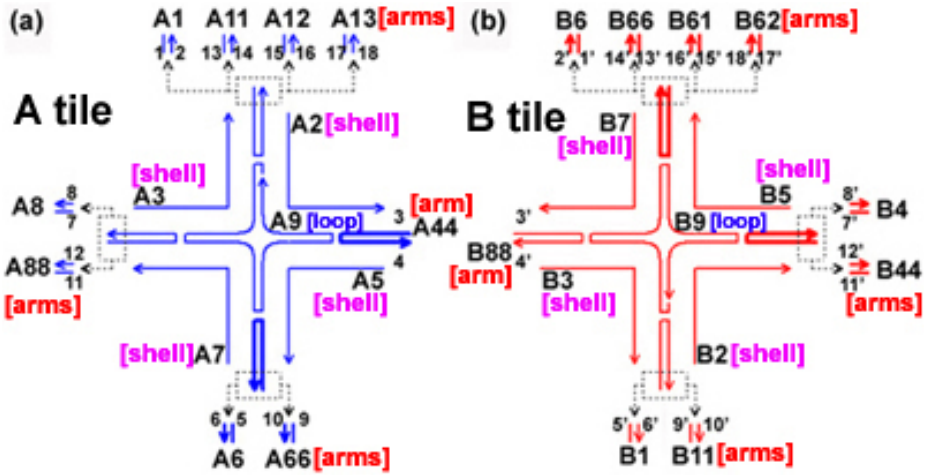

Figure 4.1: Schematic drawings of self-assembled cross tiles. Each tile, A-tile (shown in blue color) and B-tile (in red), consists of three different strand families: a central loop-strand, shell-strands, and arm-strands. Each sticky-end is in the arm-strand and the Watson-Crick complementary sticky-end of *n* is *n'*.

Schematic diagrams of the cross-tiles are shown in Figure 4.1. Arrows in drawings indicate simplified strands running from 5' to 3'. Each tile, A-tile (shown in blue color) and B-tile (in red), consists of three kinds of strands: a central loop-strand (A9 for A tile, B9 for B), shell-strands (A2, A3, A5, A7 for A tile, and B2, B3, B5, B7 for B) and arm-strands (A1x, A44, A6x, A8x for A tile, and B1x, B4x, B6x, B88 for B). Here,

loop and shells are core strands, and arms are optional for forming a unit cross-tile. All arm-strands have 5 bases of the sticky-ends at both 5'- and 3'- ends. Detailed nucleotide sequences and sets of the Watson-Crick complementary sticky-ends are given in the Figures 4.2, 4.3 and Table 4.1.

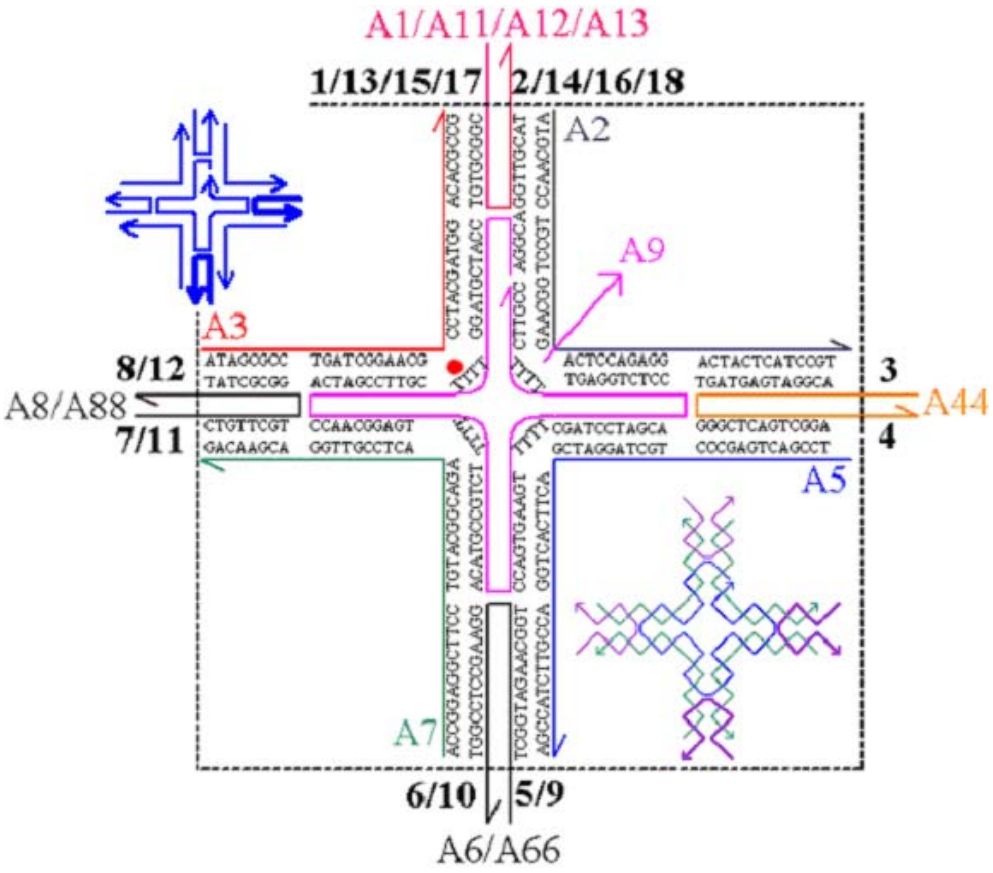

Figure 4.2: Cross-DNA motif, tile A. Schematics of strand structures and DNA sequences. Tile A consists of nine different strands indicated by different colors. The red-dot on the A9 strand indicates the site of biotin modification for demonstration of addressability. Arrows in drawings indicate simplified strands running from 5' to 3'.

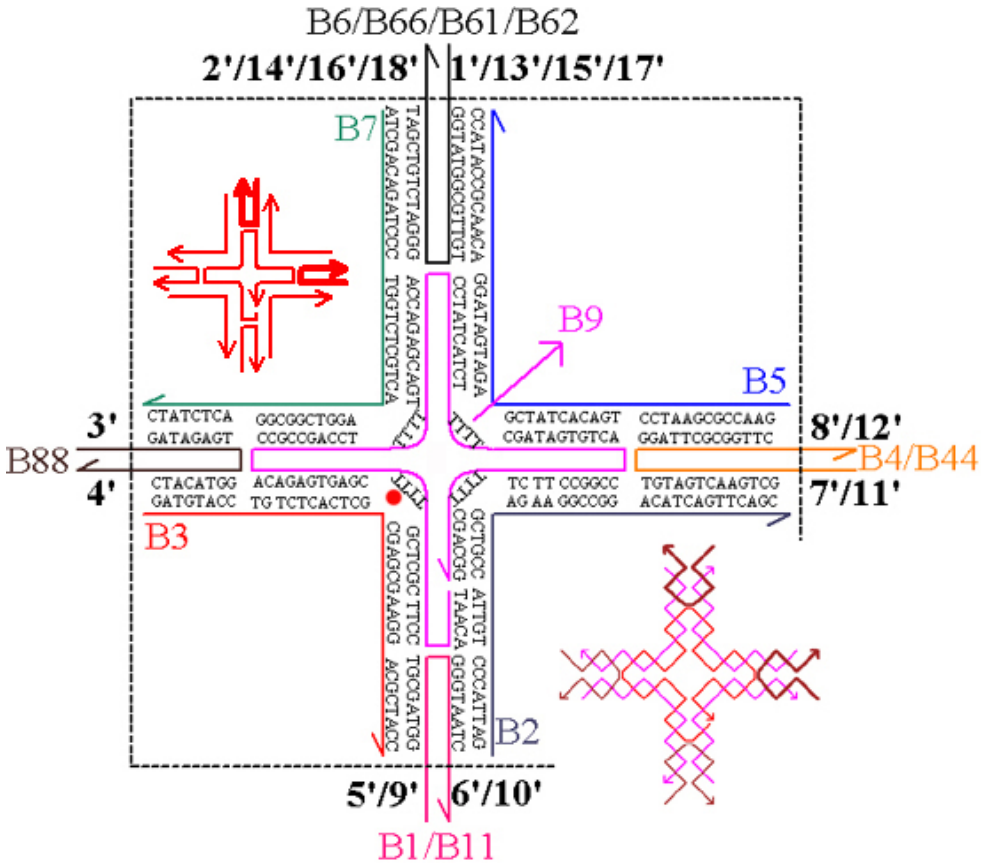

Figure 4.3: Cross-DNA motif, tile B. Schematics of strand structures and DNA sequences. Tile B consists of nine different strands as well. The red-dot on the B9 strand indicates the site of biotin modification for demonstration of addressability.

Sticky Ends	Arm-Strands	5’ to 3’	3’ to 5’	Arm-Strands	Sticky Ends
1(NS)	A1	CGCTA	GCGAT	B6	1’(NS)
2(NS)	A1	AGGTC	TCCAG	B6	2’(NS)
3(EW)	A44	TCACG	AGTGC	B88	3’(EW)
4(EW)	A44	TGAGC	ACTCG	B88	4’(EW)
5(NS)	A6	CTCGC	GAGCG	B1	5’(NS)
6(NS)	A6	GCATG	CGTAC	B1	6’(NS)
7(EW)	A8	GAGAG	CTCTC	B4	7’(EW)
8(EW)	A8	CAGTC	GTCAG	B4	8’(EW)
9(NS)	A66	TAGCA	ATCGT	B11	9’(NS)
10(NS)	A66	CCAGT	GGTCA	B11	10’(NS)
11(EW)	A88	CGTTG	GCAAC	B44	11’(EW)
12(EW)	A88	CACTA	GTGAT	B44	12’(EW)
13(NS)	A11	TTATC	AATAG	B66	13’(NS)
14(NS)	A11	ACTTA	TGAAT	B66	14’(NS)
15(NS)	A12	GTACA	CATGT	B61	15’(NS)
16(NS)	A12	CTGTA	GACAT	B61	16’(NS)
17(NS)	A13	TACCG	ATGGC	B62	17’(NS)
18(NS)	A13	GAAGA	CTTCT	B62	18’(NS)
			AATAG	B66	1”(NS)
			TGAAT	B66	2”(NS)
			CTATT	B8	3”(NS)
			ATTGA	B8	4”(NS)
			GCAAC	B44	7”(EW)
			GTGAT	B44	8”(EW)

Table 4.1: Sets of the complementary sticky-ends for constructing stepwise assembly of NMs and nanotracks. The sticky-ends are designed such that the complementary sticky-end pairs are shown as (*n* and *n’*) and (*n”* is *n’’’*). NS and EW in the first and last columns indicate the directions of arm-strands, ‘north or south’ for NS and ‘east or west’ for EW. Note that *n’’’* will be used in the double-stranded DNA nanobridges in section 4.2.

4.1.2 2 × 2 nanomatrix

We have developed a novel stepwise-assembly technique to construct finite-size 'N x N' NM. For example, 2 × 2 NM can be fabricated with 2 steps: the first step involved high-temperature annealing of equimolar mixtures of strands of '1 and 2' and '3 and 4' tiles shown in Figure 4.4a. They were cooled slowly from 95 °C to 20 °C by placing the microtubes in 2 L of boiled water in a Styrofoam box for at least 40 hours to facilitate hybridization. The second step involved low-temperature assembly, with exactly the same volume of '1 and 2' and '3 and 4' 1 × 2 NMs' mixture; they cooled slowly from 42 °C to 20 °C by placing the microtubes in 1 L of water at room temperature for ~4 hours. After each step of annealing, samples were incubated overnight at 4 °C for structure stabilization. Low-temperature annealing prevents formed lattices from dissociating, at a $T_m \approx 60$ °C, and provides enough mobility and energy -average CG base-pair concentration in sticky-ends is ~50 % with melting temperature, ~30 °C- to facilitate further hybridization for desired lattice structures.

Experimentally, we observed that matrices were fabricated rigid enough to visualize by AFM without outer arm-strands. 2 × 1 NM without outer arms is shown in Figure 4.4c (a schematic drawing) and Figure 4.4f (an AFM image). The cross-tile participation ratio of 'N × M' NM, p(N×M), is defined as the total number of tiles *participating* in 'N × M' NM divided by the total number of cross-tiles analyzed by AFM images. We notice p(2×1) varies from 0.78 ~ 0.84 and the average is ~0.81. We have performed two ways to fabricate 2 × 2 NMs utilized by the 2-step assembly: one with non-complementary sticky-ends outer arms (a cartoon in Figure 4.4a and an AFM image

in Figure 4.4d) and one without outer arm-strands (Figure 4.4b and Figure 4.4e). Here, the average participation ratio, p(2×2) with/without is 0.75/0.90. When properly addressed 2 × 2 NMs without outer arms facilitated by biotinylated loop-strands were mixed with streptavidin (SA), the interaction of biotin-SA led to artificially programmed SA protein arrays for demonstrating full addressability. The formation of the protein arrays on 2 × 2 NMs was visualized by AFM. Figures 4.5a through 4.5e are high-resolution AFM images of fully addressed 2 × 2 NMs with SA on '1st', '2nd and 3rd', '1st and 2nd', '1st, 2nd, and 3rd' and 'all' tiles, respectively. The SA's binding, height ~5 nm, to 2 × 2 NMs generates bumps at the center of the cross-tiles, which can be compared with unbounded-tiles. 2 x 2 NMs in Figures 4.5b and 4.5e are symmetrical; others are asymmetrical and they clearly support the successful assembly of the fully-addressed 2 × 2 NMs. About 75 % of all 2 × 2 NMs show correctly addressed matrices (Figures 4.5f and 4.5g).

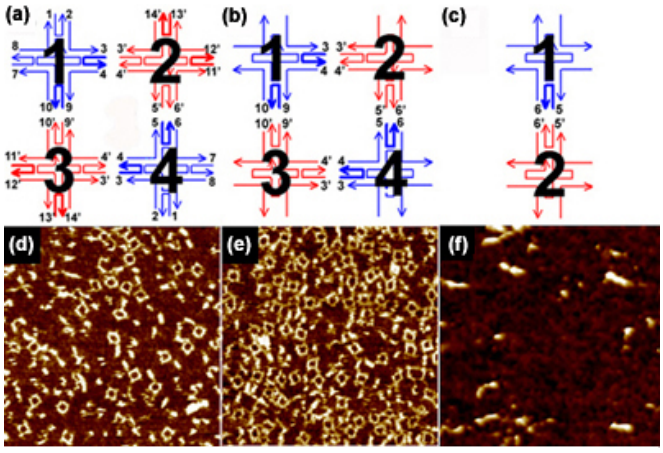

Figure 4.4: (a) and (b) are schematics of 2 × 2 NMs with outer non-complementary sticky-end arms and without, respectively. (c) A schematic diagram 2 × 1 NM. (d) and (e) are AFM images of 2 × 2 NMs with and without the outer non-complementary sticky-end arms. Each scan size is 500 nm × 500 nm. (f) An AFM image of 2 × 1 NM with 250 nm × 250 nm scan size.

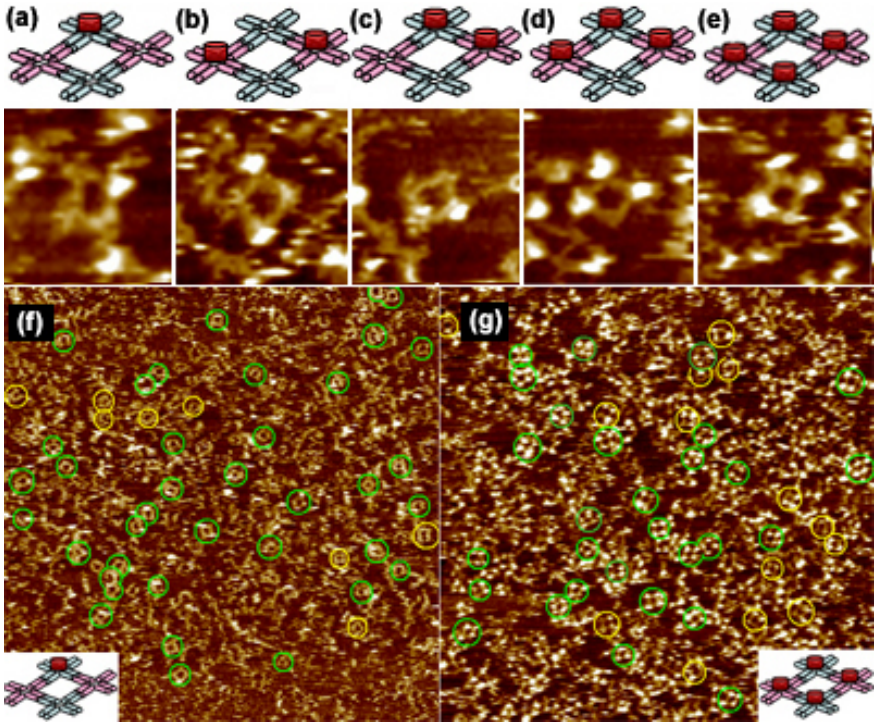

Figure 4.5: Demonstration of fully-addressable and fully-programmable 2 × 2 NM. (a) through (e) are high-resolution AFM images for demonstrating fully addressable capability of 2 × 2 NMs facilitated by programmed biotinylated loop-strands and bindings of SA on desired sites. Scan size, 80 nm × 80 nm. (f) AFM image of 2 × 2 NM with the binding of SA, final concentration of SA, 0.0625 μM, at a corner of 2 × 2 NM. Schematic is shown in the inset. Roughly 80 % of all 2 × 2 NMs show properly addressed SA on matrices, circled in green. 2 × 2 NMs circled in yellow indicate lattices with not-properly addressed SA, ~20 % of 2 × 2 NMs. Scan size is 1 μm × 1 μm. (g) AFM image of 2 × 2 NM with the binding of SA, final concentration of SA, 0.25 μM, at all four tiles of 2 × 2 NM. Roughly 69 % of 2 × 2 NMs have correctly assembled SA, circled in green. Scan size, 1 μm × 1 μm.

4.1.3 4 × 4 nanomatrix

We have further demonstrated four-step assembly of the fixed-size 4 × 4 NM. Figure 4.6a shows a four-step flow diagram and Figure 4.6b is a final structure of the self-assembled 4 × 4 NM with the detailed complementary sticky-ends. 4 × 4 NM is consisting of fully-addressable 16 cross-tiles. From AFM images of 4 × 4 NMs in Figure 4.6c after the final-step low-temperature annealing, we note p(4×4) is about 0.20 which corresponds well with $[p(1\times2)]^8 \approx 0.81^8 \approx 0.19$. In order to be more useful and effective of stepwise assembly and to increase the yield of the final product, we should maximize the yield of initial product, p(1×2). It can be achieved by the native gel electrophoresis technique so that unassociated, and/or badly associated strands, can be removed.

Figures 4.6d through 4.6f are cartoons (top) and high-resolution AFM images with 100 nm × 100 nm scan size (bottom) of three different 4 × 4 NMs without '6^{th}', '6^{th} and 11^{th}' and '6^{th}, 7^{th}, 10^{th}, and 11^{th}' tiles. They show rigidity of 4 × 4 NMs as well as verification, demonstration of addressability and programmability. Another example of fabrication of an addressable NM using biotin-SA conjugates on all B-tiles is shown in Figure 4.6g. A cartoon of programmable and symmetrical self-assembly of SA protein array on 4 × 4 NM is in the right panel and a corresponding AFM image, with scan size 1 μm × 1 μm, is in the middle of Figure 4.6g. This also provides the convincing evidence of the fully-addressable 4 × 4 NMs.

4.1.4 Generalized N × N nanomatrix

We have generalized the stepwise assembly of 'N × N' NM with three distinct features: (i) $N = 2^n$, with n = 1, 2, 3 …, (ii) utilizing two different cross-A and -B tiles, and (iii) using

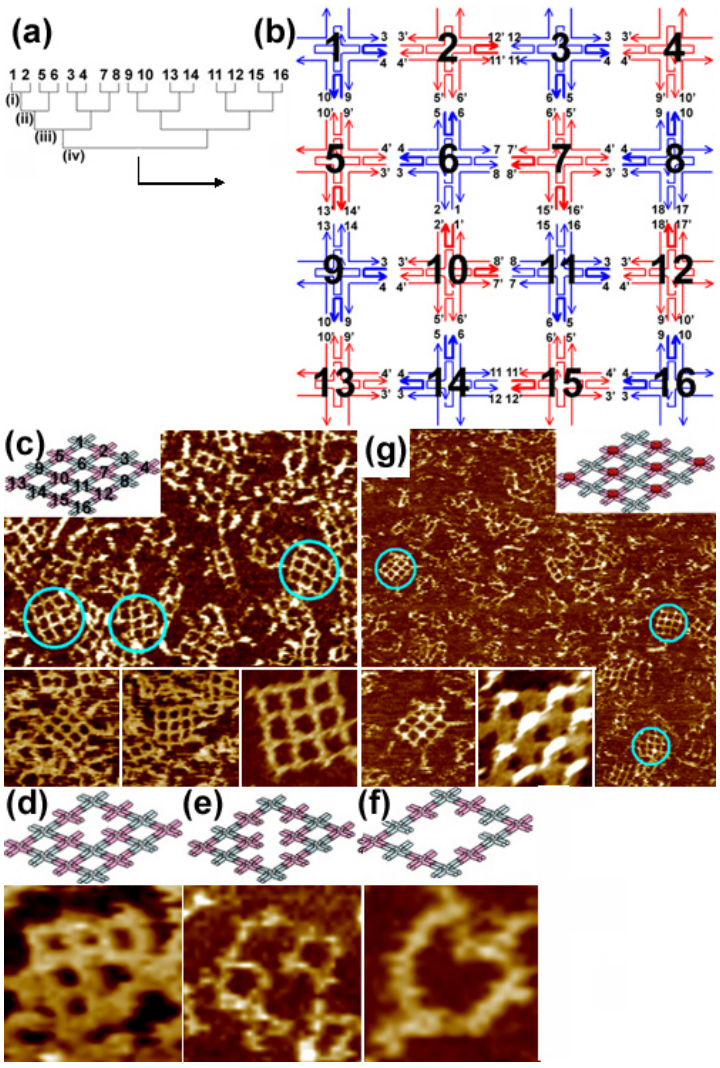

Figure 4.6: Four-step assemblies of the fixed-size 4 × 4 NM and demonstration of full addressability and programmability. (a) Four-step flow diagram of 4 × 4 NM. (b) Schematic of the self-assembled 4 × 4 NM which is consisting of fully-addressable 16 cross-tiles. (c) AFM images of 4 × 4 NM formed from the stepwise assembly. Scan size is 600 nm × 400 nm (middle). The upper-left panel is a cartoon of 4 × 4 NM and the lower-panels from left to right are zoomed-in views with scan sizes, 200 nm × 200 nm, 200 nm × 200 nm, and 100 nm × 100 nm, respectively. (d) through (f) show fully-addressable and programmable capabilities of 4 × 4 NMs. High-resolution images of 4 × 4 NMs without (d) 6^{th}, (e) 6^{th} and 11^{th}, and (f) 6^{th}, 7^{th}, 10^{th}, and 11^{th} tiles. (g) Another example of construction of addressable nanomatrices used by biotin-SA bindings on all B-tiles. AFM image of 4 × 4 NM as a template for programmable self-assembly of SA protein arrays. Scan size is 1 μm × 1 μm. The upper-right panel is a cartoon of desired 4 × 4 NM with SA indicated as red-cylinders. The lower-panels from left to right are zoomed-in images with scan sizes of 200 nm × 200 nm and 100 nm × 100 nm, respectively.

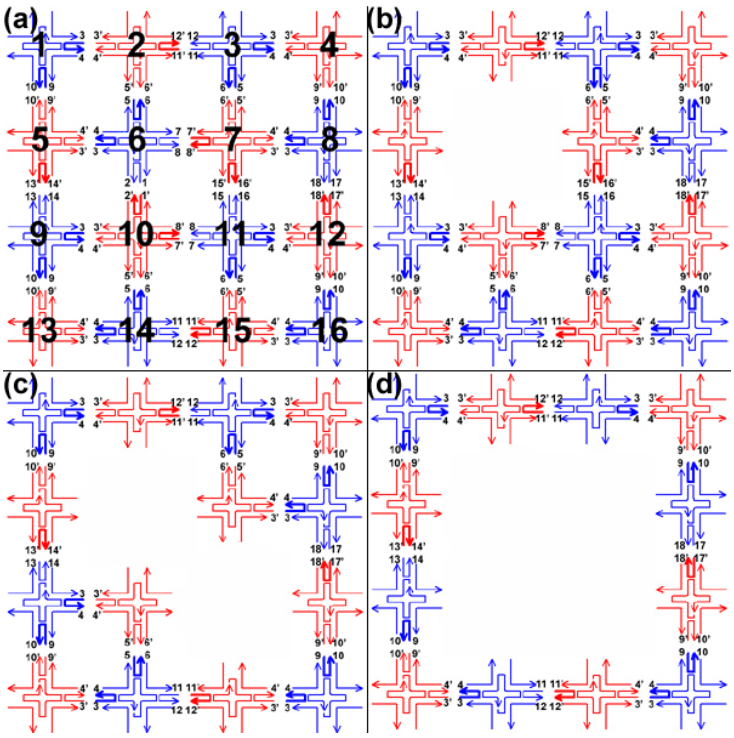

Figure 4.7: Schematic diagrams of four different 4 × 4 NMs. (a) Original 4 × 4 NM, and 4 × 4 NMs without (b) 6th, (c) 6th and 11th, and (d) 6th, 7th, 10th, and 11th tiles.

the minimum number of complementary sticky-ends sets. Using first feature, we may fabricate all subsets of 'N × N' matrices. For example, using 4 cross-tiles of 2 × 2 NM, we can construct all four fixed-size and fully-addressable subsets, 1 × 1, 1 × 2, 2 × 1, and 2 × 2 NMs. The advantage of the second condition is the reduction of one-step; we can anneal two tiles at the same time. The third feature is for use of the minimum number of strands. With these conditions, we have found that the total number of annealing steps, $n_{total\text{-}step}$, and the total number of minimum required stick-ends sets, $n_{total\text{-}sticky}$, for 'N × N' NM are $[2 + 2(m - 1)]$ and $[3\sum_{n=1}^{m} 2^{n}]$ where $m = log_2 N$, respectively (see Table 4.2). Figure 4.8 is an example of a proposed 8 × 8 NM with the detailed complementary

sticky-ends geometry. With N = 8 for 8 × 8 NM, then $n_{total\text{-}step}$ = 6 and $n_{total\text{-}sticky}$ = 42. In this way, we could build, in principle, up to 64 × 64 NM, size 1.2 μm × 1.2 μm, using 5 (pentamer) bases sticky-ends. Using 6 (hexamer), 512 × 512 NM can be constructed with size 9.9 μm × 9.9 μm (Table 4.3).

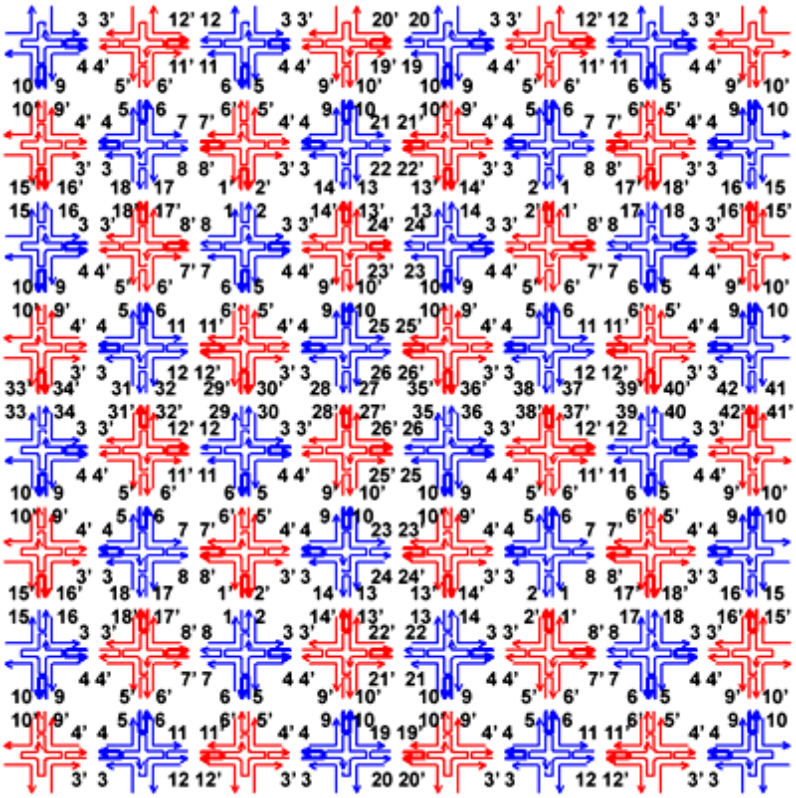

Figure 4.8: A schematic drawing of a proposed 8 × 8 NM using a stepwise-assembly technique with the minimum required Watson-Crick complementary sticky-ends sets.

	Total number of minimum required strands
1 × 1	5 (A tile) + 5 (B tile) = 10; total number of initial strands
2 × 2	10+(2+2+2) = 16
4 × 4	10+(2+2+2)+(4+4+4) = 28
8 × 8	10+(2+2+2)+(4+4+4)+(8+8+8) = 52
16 × 16	10+(2+2+2)+(4+4+4)+(8+8+8)+(16+16+16) = 100
32 × 32	10+(2+2+2)+(4+4+4)+(8+8+8)+(16+16+16)+(32+32+32) = 196
N × N (where N ≥ 2)	10+(2+2+2)+...+(N+N+N) = $10 + 3\sum_{n=1}^{m} 2^n$, where $m = log_2 N$

Table 4.2: Total number of minimum required strands utilizing two different cross-tiles for fabricating 'N × N' NM.

	Using 5 bases	Using 6 bases
Total # of unique sets	$4^5 = 1024$	$4^6 = 4096$
Total # of used sets in Tiles A and B	368	360
Available sticky-ends sets	1024 - 368 = 656 sets	4096 - 360 = 3736 sets
Largest possible NM	64 × 64 NM (i) size: $(63 \times 19.3 \text{ nm})^2 \approx$ 1.2 μm × 1.2 μm (ii) $n_{total\text{-}sticky} = 378$ (iii) $n_{total\text{-}step} = 12$	512 × 512 NM (i) size: $(511 \times 19.3 \text{ nm})^2$ ≈ 9.9 μm × 9.9 μm (ii) $n_{total\text{-}sticky} = 3066$ (iii) $n_{total\text{-}step} = 18$

Table 4.3: Possible 'N × N' NM utilizing pentamer and hexamer sticky-ends sets.

4.2 Stepwise Assembly of Superstructures Using Multipath Double-Stranded DNA Bridges

Although dsDNA molecules themselves can be utilized as templates for fabricating metallic nanowires, they are not considered much as an active motif of complicated self-assembled DNA nanostructures. Here we demonstrate construction of DNA complexes consisting of artificially designed dsDNA molecules with cross-tiles. Duplex DNA molecules can serve as functionalized bridges effectively, length up to its persistence length of ~50 nm, between complexes for controlling length and directionality of superstructures.

A schematic flow diagram of four-step self-assembly of the finite-size superstructures composed of 2 × 2 NMs and dsDNA bridges (2 full-turns, ~6.8 nm) are shown in Figure 4.9. Figures 4.11a through 4.11d show cartoons and the results of AFM images of 2 × 2 NMs (after 2^{nd}-step annealing), 2 × 2 NMs with horizontal (after 3^{rd}), with vertical (after 3^{rd}), and with both *x*- and *y*- directional bridges (after final-step), respectively. All experimental distance measurements are in excellent agreement with designed superstructures with less than 5 % (± 1.0 nm) deviation. Self-assembled superstructures, circled in cyan, show the properly assembled superstructures and the participation ratios of the cross-tiles, p(2×2), p(2×2 with *x* or *y* -bridges), and p(2×2 with *x* and *y* -bridges) are roughly 0.79, 0.33, and 0.17, respectively. Here noticeable low yields of final products, 2 × 2 NMs with horizontal or vertical, and 2 × 2 NMs with both bridges, may come from error accumulation through each annealing step. We also performed the length control of self-assembled DNA superstructures, nanotracks, utilized

by two different lengths of dsDNA bridges, 1.5 full-turns, ~5.1 nm and 2.5 full-turns, ~8.5 nm (Figures 4.13 ~ 4.14). The measured distances between nanotracks with the short/long -bridges are ~24.6/~28.2 nm, excellently matching the designed distance, 24.4/27.8 nm (Figure 4.15).

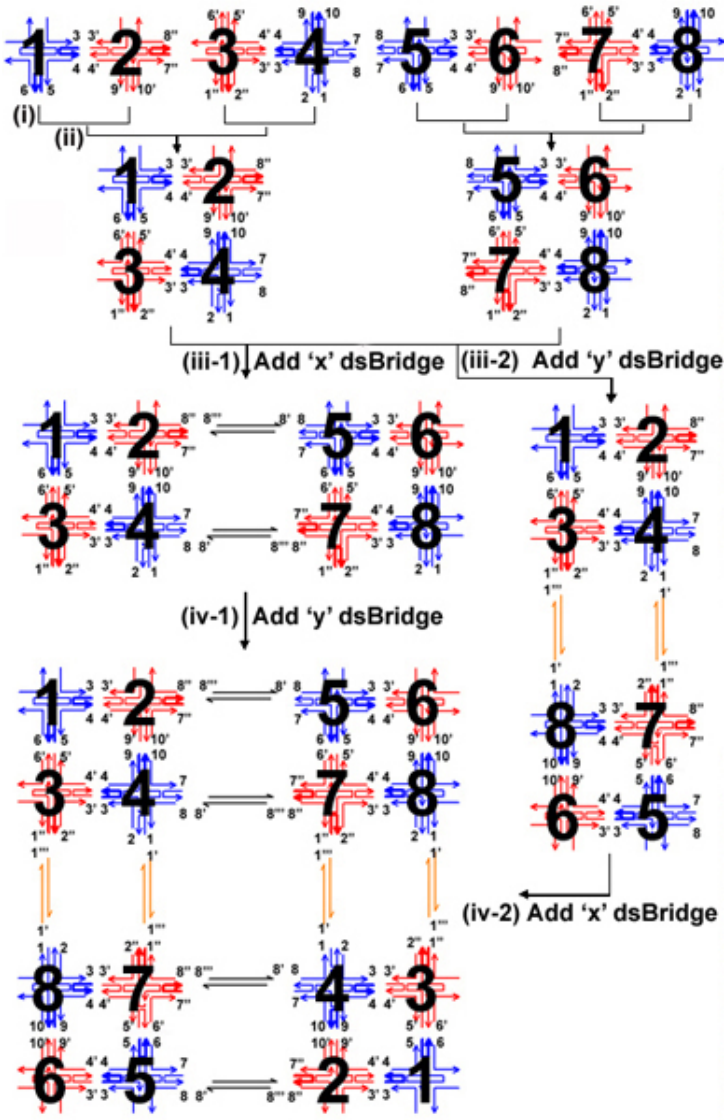

Figure 4.9: Four-step self-organization of the finite-size superstructures composed of 2 × 2 NMs and dsDNA nanobridges.

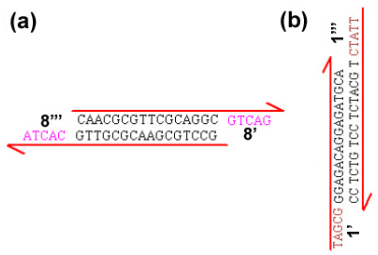

Figure 4.10: Double-stranded DNA bridges used in Figure 4.9. Schematic drawings of (a) horizontal, (*x*-direction), and (b) vertical (*y*-direction) bridges. Each bridge is composed of two strands with the two sticky-ends at the ends of dsDNA molecules. The complementary sticky-end of *n* is *n'* and of *n''* is *n'''*.

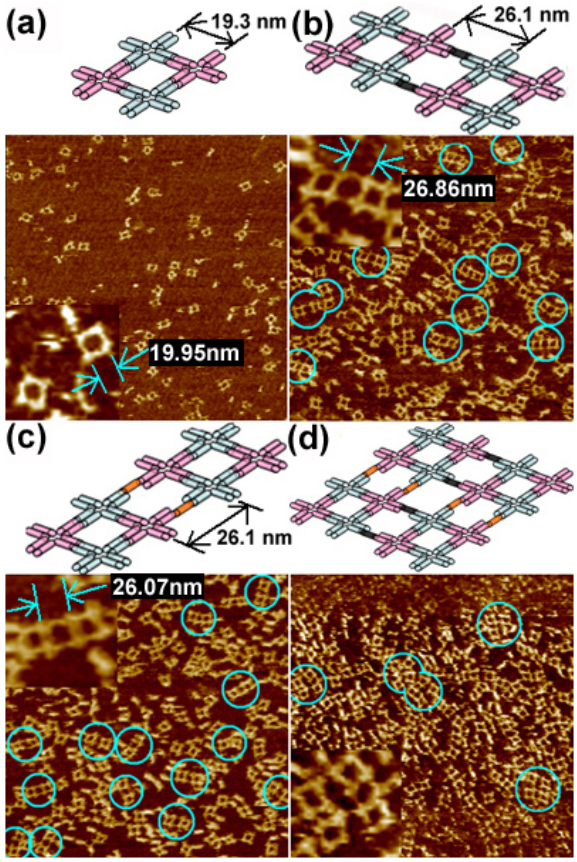

Figure 4.11: AFM images of four-step self-organization of the finite-size superstructures composed of 2 × 2 NMs and dsDNA nanobridges. (a) through (b) show (top) cartoons and (bottom) AFM images -scan sizes, 800 nm × 800 nm and (inset) 100 nm × 100 nm- of 2 × 2 NM, 2 × 2 NMs with horizontal, with vertical, and with both directional nanobridges. Self-assembled superstructures, circled in cyan, show the properly assembled superstructures.

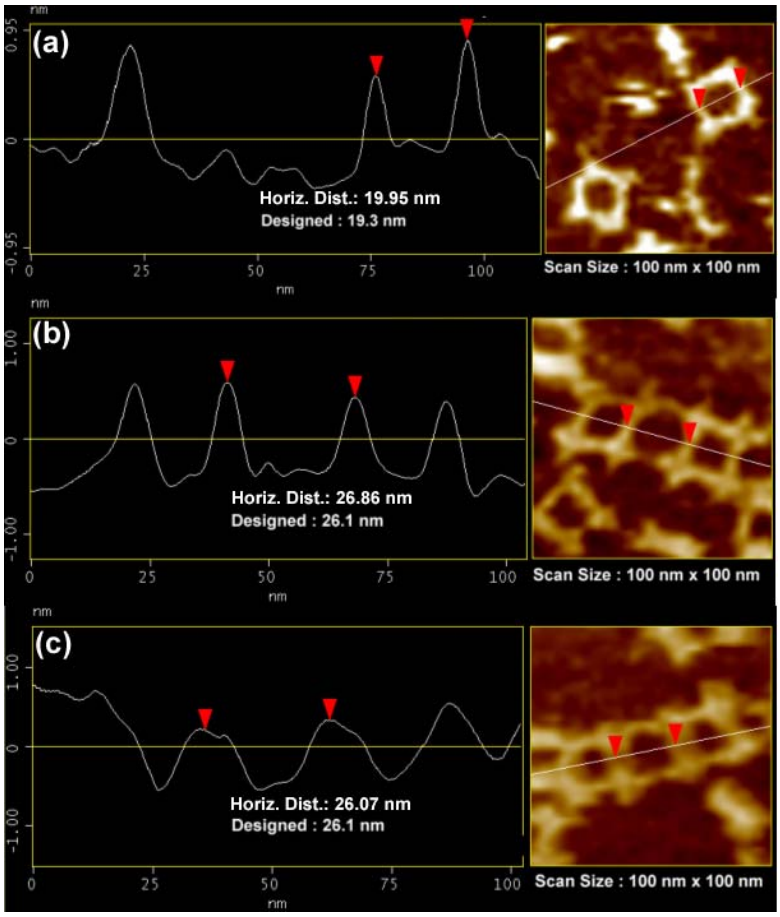

Figure 4.12: Section measurement of 2 × 2 NM + dsDNA bridges. Section profile distance measurements of (a) 2 × 2 NM, (b) 2 × 2 NM with horizontal, and (c) 2 × 2 NM with vertical dsDNA bridges. All experimental distance measurements were in excellent agreement with designed structures with less than 5% (± 1.0 nm) deviation.

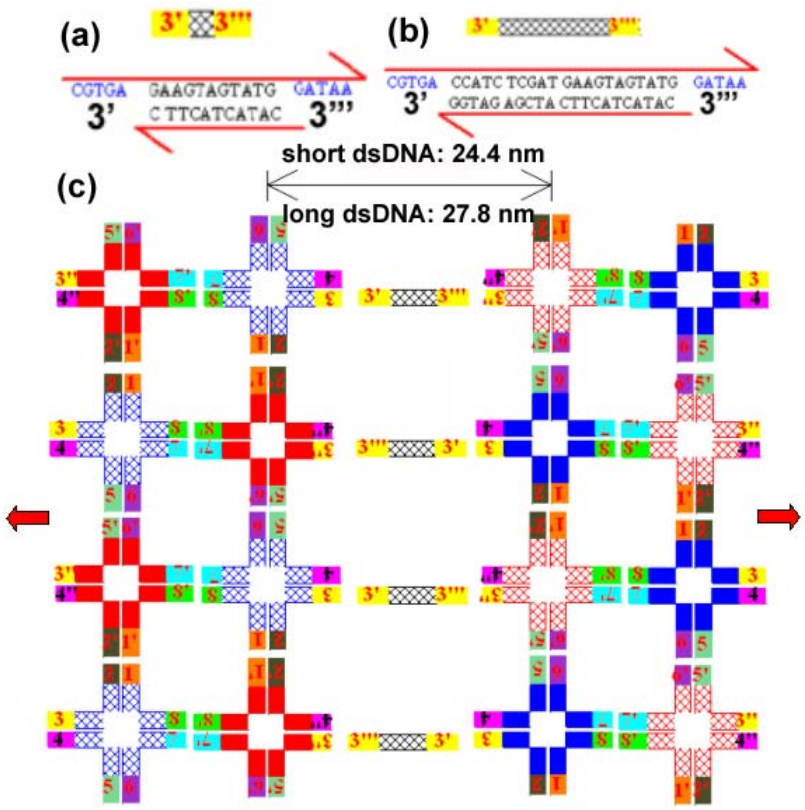

Figure 4.13: Cartoons of nanotrack + double stranded DNA bridges. Schematic drawings of (a) the short- (16 bases, 1.5 full-turns) and (b) the long- (26 bases, 2.5 full-turns) duplex DNA bridges. Each bridge consists of two strands with two sticky-ends at the ends of dsDNA molecules. The complementary sticky-end of *n* is *n'* and of *n''* is *n'''*. (c) Cartoon of nanotracks with the bridges. Here the solid and hatched cross-tiles indicate upward and downward facings, respectively. Designed distances between the nanotracks are 24.4 nm for the short-dsDNA bridge and 27.8 nm for the long.

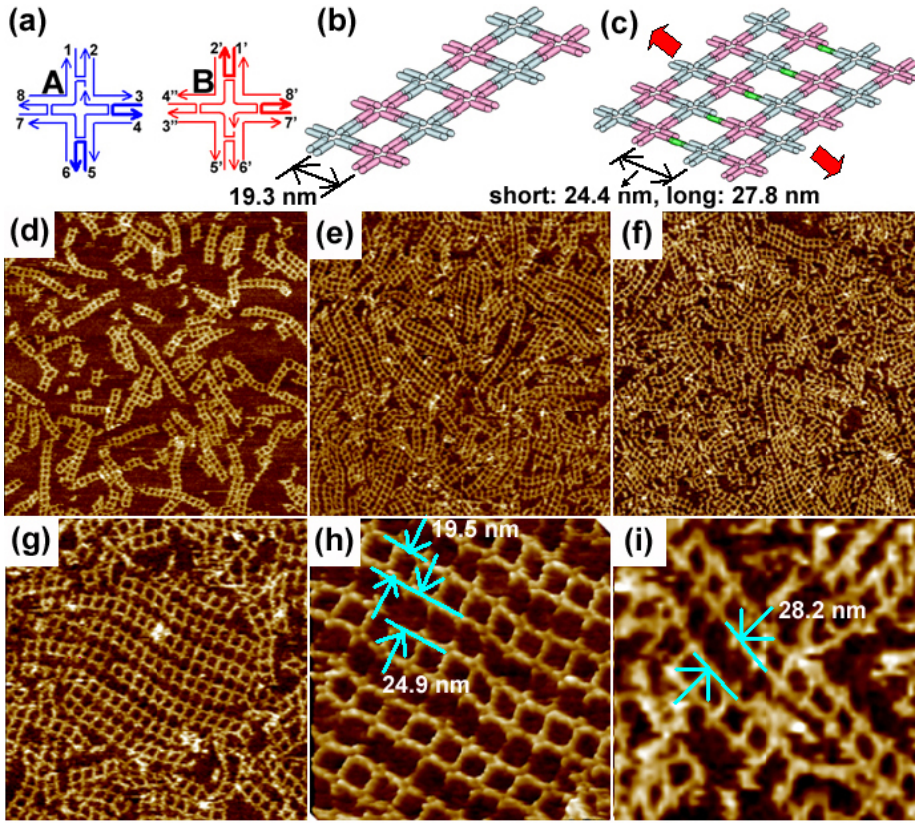

Figure 4.14: AFM images of Nanotrack + double stranded DNA bridges. (a) Simplified drawings of the cross A- and B- tiles for constructing the self-assembled one-dimensional nanotracks. (b) and (c) are cartoons of the nanotracks with and without duplex DNA bridges, respectively. (d) through (f) are AFM images, scan sizes 1 μm × 1 μm, of nanotracks, with the short-bridges and with the long-bridges, respectively. (g) and (h) are high-resolution AFM images of nanotracks with the short-bridges with 500 nm × 500 nm and 200 nm × 200 nm scan sizes. (i) is a high-resolution AFM image of nanotracks with the long-bridges with 200 nm × 200 nm scan sizes. Their dimensions are shown to be in excellent agreement with designed structures.

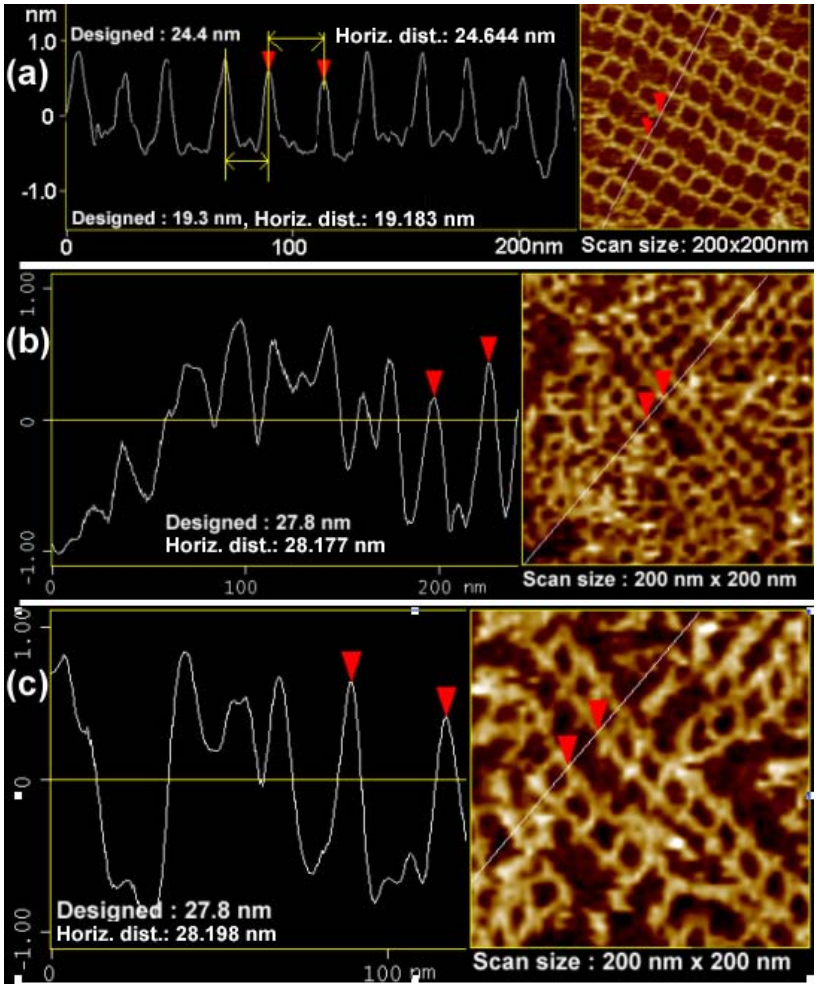

Figure 4.15: Section measurements of Nanotrack + double stranded DNA bridges. Section profile AFM images of (a) nanotracks with the short dsDNA bridges. The measured distance between nanotracks is ~24.6 nm, matching the designed distance, 24.4 nm. (b) and (c) are two examples of section profiles of nanotracks with the long dsDNA bridges. Both data are in excellent agreement with designed structures with less than ± 1 nm differences.

4.3 Summary

We have designed and performed fabrication of size-controllable, fully-addressable, and precisely programmable DNA-based NMs, consisting of two different cross-tiles utilizing a novel stepwise-assembly technique. The reliable stepwise assembly, controlled by annealing temperature with the aid of predominant DNA's properties -molecular level recognition, self-organization, and structuring properties- can be a major step toward developing DNA-based nanotechnology. We have also demonstrated construction of stepwise DNA superstructures consisting of hetero-structure DNA motifs: the cross-tiles and dsDNA molecules. The synthetic dsDNA motif, as a nanobridge for connecting complex DNA superstructures, has two distinct features: size and direction controllability with minimum cost and maximum efficiency.

Chapter 5
DNA-templated Silver Nanowires

Electrical transport measurements in DNA molecules themselves have been considered an interesting research subject for the last decade. Even though some conductivity experiments with DNA have shown wide gap semiconducting [41] or superconducting [42] behavior, most other studies have concluded that DNA molecules are insulators [43, 44]. Rather than relying on electrical transport through DNA itself, we have made use of DNA nanostructures as templates for the specific deposition of highly conductive metallic nanowires. Until recently, mostly native λ-DNA molecules have been used as template for fabricating various metallic nanowires, such as silver [45, 46], gold [47-49], palladium [50-53], platinum [54], copper [55] and semiconducting copper sulfide chains [56]. In this chapter, we present metallic silver nanowires templated by a novel electroless deposition technique (see appendix A2) on artificially designed 1D DNA nanostructures which include the cross-tile nanoribbons, triple-crossover nanotubes, 3HB filaments and synthetic double-stranded DNA (dsDNA) nanowires as well as native λ-DNA molecules. We study electrical transport properties of these silver nanowires.

5.1 Significances of DNA-templated Electronics

Utilizing DNA molecules as scaffolds for making functionalized nanowires have certain advantages such as site-specific alignment [45], site-specific molecular lithography [47], DNA-templated nanoelectronic devices [48] with massive and parallel self-assembly on the near future electronics. A series of breakthrough DNA-based electronic devices was presented by Braun, Sivan, and their collaborators [45-48]. The first direct electrical transport measurement on a native λ-DNA, was published in 1998 by Braun *et al.* [45]. In this experiment, the λ-DNA molecules were stretched onto a mica surface and connected to two metal leads with the gap distance of ~12 μm. This was accomplished using the double-strand molecular recognition between a short single-strand in the end of the long λ-DNA and a complementary single-strand that was connected to the metal lead on each side of the molecule (Figure 5.1a). Conductivity measurements through the λ-DNA that was placed on the mica surface yielded no observable current up to 10 V.

The advances in the recognition of individual molecular-scale electronic devices highlight the demand for useful tools and concepts capable of assembling such devices into macroscale functionalized structures. Keren *et al.* [47] demonstrated sequence-specific molecular lithography on substrate DNA molecules by harnessing homologous recombination by RecA protein (Figure 5.1b). In a sequence-specific manner, they fabricated the coating of DNA with metal, localized labeled molecular objects and grew metal wires on specific sites along the DNA template, and constructed molecular-level accurate, stable DNA junctions for patterning the DNA substrate connectivity. In

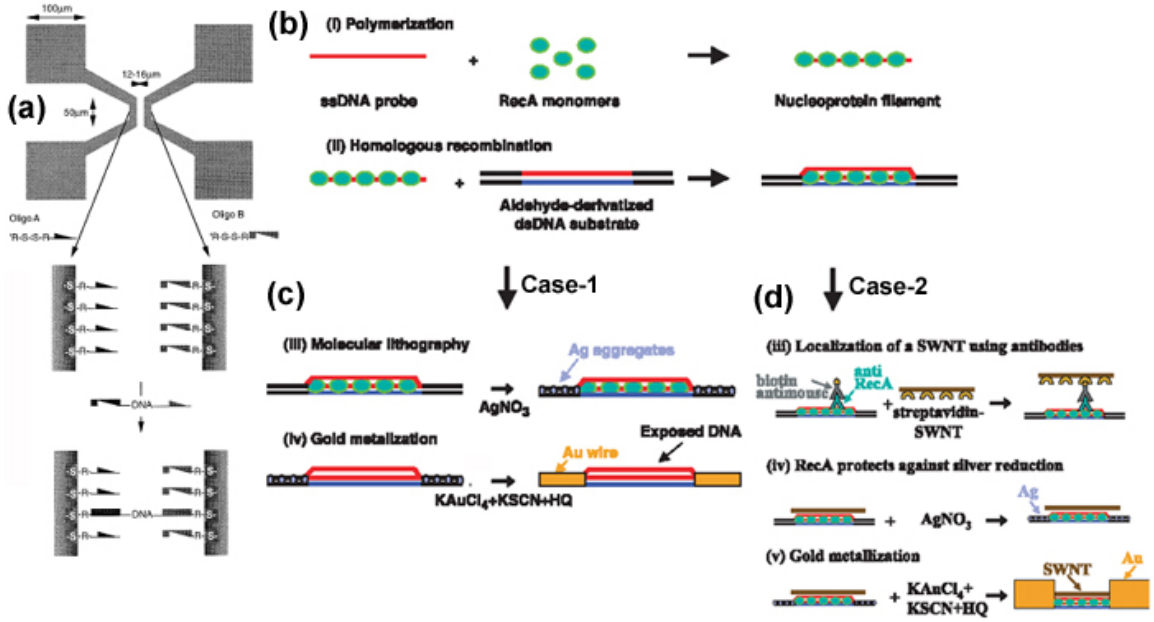

Figure 5.1: (a) λ-DNA oligos with two different sequences attached to the electrodes. λ-DNA bridge connects the two electrodes. (b) Schematics of the homologous recombination reaction and molecular lithography. In part (i), RecA monomers polymerize on a single stranded DNA probe molecule to form a nucleoprotein filament. In part (ii), the nucleoprotein filament binds to an aldehyde-derivatized dsDNA substrate molecule at a homologous sequence. (c) In part (iii), incubation in $AgNO_3$ solution results in the formation of Ag aggregates along the substrate molecule at regions unprotected by RecA. In part (iv), the Ag aggregates serve as catalysts for specific gold deposition, converting the unprotected regions to conductive gold wires. (d) Assembly of a DNA-templated FET and wires contacting it. In part (iii), the DNA-bound RecA is used to localize a streptavidin-functionalized SWNT, utilizing a primary antibody to RecA and a biotin-conjugated secondary antibody. In part (iv), incubation in an $AgNO_3$ solution leads to the formation of silver clusters on the segments that are unprotected by RecA. (v) Electroless gold deposition, using the silver clusters as nucleation centers, results in the formation of two DNA-templated gold wires contacting the SWNT bound at the desired gap. (From Ref. [45, 47, and 48].)

molecular lithography, the information encoded in the DNA molecules replaces the masks used in conventional microelectronics, and the RecA protein serves as the resist. The molecular lithography with the DNA molecules works with high resolution over a broad range of length scales from nanometers to many micrometers (Figure 5.1c).

Keren *et al.* [48] further demonstrated DNA-templated functionalized electronic devices using carbon nanotubes (Figure 5.1d). The combination of their fascinating electronic properties and nanometer-scale dimensions makes carbon nanotubes ideal building blocks for nanoelectronics. The advancement of carbon nanotube–based electronics requires assembly strategies that allow their precise localization and interconnection. Utilizing a scheme based on molecular recognition between building blocks, authors report the realization of a self-assembled carbon nanotube field-effect transistor operating at room temperature. DNA-templated nanostructures provide the full address for precise localization of a semiconducting carbon nanotube as well as the template for the various functionalized metallic wires contacting it.

5.2 Silver Nanowires Templated on Artificially Designed 1D DNA Nanostructures

5.2.1 Nanowire templated on nanoribbon

Here we report on metallized nanoribbons (see section 3.2 for design and characteristics of 1D nanoribbon) with silver using a novel electroless chemical deposition technique (appendix A2) and demonstrate electrical measurements through silver nanowires. The resulting silver nanowires have been characterized by scanning electron microscopy

(SEM) shown in Figure 5.2. The metallized nanoribbons have average heights of 35 nm, average widths of 43 nm, and lengths of up to ~5 μm. The two-probe current-voltage (I-V) curve of the metallic silver nanoribbon shows linear ohmic behavior and the resistance of this sample is ~200 Ω as measured between the two central contacts at bias-voltage, 0.1 V (Figure 5.2c). This resistance corresponds to a bulk resistivity of 2.4×10^{-6} Ω-m. This silver nanowire is easily reproducible and has markedly higher conductivity than previously reported double-helix DNA–templated silver nanowires [45]. The bulk resistivity of polycrystalline silver is much lower (1.6×10^{-8} Ω-m) than that of nanoribbon templated nanowires. The higher resistivities of nanowires that we extract from our measurements may result from granularity of the silver structure and/or high contact resistance between the nanowire and the metal leads.

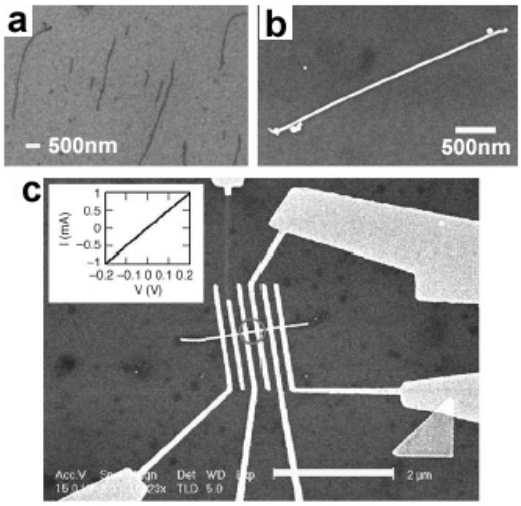

Figure 5.2: Metallization and a conductivity measurement of cross-tile nanoribbon. (a) SEM image of nonmetallized nanoribbons. (b) SEM image of silver-seeded silver nanoribbon. The change in the signal contrast between (a) and (b) is apparent. (c) SEM image of the actual device (scale bar: 2 um). (Inset) The two-probe current-voltage curve of the metallic silver nanowires.

5.2.2 Nanowire templated on triple-crossover nanotube

The construction and characterization of DNA nanotubes, a self-assembling superstructure composed of triple-crossover (TX) tiles and TX nanotube templated silver nanowires are presented. The TX tiles used here have been extensively characterized and described by LaBean *et al.* [37]. The DNA self-assemblies described here were formed

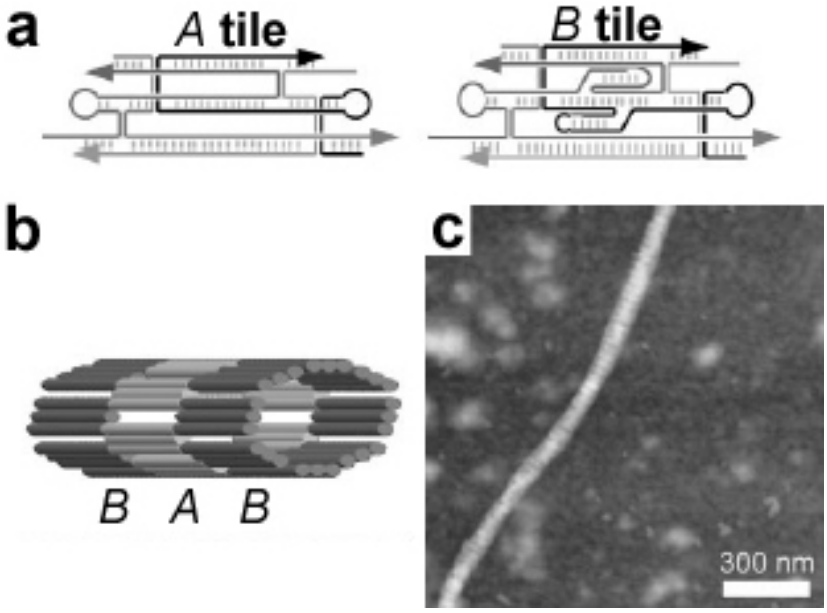

Figure 5.3: (a) Line drawings showing the strand traces through the two tile types used in the constructions. Oligonucleotides are shown in different shades of gray and with arrowheads marking the 3' ends. Short vertical hash marks indicate base-pairing within double-helical regions; paired vertical lines represent crossover points. The central helices of both tile types are terminated with –TTTT– loops. Two extra stem-loops (2J) on the central helix of the B tile are designed to protrude, one into and one out of the tile plane. (b) Cartoon model of a section of TAO nanotube shown with eight tiles per layer of tube. Tubes represent double-helical regions; for simplicity, the 2J stem-loops on the B tiles are not shown. (c) AFM image of TAO nanotube taken by tapping mode in air. The B tile layers are visible as brighter stripes (because of increased height) oriented perpendicular to the long axis of the tube.

from two DNA tile building blocks, a TAO (tile A) and a TAO with two step-loops (2J) (tile B) as shown in Figure 5.3a. Names begin with 'T' for triple-crossover. The second character indicates the relative orientations of their two double-helical domains. Here 'A' stands for anti-parallel. The third character refers to the number of helical half-turns between crossovers, 'O' for an odd number. The B-tile contains two extra dsDNA stems, which form junctions with the central helix of the tile such that they project out of the tile plane, with one stem protruding on each side of the tile. The B-tiles used here are modified by the replacement of the loop on one protruding stem with two thiol groups, one on a 3' and the other on a 5' strand terminus. Burial of the sulfur moieties within the tubes makes logical sense because disulfide bridges are preferred structures formed by thiol groups under physiologic-like solution conditions such as those used here. The formation of disulfide bonds between neighboring B tiles would cause the lattice to curve and form tubes. The left panel in Figure 5.3b shows a section of the proposed structure of the nanotubes with B-tile layers alternating with A-tile layers, dsDNA helix axes aligned parallel with the tube axis, and thiol groups located inside the tubes. Figure 5.3c is a typical AFM Image of TX nanotube which exhibits uniform widths of ~25 nm for lengths of up to 20 μm. Stripes perpendicular to the long axis of the filaments are visible and indicate closed ring structures in successive layers rather than a spiral structure, which would have given stripes with noticeable diagonal slant.

We have also metallized the TX nanotubes with silver using a two-step procedure described in appendix, A2. The resulting nanowires have been characterized by SEM (Figure 5.4). The metallized nanowires have heights of ~35 nm, widths of ~40 nm and

lengths of up to ~5 μm. We have patterned chromium/gold electrodes onto the wires by electron-beam lithography (5 nm Cr followed by 30 nm Au). SEM images of nanowires with attached electrodes are shown in Figures 5.4c and 5.4d. The two-terminal current-voltage (I-V) measurements were conducted on these devices (Figure 5.4e) with various gap distances: 180, 80, and 100 nm, between electrodes 'A and B', 'C and D' and 'D and E' respectively. The I-V curves show mostly linear (ohmic) behavior and give resistances of 2.80, 2.35 and 2.82 kΩ as measured at 0.1 V. Measurements were done at room temperature, 300K. These numbers correspond to bulk resistivities of ~1.4, 3.2, and 3.1 $\times 10^{-5}$ Ω-m, respectively. These nanowires demonstrate much higher conductivity than previously reported dsDNA-templated silver nanowires [45], although their conductivity is slightly lower than reported for dsDNA-templated palladium nanowires [51] and slightly lower than a nanoribbon templated silver nanowire. The silver nanowires reported here as well as the nanoribbon templated silver wire are of much more uniform width and smooth appearance than the rather bumpy and grainy metallic nanowires templated on dsDNA [50-55]. Although the tile-assembly templates (~25 nm) are much wider than dsDNA (~2 nm), the resulting nanowires are generally thinner (~40 nm) than nanowires templated on duplex DNA molecules. These desirable properties may result from tile-assemblies' ability to bind relatively more glutaraldehyde in the first step of the metallization, which then results in smaller grain-size leading to complete fusion of the wires in the second step (see appendix A2 for the two-step metallization).

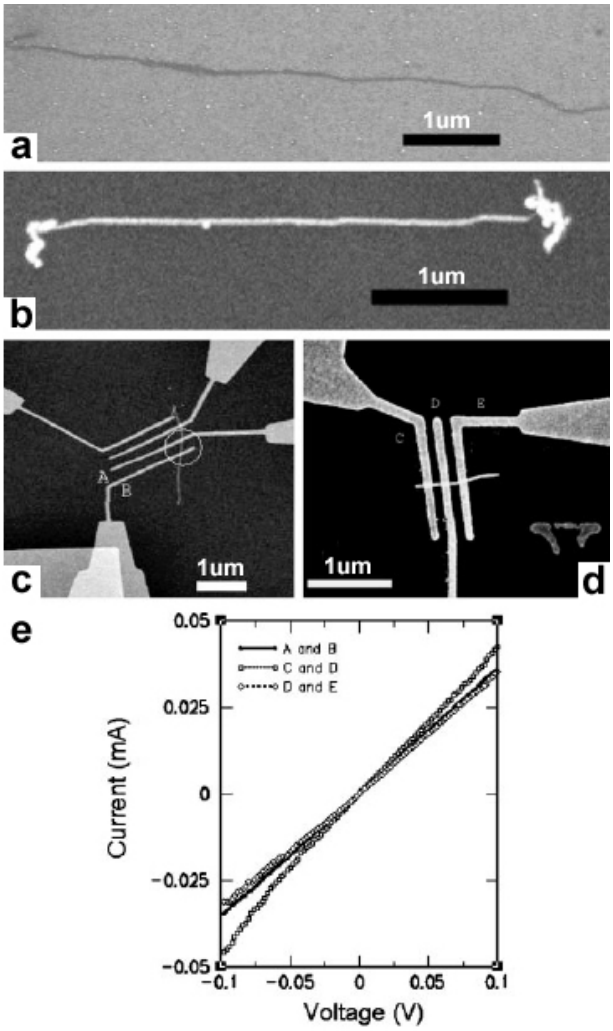

Figure 5.4: (a) SEM image of TX nanotube on the silicon substrate before metallization. (b) SEM image of fully metallized TX nanotube on silicon substrate. The brighter tone of the nanotube in 'b' versus 'a' indicates the increased ability of the metallized nanotube (nanowire) to emit secondary electrons. (c) and (d) SEM images showing metallized TX nanotubes (circled in 'c'), overlaid with chromium/gold electrodes patterned by electron beam lithography and deposited by thermal vapor deposition. The electrodes are labeled A–E. (e) The current–voltage curves measured through the sections of TX templated nanowire between the indicated electrodes.

5.2.3 Nanowire templated on 3HB filament

We performed conductivity measurements using metallized 1D-3HB (see chapter 2 for design and characteristics of 1D-3HB filaments) nanowires at room temperature. Chromium-gold double layer electrodes were deposited onto the nanowires by electron-beam lithography, with 5 nm of Cr followed by 25 nm of Au patterned onto the silicon substrate. An SEM image of a nanowire with attached electrodes is shown in Figure 5.5e (inset). The I-V measurement was conducted on this device with electrode gap distances (wire lengths) of 430 nm, labeled as 'a', and 320 nm, 'b'. The two-terminal I-V curves show mostly linear behavior (obeyed Ohm's law) and give resistances of 1.42 kΩ for 'a' and 1.21 kΩ for 'b' measured at 0.1 V. These numbers correspond to bulk resistivities of 2.25×10^{-6} Ω-m and 2.57×10^{-6} Ω-m for 'a' and 'b' respectively. These nanowires are compatible with conductivity of nanoribbon templated silver nanowires. 3HB templated nanowires have a uniform average width of ~30 nm with negligible granularity compared with the original report of double-stranded DNA (dsDNA) templated silver nanowires by Braun *et al.* [45] which gave ~100 nm widths with clearly visible 30~50 nm grains. Repeatable and reliable metallization processes and successful conductivity measurement show that we have taken a major step toward producing electronic nanodevices using DNA's scaffolding capability and programmability.

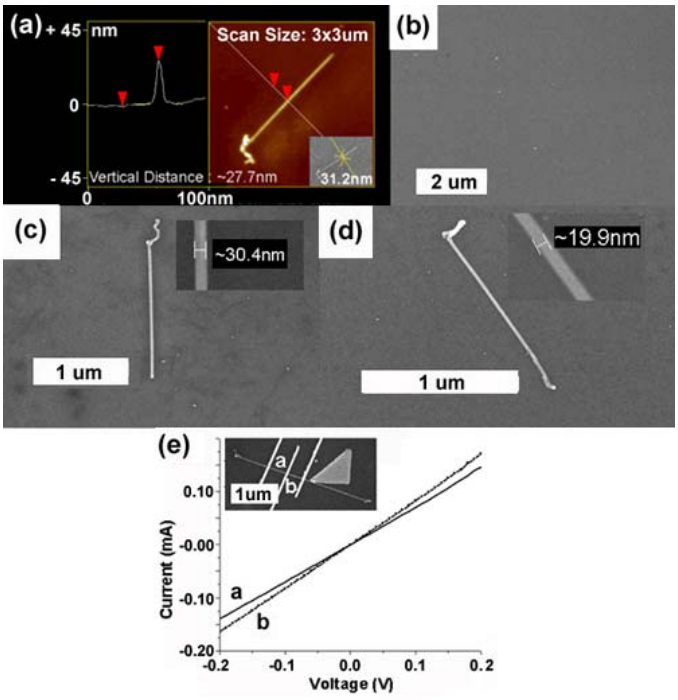

Figure 5.5: (a) Section profile AFM image of a silver nanowire templated on a 1D-3HB filament. (Inset) SEM image of the same nanowire. (b) Control experiment. Without DNA, we do not see any wire-like objects after the metallization process. (c) and (d) SEM images of ~30 nm and ~20 nm width silver nanowires. (e) Current-voltage measurement through a section of 1D-3HB templated silver nanowire. (Inset) an actual electronic device patterned by electron beam lithography.

5.2.4 Nanowire templated on native and synthetic duplex DNA molecules

In this section, we report on the electrical conductivity measurement of metallic silver nanowires templated on native λ-bacteriophage and synthetic dsDNA molecules. After fabricating metallic nanowires by an electroless chemical deposition method, the metallized nanowires have a diameter down to 15 nm which are among the thinnest metallic nanowires available to date by any method. After two-terminal I-V measurements over 70 different samples, we observe DNA templated silver nanowires with electrodes results in three distinct electrical behaviors at room temperature: ohmic (~40 %), nonohmic (~15 %), and insulating (~45 %). DNA-templated functionalized nanowires represent a potential breakthrough in the self-assembly of nanometer-scale structures for electronics-layout because they can be targeted to connect at specific locations on larger-scale circuits [45].

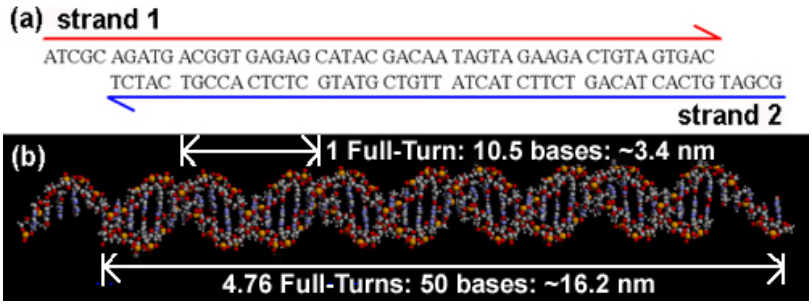

Figure 5.6: (a) DNA base sequences of synthetic dsDNA molecules. Arrows indicate simplified strands running from 5' to 3'. The complementary sticky-end of *a* is *a'*. (b) An atomic-resolution cartoon of a unit dsDNA molecule which consists of 50 base-pairs and has a length, ~16.2 nm.

DNA base sequence of the synthetic unit dsDNA tile was designed to minimize the chance of sequence symmetry and undesired associations. The strand sequence for the molecules used here is given in Figure 5.6a. A unit dsDNA molecule consists of 50 base-pairs and has a length ~16.2 nm. Native λ-DNA with the concentration of 1.6 nM and synthetic dsDNA molecules of 1.0 μM are visualized by taping mode AFM in air and under buffer, respectively. Figure 5.7a is an AFM image of λ-DNA and Figure 5.7b, synthetic. From the inset in Figure 5.7b, we clearly see helixes of DNA molecules with a pitch-to-pitch distance of 3.4 ± 0.3 nm, in excellent agreement with the original distance of ~3.4 nm. Representative section profiles of single λ-DNA height of ~0.7 nm and synthetic dsDNA of ~1.1 nm are shown in Figures 5.7c and 5.7d. Empirically, we noticed that the tapping mode AFM heights of single layer duplex DNA molecules were 0.6 ± 0.2 nm in air [57] and 1.2 ± 0.2 nm under physiological 1×TAE/Mg^{2+} buffer (see appendix A1) where the known diameter of the double-helix DNA molecules was ~2 nm. We applied a two-step metallization process to coat λ-DNA and synthetic dsDNA molecules in silver on a silicon substrate. Figures 5.7e and 5.7f are SEM images of λ- and synthetic-dsDNA templated silver nanowires. The average width of metallized nanowires is ~25 nm and length up to 7 μm. We observed that metallized nanowires were slightly wider (measured by SEM) than their height (measured by AFM); the ratio of height to width was ~0.9.

This DNA molecule's poor conductivity prevents its direct use in electronic nanodevices. Here we perform two-terminal I-V measurements using silver nanowires templated on both λ- and synthetic- dsDNA molecules. Initially, almost all nanowires

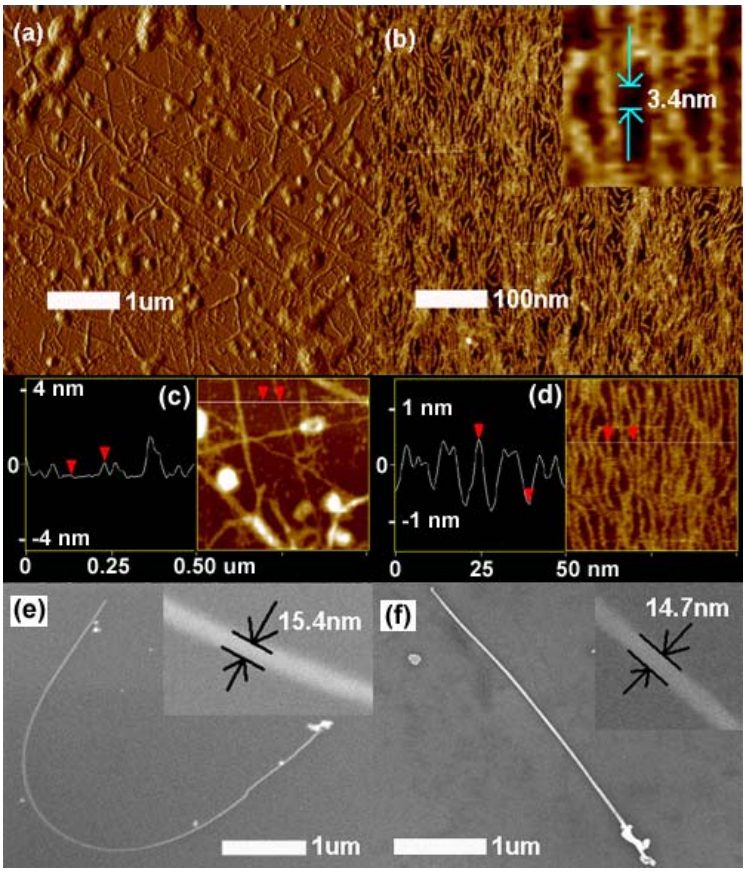

Figure 5.7: (a) AFM image of λ-DNA in air. (b) AFM image of synthetic dsDNA in liquid-phase. (Inset) High resolution AFM image. We observed pitch-to-pitch distance on dsDNA was 3.4 ± 0.3 nm which exactly corresponds to a known full-turn distance of duplex DNA molecules. (c) and (d) are height measurements of single λ-DNA (~0.7 nm) in air and synthetic dsDNA (~1.1 nm) molecules under buffer. (e) and (f) are SEM images of λ- and synthetic- dsDNA after two-step silver metallization process.

showed no currents probably due to a contamination layer between the wire and the electrode and/or due to the native silver oxide. After first few scans of voltages with careful monitoring of current, 30 samples out of 70 measured nanowires resulted in resistances (R) ≥ 10 GΩ and did not show substantial current even at voltages higher than 5 V. After applying bias voltages higher than 5 V, most nanowires were damaged severely and became disconnected. Nonlinear characteristics of two-terminal I-V curves of silver nanowires were also observed after initial scans of bias voltage. About 15 % of nanowires are nonohmic and have slightly asymmetrical I(V) with respect to the zero bias. The length of the zero bias plateaus varies from a few mV to ~6 V. Four I-V nonlinearities are shown in Figure 5.8.

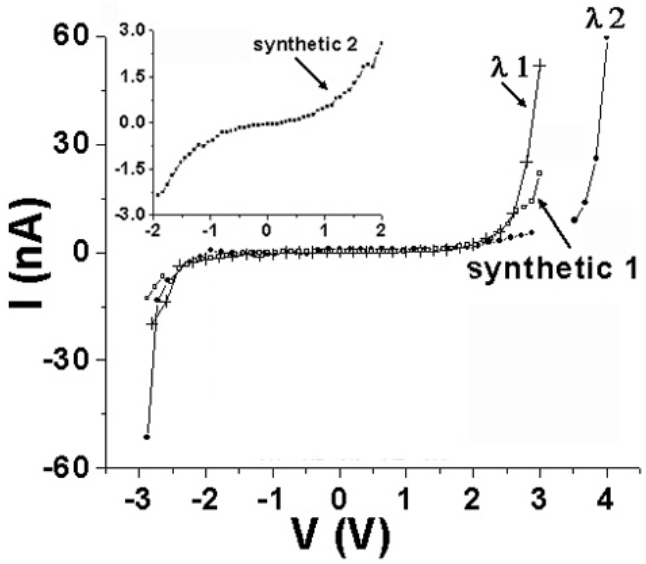

Figure 5.8: Nonlinear characteristics of two-terminal I-V curves of silver nanowires. About 15 % of total measured nanowires are nonohmic and have slightly asymmetrical I(V) with respect to zero bias. The width of the zero bias plateaus varies from a few mV to ~6 V. Among them, four sets of data are shown above.

About 40 % of the measured nanowires were highly conductive and showed ohmic behavior. In many samples, the as-prepared wire resistance is very high, and could dramatically decrease following several voltage sweeps in the range of about +/- 3V (Figure 5.9a). Most probably the initial high resistance is caused by an oxide or contamination layer covering the nanowire, which prevents formation of an adequate contact between the nanowire and the metal leads. This layer is evidently destroyed upon application of a large enough critical source-drain voltage, V_c. The magnitude of V_c in different nanowires varies from a few mV to roughly 3 V. The two-terminal I-V curves of the samples in the low-resistance state show mostly linear behavior and demonstrate resistances of 895 Ω for a first λ-DNA templated nanowire (λ1), 597 Ω for a λ2, 798 Ω for a first synthetic dsDNA templated nanowire (synthetic-1), and 784 Ω for a synthetic-2 measured at 0.1 V. These numbers correspond to bulk resistivities (ρ) of ~22.4, 10.0, 4.7, 3.8×10^{-6} Ω-m for λ1, λ2, synthetic-1, and synthetic-2 respectively. We observed that larger V_c were roughly proportional to larger R. Finally Figure 5.9b shows I-V curves of ~30 nm width nanowire with ~110 nm between electrodes and shows R of ~500 Ω at 300 K and ~30 Ω at 77 K. This change of resistance (~17 times for a change in temperature of about 4 times) is unexpectedly large, comparable to the available data on nanostructured silver films of a significantly higher conductivity [58]. It is possible that the cross-section of wire is much smaller than the apparent wire width. So the actual wire conductance is higher than our estimate.

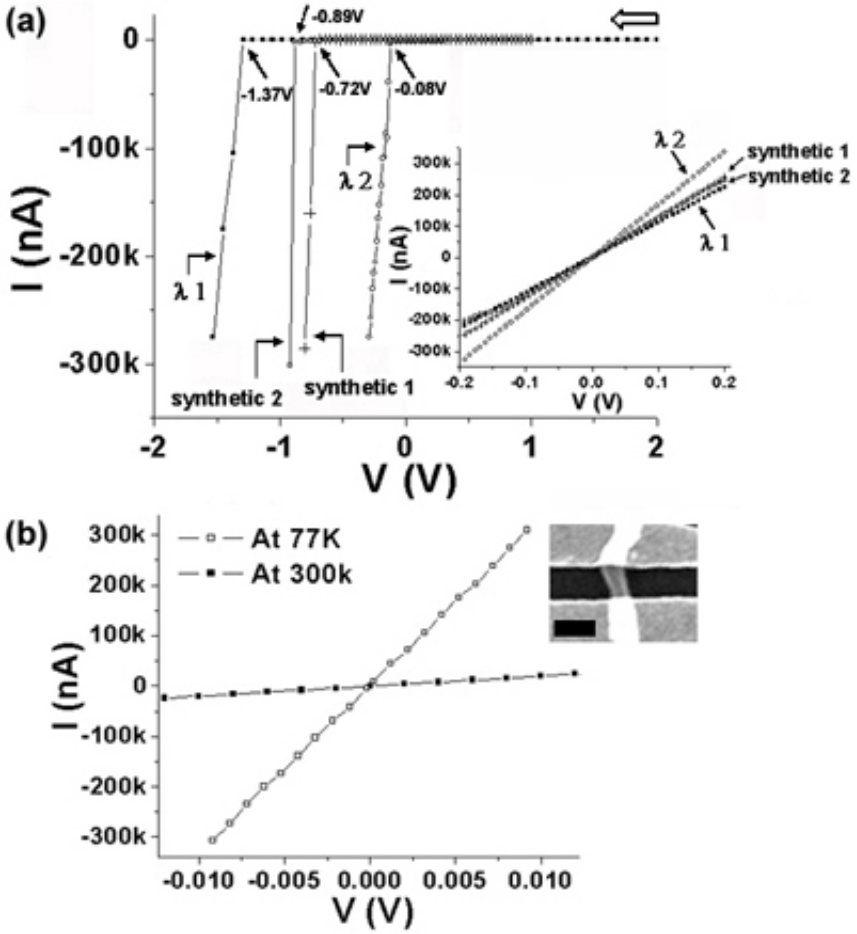

Figure 5.9: Linear characteristics of the two-terminal I-V measurement of silver nanowires. About 40% of total measured nanowires are highly conductive and show ohmic behavior. (a) Removal process of the barrier layers between electrodes and silver nanowires by applying bias voltages. White arrow indicates voltage scan direction. After the first few scans of bias voltages, current dramatically changes at certain critical voltage, V_c. (Inset) The I-V curves after breakdown of the barrier layers. (b) I-V curves of a silver nanowire measured at two different temperatures, 300 K and 77 K. (Inset) SEM image of an actual device with scale bar, 100 nm. Cr-Au double layer electrodes onto the nanowires, with 5 nm of Cr followed by 25 nm of Au were patterned by electron beam lithography on the silicon substrate.

5.3 Summary

We have presented fabrication of metallic silver nanowires templated on artificially designed 1D DNA nanostructures, as well as native λ-DNA molecules by an electroless deposition technique and demonstration of electrical measurements through silver nanowires. DNA-templated silver nanowires have a uniform width with a diameter down to ~15 nm. The wires have been contacted by leads formed by electron beam lithography and show various interesting electronic behaviors: nonconducting, nonlinear, and ohmic.

Chapter 6
Conclusions and Perspectives

In the final chapter of this thesis, we review the main results of our experiments and discuss the direction of future work in DNA self-assembly and DNA-based nanoelectronics: the possibility of the construction of functionalized electronic devices such as single electron transistors (SET) [59, 60], spin-related devices [61, 62], and quantum-dot cellular automata [63] based on properly designed DNA superstructures as templates.

6.1 Conclusions

About 50 years ago, Watson and Crick put the model and the data together to explain the double-helical molecular structure of DNA to the world. Today people are able to manipulate DNA molecules for use as an engineering material with unprecedented predictability and repeatability. In this thesis, we have presented several 1D- and 2D-DNA nanostructure including 3HB filaments, lattices, cross-tile nanoribbons, nanotracks, and nanogrids:

- 3HB consists of three double-helical DNA domains connected by six immobile crossover junctions such that the helix axes are not coplanar. The 3HB motif presents a triangular cross-section with one helix lying in the groove formed by

the other two. By differential programming of sticky-ends, 3HB tiles can be arrayed in two distinct lattice conformations: 1D-filaments and 2D-lattices.

- A unique and versatile cross-tile consisting of four four-arm junctions oriented with a square aspect ratio was also designed and constructed. Programmable self-assembly of cross-tiles resulted in four distinct lattice morphologies: uniform-width nanoribbons and nanogrids made from a single unit cross-tile, and nanotracks and nanogrids using two unit cross-tiles. We have reported on fabrication of size-controllable and fully-addressable DNA-based nanomatrices which consist of two different cross-tiles using a novel stepwise-assembly technique. The reliable and easily reproducible fixed-size DNA nanostructures as templates should lead to a big step toward developing nano/bio technologies. Construction of DNA superstructures consisting of cross-tiles and duplex DNA molecules for controlling length and directionality of superstructures were also demonstrated.

- Rather than relying on electrical transport through DNA itself, we have made use of DNA nanostructures as templates for the specific deposition of highly functionalized nanowires. DNA-templated silver nanowires represent a potential breakthrough in the self-assembly of nanometer-scale structures for electronics-layout because they can be targeted to connect at specific locations on larger-scale circuits. We have succeeded in fabrication silver nanowires templated on artificially designed 1D DNA nanostructures, such as the cross-tile nanoribbons,

triple-crossover nanotubes, 3HB filaments and synthetic double stranded DNA nanowires as well as native λ-DNA molecules by a two-step metallization technique and demonstration of electrical measurements through silver nanowires at room temperature.

These DNA tiles, lattices and nanowires, are promising candidate structures for targeted self-assembly of nanoelectronic components and circuits. This interdisciplinary work has implications for a large number of fields of science and technology; it adds to the toolbox available for studying artificial self-assembling systems which may model some aspects of biological systems and enables nanofabrication techniques which may lead to programmable nanomachines and nano- and micro- molecular electronics.

6.2 Perspectives

DNA-based nanotechnology is the latest realm in bio/nano science and technology. However, the future of DNA-based nanotechnology depends mainly on the highly efficient, reliable fabrication of self-assembled DNA nanostructures and device applications of nanoscale objects organized by DNA templates for real-world applications. Among the different biomaterials, DNA is of great interest as a template for the construction of nano-circuitries and opens great possibilities for the construction of functionalized electronic devices in the near future.

Appendices

A.1 DNA Sample Preparation

The design of the DNA tiles and superstructure assemblies analyzed were based on the structure of immobile branched junctions. DNA base sequences were designed with the program SEQUIN [35] (see section 1.3) to minimize the chance of undesired complementarity and base sequence symmetry. Custom oligonucleotides were purchased from Integrated DNA Technology (www.idtdna.com) and purified by PAGE. Complexes were formed by mixing a stoichiometric quantity of each strand, as estimated by OD_{260} in 1×TAE/Mg^{2+} buffer (20 mM Tris-acetate (pH 7.6), 2 mM EDTA, 12.5 mM $MgCl_2$). The final concentration of DNA was between 0.1 and 1.0 μM, and the final volume was 30 ~ 120 μL. Oligo mixtures were cooled slowly from 90 °C to 20 °C by placing the microtubes in 2 L of boiled water in a styrofoam box for at least 40 hours to facilitate hybridization. Non-denaturing polyacrylamide gel electrophoresis in A.4 and thermal profile experiments were described in Ref. 37.

A.2 Denaturing Polyacrylamide Gel Electrophoresis

Protocols:

(1) Turn on water bath at 50 °C.

(2) Clean spacer/glasses/comb with dI H_2O and acetone.

(3) Assemble them, using high vacuum grease on edges to prevent leakage.

(4) For 10 % (12 %), denature PAGE gel, add 20 % denature PAGE gel 20 mL (24 mL), 0 % denature PAGE gel 20 mL (16 mL), 10 % Ammonium persulfate 300 μL, and TEMED 16.8 μL. Mix by swirling.

(5) Leave the mixture on the bench at room temperature for 30 ~ 60 minutes for it to polymerize.

(6) Take out comb and cover with "cover head". Use high vacuum grease to prevent leakage.

(7) Add in dI H_2O and rinse the wells.

(8) Prepare DNA sample. Use 2×denaturing dye (1:1) with the sample. Incubate it at 90 °C for 5 minutes. Load sample up to 50 μL per well for thick spacer.

(9) Run gel at 200 ~ 300 V for around 0.5 ~ 3 hours depending on the length of the interested DNA fragments.

(10) Process the Gel. Stain with EB for 5 minutes and use fluorescence for taking a picture.

A.3 Purification of DNA

Protocols:

(1) Add in 500 μL elution buffer to the cut gel. Shake in cold room over night.

(2) Take the 500 μL elution buffer to a new microcentrifuge tube.

(3) Add in 1000 μL Butyl Alcohol, vortex the microcentrifuge tube for 1 minute, and centrifuge it at 800 rpm for 1 minute.

(4) After the spin, discard the upper layer of Butyl Alcohol with pipette.

(5) Add in 99 % EtOH 1000 μL, and mix well. Leave the mixture on dry ice for 30 minutes.

(6) Spin at 13K rpm for 30 minutes at cold room, 4 ºC.

(7) Pour out EtOH, and add in 70 % EtOH 1000 μL and mix well.

(8) Centrifuge it at 13K rpm for 20 minutes at cold room. Pour the liquid out.

(9) Use vacufuge to dry the sample for 4 hours at 30 ºC.

(10) Add in 50 μL dI H_2O, vortex violently for 1 minute to dissolve the DNA fragments.

A.4 DNA Concentration Measurement

Protocols:

(1) The following protocol measure DNA concentration by measuring light absorbance at 260 nm wavelength.

(2) Turn on UV spectrophotometer to warm up.

(3) UV spectrometer initialization. Choose mode 1, photometric; parameter change: yes; program number 1, set at 260 nm; program number 5, set at 260 nm; got to λ = 260 nm, λ1 = 260 nm; enter scanning.

(4) Clean cubic tube. dI H_2O wash, 3 times; acid/ethanol wash, 3; dI H_2O wash; finally 95 % EtOH wash; and dry.

(5) Add in 200 μL dI H_2O. Set Auto Zero.

(6) Prepare sample. Add 50 μL dI H_2O into each microcentrifuge tube containing DNA fragments, vortex vigorously; take 1 μL DNA fragments sample, and add 199 μL dI H_2O

so that the total volume is 200 μL. Mix well; transfer the solution to the cubic box; after each measurement, wash the cubic box, and set Auto Zero.

(7) To calculate OD, use the work sheet DNA Spec measurement.

A.5 Non-denaturing Polyacrylamide Gel Electrophoresis

Protocols:

(1) Clean spacer/glasses/comb with dI H_2O and acetone.

(2) Assemble them, using high vacuum grease on edges to prevent leakage.

(3) For 8 % (12 %), 40 % Acrg-Stock solution 8 mL (12 mL), 10×TAE/ Mg^{2+} 4 mL, dI H_2O 28 mL (24 mL), 10 % Ammonium persulfate 300 μL, and TEMED 16.8 μL. Mix by swirling.

(4) Leave the mixture on the bench at room temperature for 30 ~ 60 minutes for it to polymerize.

(5) Take out comb and cover with "cover head". Use high vacuum grease to prevent leakage.

(6) Add in dI H_2O and rinse the wells.

(7) Prepare DNA sample. Add non-denaturing dye (10:1) with the annealed sample. Load sample up to 50 μL per well for thick spacer.

(8) Run gel at 200 ~ 300 V for around 0.5 ~ 3 hours depending on the length of the interested DNA fragments.

(9) Process the Gel. Stain with EB for 5 minutes and use fluorescence for taking a picture.

A.6 Streptavidin Attachment

Protocols:

(1) After DNA assembly (usually incubated 4 °C for 8 hours after annealing), add streptavidin purchased from Rockland (www.rockland-inc.com, code no: S000-01, Lot no: 12088) of same volume of equal concentration of biotin in annealed DNA sample, mostly 0.2 uM to 1uM.

(2) After adding streptavidin in sample, leave 1 hour at room temperature, then incubate 4 °C for overnight.

A.7 Two-step Silver Metallization

A DNA sample was seeded with silver using the glutaraldehyde method. Annealed DNA was incubated with 0.2 % glutaraldehyde in 1×TAE/Mg^{2+} buffer on ice for 20 minutes, then at room temperature for 20 minutes, then the sample was loaded into a Slide-A-Lyzer Mini Dialysis unit, (7000 MWCO, Pierce, Rockford, IL) and dialysised overnight at 4 °C in 1 L of 1×TAE/Mg^{2+} buffer. The published method [45] was modified in that the silver seeding was done in aqueous solution for 20 minutes instead of on substrate. Then 10 μL was deposited onto silicon substrate, allowed to absorb for 5-10 minutes; then excess reagent was rinsed off with distilled water, and dried under a stream of nitrogen. Silicon substrate was treated with aminopropyltriethoxysilane (APS) prior to DNA sample deposition for better adhesion to the substrate. In the second step, HQ SILVER^{TM}-EM Formulation (www.nanoprobes.com) was used according to the

manufacturer's instructions. One unit of initiator (A) was mixed with one unit of moderator (B) and one unit of activator (C). Then 10 μL of this fresh mixture was pipetted onto the substrate and left for 5-10 minutes. Finally excess reagent was rinsed off with distilled water and dried under a stream of nitrogen.

Protocols:

(1) Prepare DNA sample (DNA concentration, 1.0 ~ 0.2 μM) in 1×TAE/Mg^{2+} buffer (20 mM Tris-acetate (pH 7.6), 2 mM EDTA, 12.5 mM $MgCl_2$).

(2) Prepare 0.4 % glutaraldehyde aqueous solution. Mix 25 % glutaraldehyde aqueous solution (Tousimis Research Corporation) 1.6 μL in 1×TAE/Mg^{2+} buffer 98.4 μL. Total volume of the mixture is 100 μL.

(3) Mix equal volumes of DNA sample (say, 50 μL) and 0.4 % glutaraldehyde (50 μL). Do not vortex it if DNA sample was annealed.

(4) Incubate the mixture for 20 minutes at room temperature and then for 20 minutes on ice.

(5) Excess glutaraldehyde was filtered out by overnight dialysis. The sample was loaded into a Slide-A-Lyzer Mini Dialysis unit, (7000 MWCO, Pierce, Rockford, IL) and dialysised overnight at 4 °C in 1 L of 1×TAE/Mg^{2+} buffer.

(6) Take out 50 μL of aldehyde-derivatized DNA sample to a new microcentrifuge tube.

(7) Add the initiator (Solution A) (HQ SILVER™-EM Formulation, Nanoprobes Inc.) 50 μL into the aldehyde-derivatized DNA sample and leave for 20 minutes at dark room.

(8) Silicon substrate was treated with 1 % Aminopropyltriethoxysilane (APS) prior to DNA sample deposition for better adhesion to the substrate. Deposit 1 % APS 20 μL to a substrate, 5 mm × 5 mm, and then leave it for 10 minutes.

(9) Rinsed off with dI H_2O and dried under a stream of nitrogen.

(10) Deposit 15 μL of the silver seeded DNA sample on the substrate and leave for 10 minutes at dark room. Rinsed with dI H_2O and dried under a stream of nitrogen.

(11) In the second step, HQ SILVER^{TM}-EM Formulation was used according to the manufacturer's instructions. One unit of initiator (Solution A) was mixed with one unit of moderator (Solution B) and one unit of activator (Solution C). Vortex the mixture for 1 minute. Then 15 μL of this fresh mixture was pipetted onto the silicon substrate and left for 5-10 minutes at dark room.

(12) Finally excess reagent was rinsed off with dI H_2O and dried under a stream of nitrogen.

A.8 AFM Imaging

AFM imaging was obtained on a Digital Instruments Nanoscope IIIa with a multimode head by tapping mode under buffer. For AFM imaging in air, samples were prepared by pipetting annealed DNA solution (~10 μL) onto freshly cleaved mica (Ted Pella, Inc.), allowed to adhere for 2 minutes, rinsed gently by doming a drop of DI water onto the mica, then air dried either under a stream of nitrogen or by gentle waving. For AFM imaging under buffer, ~5 μL sample was spotted on freshly cleaved mica and left to adhere to the surface for 5 minutes. Then, 30 μL 1×TAE/Mg^{2+} buffer was placed onto the

mica and another 30 μL of buffer was pipetted onto the AFM tip. Imaging was performed under 1×TAE/Mg^{2+} in a tapping mode fluid cell on a Multimode NanoScope IIIa (Digital Instruments), using NP-S tips (Veeco Inc.).

References

[1] Watson, J. D., and Crick, F. H., Molecular structure of nucleic acids, *Nature*, **171**, 737-738, 1953.

[2] Hancock, J. T., Molecular genetics, *Butterworth-Heinemann*, 1999.

[3] Seeman, N. C., DNA in a material world, *Nature*, **421**, 427-431, 2003.

[4] Seeman, N. C., Nucleic acid nanostructures and topology, *Angew. Chem. Int. Ed.*, **37**, 3220-3238, 1998.

[5] Ito, Y., and Fukusaki, E., DNA as a nanomaterial, *J. Mol. Catalysis B: Enzymatic*, **28**, 155-166, 2004.

[6] Seeman, N. C., Nucleic-acid junctions and lattices, *J. Theor. Biol.*, **99**, 237-247, 1982.

[7] Seeman, N. C., Wang, H., Yang, X., Liu, F., Mao, C., Sun, W., Wenzler, L., Shen, Z., Sha, R., Yan, H., Wong, M. H., Sa-Ardyen, P., Liu, B., Qiu, H., Li, X., Qi, J., Du, S. M., Zhang, Y., Mueller, J. E., Fu, T., Wang Y., and Chen, J., New motifs in DNA nanotechnology, *Nanotechnology*, **9**, 257-273, 1998.

[8] Zhang, X., Yan, H., Shen, Z., and Seeman, N. C., Paranemic cohesion of topologically-closed DNA molecules, *J. Am. Chem. Soc.*, **124**, 12940-12941, 2002.

[9] Winfree, E., Liu, F., Wenzler, L. A., and Seeman, N.C., Design and self-assembly of two-dimensional DNA crystals, *Nature*, **394**, 539-544, 1998.

[10] Mao, C., Sun, W., and Seeman, N.C., Designed two-dimensional DNA Holliday junction arrays visualized by atomic force microscopy, *J. Am. Chem. Soc.*, **121**, 5437-5442, 1999.

[11] Rothemund, P., Ekani-Nkodo, A., Papadakis, N., Kumar, A., Fygenson, D. K., and Winfree, E., Design and characterization of programmable DNA nanotubes, *J. Am. Chem. Soc.*, **126**, 16344-16352, 2004.

[12] Ekani-Nkodo, A., Kumar, A., and Fygenson, D. K., Joining and scission in the self-assembly of nanotubes from DNA tiles, *Phys. Rev. Lett.*, **93**, 2683011-2683014, 2004.

[13] Mitchell, J. C., Robin-Harris, J., Malo, J., Bath, J., and Turberfield, A. J., Self-assembly of chiral DNA nanotubes, *J. Am. Chem. Soc.*, **126**, 16342-16343, 2004.

[14] Li., H., Park, S. H., Reif, J. H., LaBean, T. H., and Yan, H., DNA-templated self-assembly of protein and nanoparticle linear arrays, *J. Am. Chem. Soc.*, **126**, 418-419, 2004.

[15] Liu, D., Park, S. H., Reif, J. H., and LaBean, T. H., DNA nanotubes self-assembled from triple-crossover tiles as templates for conductive nanowires, *Proc. Natl. Acad. Sci.*, **101**, 717-722, 2004.

[16] Zhang, Y., and Seeman, N. C., The construction of a DNA truncated octahedron, *J. Am. Chem. Soc.*, **116**, 1661-1669, 1994.

[17] Shih, W. M., Quispe, J. D., and Joyce, G. F., A 1.7-kilobase single-stranded DNA that folds into a nanoscale octahedron, *Nature*, **427**, 618-621, 2004.

[18] Mao, C., Sun, W., Shen, Z., and Seeman, N.C., A DNA nanomechanical device based on the B-Z transition, *Nature*, **397**, 144-146, 1999.

[19] Yurke, B., Turberfield, A. J., Mills, A. P., Simmel, F., and Neumann, J. L., A DNA-fueled molecular machine made of DNA, *Nature*, **406**, 605-608, 2000.

[20] Yan, H., Zhang, X., Shen, Z., and Seeman, N.C., A robust DNA mechanical device controlled by hybridization topology, *Nature*, **415**, 62-65, 2002.

[21] Turberfield, A. J., and Mitchell, J. C., DNA fuel for free-running nanomachines, *Phys. Rev. Lett.*, **90**, 1181021-1181024, 2003.

[22] Shen, Z., Yan, H., Wang, T., and Seeman, N.C., Paranemic crossover DNA: A generalized holliday structure with applications in nanotechnology, *J. Am. Chem. Soc.*, **126**, 1666-1674, 2004.

[23] Peng, L., Park, S. H., Reif, J. H., and Yan, H., A two-state DNA lattice switched by DNA nanoactuator, *Angew. Chem. Int. Ed.*, **42**, 4342-4346, 2003.

[24] Yin, P., Yan, H., Daniell, X. G., Turberfield, A. J., and Reif, J. H., A unidirectional DNA walker that moves autonomously along a track, *Angew. Chem. Int. Ed.*, **43**, 4906-4911, 2004.

[25] Adleman, L., Molecular computation of solutions to combinatorial problems, *Science*, **266**, 1021-1024, 1994.

[26] Winfree, E., Algorithmic self-assembly of DNA: theoretical motivations and 2D assembly experiments, *J. Biomol. Struct. Dyns.*, **11**, 263-270, 2000.

[27] Mao, C., LaBean, T. H., Reif, J. H., and Seeman, N. C., Logical computation using algorithmic self-assembly of DNA triple crossover molecules, *Nature*, **407**, 493-496, 2000.

[28] Benenson, Y., Paz-Elizur, T., Adar, R., Keinan, E., Livneh, Z., and Shapiro, E., Programmable and autonomous computing machine made of biomolecules, *Nature*, **414**, 430-434, 2001.

[29] Ravinderjit B., Chelyapov, N., Johnson, C., Rothemund, P., and Adleman, L., Solution of a 20-variable 3-SAT problem on a DNA computer, *Science*, **296**, 499-502, 2002.

[30] Dwyer, C., Poulton, J., Taylor, R., and Vicci, L., DNA self-assembled parallel computer architectures, *Nanotechnology*, **15**, 1688-1694, 2004.

[31] Rothemund, P., Papadakis, N., and Winfree, E., Algorithmic self-assembly of DNA Sierpinski triangles, *PLOS Biology*, **2**, 2041-2053, 2004.

[32] Niemeyer, C. M., Burger, W., and Peplies, J., Covalvent DNA-streptavidin conjugates as building blocks for novel biometallic nanostructures, *Angew. Chem. Int. Ed.*, **37**, 2265-2268, 1998.

[33] Storhoff, J. J., and Mirkin, C. A., Programmed materials synthesis with DNA, *Chem. Rev.*, **99**, 1849-1862, 1999.

[34] Baker, S. E., Cai, W., Lasseter, T. L., Weidkamp, K. P., and Hamers, R. J., Covalently bonded adducts of deoxyribonucleic acid oligonucleotides with single-wall carbon nanotubes, *Nano. Lett.*, **2**, 1413-1417, 2002.

[35] Seeman, N C., De Novo design of sequences for nucleic acid structural engineering, *J. Biomol. Struct. Dyns.*, **8**, 573-581, 1990.

[36] Fu, T., and Seeman, N. C., DNA double-crossover molecules., *Biochemistry*, **32**, 3211-3220, 1993.

[37] LaBean, T. H., Yan, H., Kopatsch, J., Liu, F., Winfree, E., Reif, J. H., and Seeman, N. C., Construction, analysis, ligation, and self-assembly of DNA triple crossover complexes, *J. Am. Chem. Soc.*, **122**, 1848-1860, 2000.

[38] Yan, H., Park, S. H., Finkelstein, G., Reif, J. H., and LaBean, T. H., DNA-templated self-assembly of protein arrays and highly conductive nanowires, *Science*, **301**, 1882-1884, 2003.

[39] LaBean, T. H., and Park, S. H., Edited by Kumar, C., Self-assembled DNA Nanotubes, *Nanotechnologies for the Life Sciences (Book Series): Vol.* **2**. *Biological and Pharmaceutical Nanomaterials*, 2005.

[40] Chworos, A., Severcan, I., Koyfman, A., Weinkam, P., Oroudjev, E., Hansma, H., and Jaeger, L., Building programmable jigsaw puzzles with RNA, *Science*, **306**, 2068-2072 2004.

[41] Porath, D., Bezryadin, A., de Vries, S., and Dekker, C., Direct measurement of electrical transport through DNA molecules, *Nature*, **403**, 635-638, 2000.

[42] Kasumov, A., Kociak, M., Gueron, S., Reulet, B., Volkov, V. T., Klinov, D. V., and Bouchiat, H., Proximity-induced superconductivity in DNA, *Science*, **291**, 280-282, 2001.

[43] Storm, A., van Noort, J., de Vries, D., and Dekker, C., Insulating behavior for DNA molecules between nanoelectrodes at the 100 nm length scale, *Appl. Phys. Lett.*, **79**, 3881-3883, 2001.

[44] de Pablo, P. J., Moreno-Herrero, F., Colchero, J., Herrero, J., Herrero, P., Baro, A. M., Ordejon, P., Soler, J., and Artacho, E., Absence of dc-conductivity in λ-DNA, *Phys. Rev. Lett.*, **85**, 4992-4995, 2000.

[45] Braun, E., Eichen, Y., Sivan, U., and Ben-Yoseph, G., DNA-templated assembly and electrode attachment of a conducting silver wire, *Nature*, **391**, 775-778, 1998.

[46] Eichen, Y., Braun, E., Sivan, U., and Ben-Yoseph, G., Self-assembly of nanoelectronic components and circuits using biological templates, *Acta Polym.*, **49**, 663-670, 1998.

[47] Keren, K., Krueger, M., Gilad, R., Ben-Yoseph, G., Sivan, U., and Braun, E., Sequence specific molecular lithography on single DNA molecules, *Science*, **297**, 72-75, 2002.

[48] Keren, K., Berman, R. S., Buchstab, E., Sivan, U., and Braun, E., DNA-templated carbon nanotube Field-Effect Transistor, *Science*, **302**, 1380-1382, 2003.

[49] Patolsky, F., Weizmann, Y., Lioubashevski, O., and Willner, I., Au-nanoparticle nanowires based on DNA and polylysine templates, *Angew. Chem. Int. Ed.*, **41**, 2323-2327, 2002.

[50] Richter, J., Seidel, R., Kirsch, R., Mertig, M., Pompe, W., Plaschke, J., and Schackert, H. K., Nanoscale palladium metallization of DNA, *Adv. Mater.*, **12**, 507-510, 2000.

[51] Richter, J., Mertig, M., Pompe, W., Monch, I., and Schackert, H. K., Construction of highly conductive nanowires on a DNA template, *Appl. Phys. Lett.*, **78**, 536-568, 2001.

[52] Richter, J., Mertig, M., Pompe, W., and Vinzelberg, H., Low-temperature resistance of DNA-templated nanowires, *Appl. Phys. A*, **74**, 725-728, 2002.

[53] Deng, Z., and Mao, C., DNA-templated fabrication of 1D parallel and 2D crossed metallic nanowire arrays, *Nano Lett.*, **3**, 1545-1548, 2003.

[54] Ford, W. E., Harnack, O., Yasuda, A., and Wessels, J., Platinated DNA as precursors to templated chains of metal nanoparticles, *Adv. Mater.*, **13**, 1793-1797, 2001.

[55] Monson, C. F., and Woolley, A. T., DNA-templated construction of copper nanowires, *Nano Lett.*, **3**, 359-363, 2003.

[56] Dittmer, W. U., and Simmel, F. C., Chains of semiconductor nanoparticles, *Appl. Phys. Lett.*, **85**, 633-635, 2004.

[57] Antognozzi, M., Szczelkun, M. D., Round, A. N., and Miles, M. J., Comparison between shear force and tapping mode AFM - high resolution imaging of DNA, *Single Mol.*, **3**, 105-110, 2002.

[58] Qin, X. Y., Zhang, L. D., Cheng, G. S., Liu, X. J., and Jin, D., The low-temperature resistance and its density effects of bulk nanostructured silver, *J. Phys. D: Appl. Phys.,* **31**, 24-31, 1998.

[59] Dorogi, M., Gomez, J., Osifchin, R., Andres, R. P., and Reifenberger, R., Room-temperature Coulomb blockade from a self-assembled molecular nanostructure, *Phys. Rev. B*, **52**, 9071-9077, 1995.

[60] Parthasarathy, R., Lin, X. M., and Jaeger, H. M., Electronic transport in metal nanocrystal arrays: the effect of structural disorder on scaling behavior, *Phys. Rev. Lett.*, **87**, 1868071-1868074, 2001.

[61] Wolf, S. A., Awschalom, D. D., Buhrman, R. A., Daughton, J. M., von Molnar, S., Roukes, M. L., Chtchelkanova, A. Y., and Treger, D. M., Spintronics: a spin-based electronics vision for the future, *Science*, **294**, 1488-1495, 2001.

[62] Zwolak, M., and Di Ventra, M., DNA spintronics, *Appl. Phys. Lett.*, **81**, 925-927, 2002.

[63] Lieberman, M., Chellamma, S., Varughese, B., Wang, Y., Lent, C., Bernstein, G. H., Snider, G., and Peiris, F. C., Quantum-dot cellular automata at a molecular scale, *Ann. N. Y. Acad. Sci.*, **960**, 225-239, 2002.

Biography

Sung Ha Park was born on October 25, 1969. He was raised in the harbor city, Busan, Korea during a period of growth, change and democratic thinking. Against the backdrop of society's enthusiasm for growth and discovery, his childhood dream was to rub an *Aladdin's Magic Lamp* which would unlock the mysteries of nature so that he could meet the God of the Nature. Following his desire, he entered Kyung Hee University in the Department of Astronomy and Space Science in Korea, studying astronomy. Sensing that there was greater knowledge to be won overseas, he transferred to California State University at Northridge in the United States of America. He earned a Bachelor of Sciences in August, 1996 and a Master of Sciences in physics in May 1998, studying theoretical computational condensed matter physics with Sigma Pi Sigma. After completion of the Master's Program in Physical Sciences at the University of Chicago, studying experimental condensed matter physics in June, 2000, he moved to Duke University for further study in nano/bio science in the Fall, 2000.

Publications

Park, S. H., Ahn, S. J., Reif, J. H., and LaBean, T. H., Fully addressable stepwise assembly of finite-size nanomatrices from simple cross tiles, in preparation, 2005.

Park, S. H., Reif, J. H., LaBean, T. H., and Finkelstein, G., Metallic nanowires templated on native and synthetic double-stranded DNA molecules, in preparation, 2005.

Park, S. H., Barish, R., Li, H., Reif, J. H., Finkelstein, G., Yan, H., and LaBean, T. H., Three-helix bundle DNA tiles self-assemble into 2D lattice or 1D templates for silver nanowires, *Nano Lett.*, **5**, 693-696, 2005.

Park, S. H., Yin, P., Liu, Y., Reif, J. H., LaBean, T. H., and Yan, H., Programmable DNA self-assemblies for nanoscale organization of ligands and proteins, *Nano Lett.*, **5**, 729-733, 2005.

Park, S. H., Yan, H., Reif, J. H., LaBean, T. H., and Finkelstein, G., Electronic nanostructures templated on self-assembled DNA scaffolds, *Nanotechnology*, **15**, S525-S527, 2004.

Liu, D., Park, S. H., Reif, J. H., and LaBean, T. H., DNA nanotubes self-assembled from triple-crossover tiles as templates for conducting nanowires, *Proc. Natl. Acad. Sci.*, **101**, 717-722, 2004.

Li, H., Park, S. H., Reif, J. H., and LaBean, T. H., and Yan, H., DNA-templated self-assembly of protein and nanoparticle linear arrays, *J. Am. Chem. Soc.*, **126**, 418-419, 2004.

Feng, L., Park, S. H., Reif, J. H., and Yan, H., A two state DNA lattice actuated by DNA motors, *Angew. Chem. Int. Ed.*, **42**, 4342-4346, 2003.

Yan, H., Park, S. H., Finkelstein, G., Reif, J. H., and LaBean, T. H., DNA-templated self-assembly of protein Arrays and highly conductive nanowires, *Science*, **301**, 1882-1884 2003.

Kocharian, A., Kioussis, N., and Park, S. H., Magnetic crossover in the one-dimensional Hubbard model in the presence of magnetic field, *J. Phys.: Condensed Matt.*, **13**, 6759-6772, 2001.

Papatriantafillou, C., Kioussis, N., Park, S. H., and Kocharian, A., The one-dimensional periodic Anderson model: A Mean Field study, *Physica B*, **259-261**, 208-209, 1999.

Papatriantafillou, C., Kioussis, N., and Park, S. H., Antiferromagnetism of the half-filled Anderson lattice in one-dimension, *Phys. Rev. B*, **60**, 13355-13360, 1999.

Kioussis, K., Kocharian, A., and Park, S. H., One-dimensional Hubbard model in the presence of magnetic field, *J. of Magnetism and Magnetic Mater.*, **177-181**, 575-576, 1998.

Book Chapter

LaBean, T. H., and Park, S. H., Self-assembled DNA Nanotubes, *Nanotechnologies for the Life Sciences (Book Series): Vol.* **2***. Biological and Pharmaceutical Nanomaterials*, Edited by Kumar, C., 2005.

Presentations

Park, S. H., Li, H., Yan, H., Reif, J. H., Finkelstein, G., and LaBean, T. H., Self-assembled 1D DNA nanostructures as templates for silver nanowires, the 2nd Foundations of Nanoscience: Self-assembled Architectures and Devices, Snowbird, Utah, April 24-28, 2005.

Park, S. H., DNA self-assembly and DNA-based nanoelectronics, Center for the Physics of Information, California Institute of Technology, Pasadena, CA, February 21, 2005.

LaBean, T. H., Yan, H., Park, S. H., Feng, L., Yin, P., Li, H., Ahn, S. J., Liu, D., Guan, X., and Reif, J. H., Overview of the new structures for DNA-based nanofabrication and computation, the 1st Conference on Advanced Nanotechnology: Research, Applications, and Policy, Washington DC, October 22-24, 2004.

Park, S. H., Ahn, S. J., Yin, P., Yan, H., Reif, J. H., and LaBean, T. H., Effect of corrugating schemes on the morphologies of DNA lattices, the 1st Foundations of Nanoscience: Self-assembled Architectures and Devices, Snowbird, Utah, April 21-23, 2004.

Park, S. H., Yan, H., Reif, J. H., Finkelstein, G., and LaBean, T. H., Conductive nanowires, programmable attachment chemistry and molecular computers using self-assembled DNA nanostructures, the 4th Annual Graduate Student Research Day at Duke University, Durham, NC, March 24, 2004.

Park, S. H., Yan, H., Finkelstein, G., Reif, J. H., and LaBean, T. H., Self-assembling DNA nanostructures for DNA-based computation and nanoelectronics fabrication, the IBM University Day, Research Triangle Park, NC, February 26, 2004.

Finkelstein, G., Park, S. H., Yan, H., Reif, J. H., and LaBean, T. H., Highly conductive metallic nanostructures based on self-assembled DNA templates, IEEE-Nanoscale Devices and System Integration, Miami, FL, February 15-19, 2004.

Yan, H., Park, S. H., Finkelstein, G., Reif, J. H., and LaBean, T. H., 4 × 4 DNA tile and lattices: characterization, self-assembly and metallization of a novel DNA nanostructure motif, the 13th Conversation, Biomolecular Stereodynamics, SUNY, Albany, NY, June 17-21, 2003.

Park, S. H., Yan, H., Feng, L., Finkelstein, G., Reif, J. H., and LaBean, T. H., DNA nanogrids and nanoribbons for templated self-assembly of highly conductive nanowires, Duke University, NANO-2003, Workshop, Durham, NC, May 5-6, 2003.

Park, S. H., and Finkelstein, G., Iron nanoparticle single electron transistor, the 2nd Annual Graduate Student Research Day at Duke University, Durham, NC, March 20, 2002.

Park, S. H., Kioussis, N., and Kocharian, A., Phase diagram of the symmetric and asymmetric one-dimensional Anderson lattice, American Physical Society, March Meeting, L. A., CA, March, 1998.